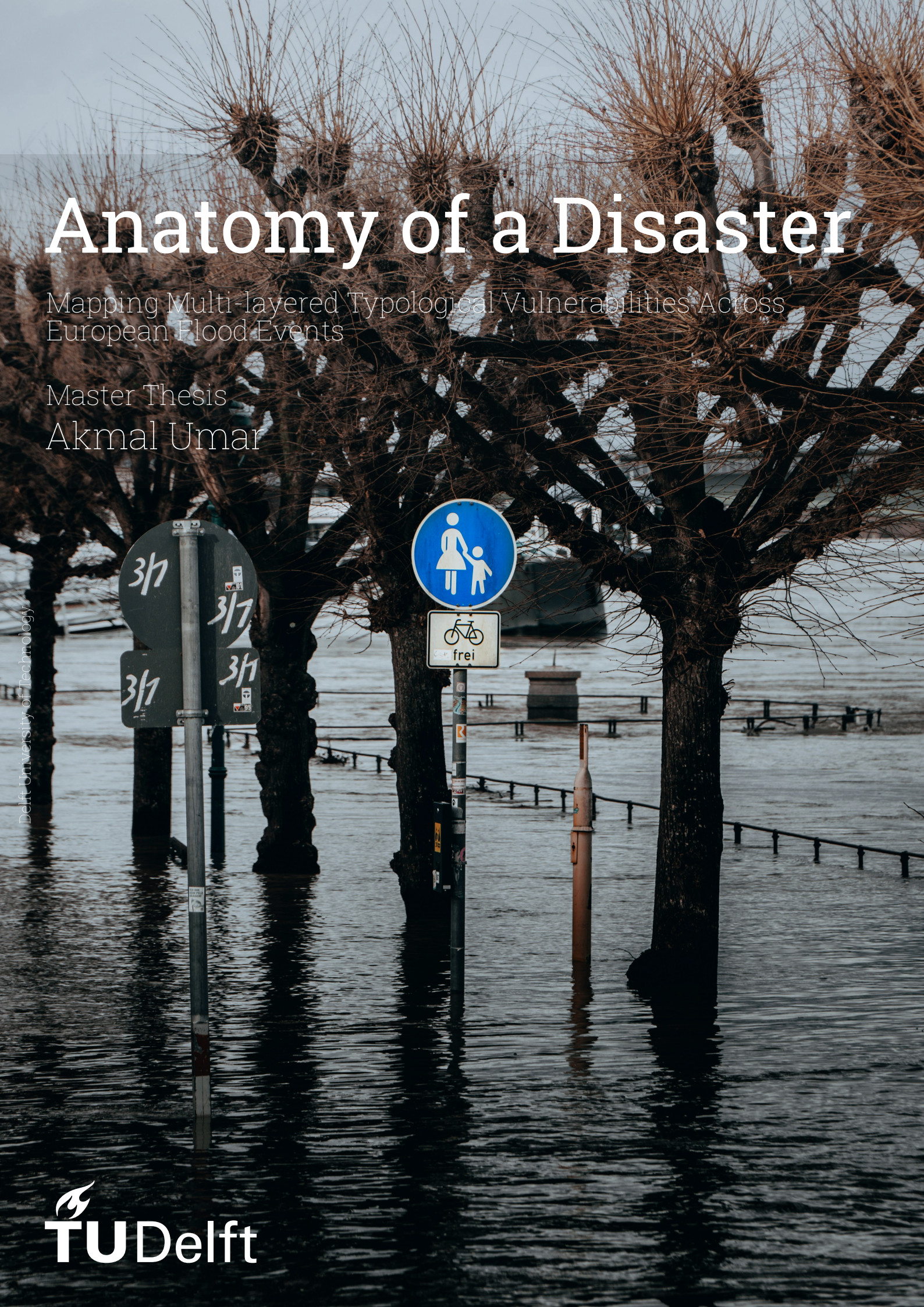
Anatomy of a Disaster

Mapping Multi-layered Typological Vulnerabilities Across European Flood Events

Master Thesis

Akmal Umar



Delft University of Technology

TU Delft

Anatomy of a Disaster

Mapping Multi-layered Typological Vulnerabilities Across European Flood Events

by

Akmal Umar

to obtain the degree of Master of Science

at the Delft University of Technology,

to be defended publicly on Wednesday, August 26th, 2026 at 01:00 PM.

Student number:	6128971	
Thesis committee:	Dr. N. Y. Aydin,	First supervisor & Chair
	Dr. S. Balakrishnan,	Second supervisor

Cover:	Black and white street sign near brown trees during daytime, photo by Jonathan Kemper from Unsplash (Modified)
Style:	TU Delft Report Style, with modifications by Daan Zwaneveld (Modified)

An electronic version of this thesis is available at http://repository.tudelft.nl/. Data and code used in this thesis are available from the author upon request.

TU Delft

lpdp

lembaga pengelola dana pendidikan

Acknowledgments

I believe that education can be a means of emancipation. It empowers learners with the knowledge to critically engage with and transform their world, ultimately allowing them to take greater ownership of their own futures. Studying in the Engineering and Policy Analysis program has been a strong demonstration of this idea. Every model result, visualization, and iteration of parameters can be used to inform and guide, as opposed to imposing a single answer.

Throughout the program, we have learned to work with numbers and data, while recognizing that these must be communicated clearly and understood by the people who encounter them. We have learned to engage with policy stakeholders, while recognizing that policymaking must remain participatory and communicative among analysts, institutions, and affected communities. We have learned to address Grand Challenges and Wicked Problems, yet the phrase ”it depends” persistently reminds us that there is rarely one final answer to a complex problem. Information can expand how stakeholders understand a problem and open a clearer range of possible solutions. At the same time, analysts must not become absorbed in their model-world and must remain attentive to the nuances and complexities of the real world.

This thesis has been shaped by that perspective. Its models, maps, and typologies are intended to support an understanding of how flood vulnerability and damage are distributed in space. They are not intended to prescribe solutions on their own. I hope they can contribute, however modestly, to more informed and participatory decisions for communities facing flood risk. This way of thinking has greatly shaped how I understand my work and how I hope to carry myself moving forward.

I am especially thankful to the Indonesia Endowment Fund for Education Agency (LPDP) for giving me the opportunity to experience this program firsthand. This journey would not have been possible without the support of this scholarship and the many efforts involved in obtaining it.

I would also like to extend my gratitude to my thesis committee. To Nazli, my first supervisor and chair, thank you for the sparks, encouragement, and guidance that helped this thesis move in the right direction and retain its focus on benefiting people. To Srijith, my second supervisor, thank you for your ideas, feedback, and challenges that pushed this thesis to become firmer and more detailed. Thank you both for your trust and support throughout the past seven months.

To the people who experienced the past two years with me, Atha, Memeng, Rachel, Anin, Raissa, thank you for being there whether in joy or when things get too rough. I look forward to seeing each of you succeed in whatever you consider worthy of your efforts.

Lastly, I offer heartfelt appreciation to my support systems in Delft and beyond. To my family back home, thank you for your continual support. Much of what is good in me comes from you. To my fellow EPA classmates, Polakweg housemates, Vijzelgracht regulars, and PPI Delft, thank you for illuminating these two years away from home. And to Nisa, thank you for holding me to a higher standard at every step.

I hope this thesis brings some light to the complex world around us, encourages further exploration and curiosity, and serves as a small step toward more resilient, expressive, and emancipated communities.

Akmal Umar
Delft, August 2026

Summary

Floods are Europe's most frequent natural hazard and increasingly its most damaging, with the past three decades ranking among the most flood-intensive periods of the last 500 years. Despite growing exposure, flood vulnerability assessments have suffered from two persistent gaps, a lack of empirical validation against observed damage and a tendency to study single events in isolation rather than compare across cases. This thesis addresses both gaps by asking *to what extent do theoretical flood vulnerability indicators align with actual post-disaster impact zones to define spatial typologies across recent European flood events?*

The research compares four major European floods, the 2021 Ahr Valley floods in Germany, the 2023 Emilia-Romagna floods in Italy, the 2024 Klodzko Valley floods in Poland, and the 2024 Valencia floods in Spain, chosen for their high fatality counts and their diversity in flood mechanism, terrain, and institutional context. A literature-derived indicator set, grounded in the Integrated Risk Linkages framework and informed by country-specific vulnerability studies, was operationalized on a harmonized 100 m grid. Copernicus products supplied hazard, built-environment, and damage data. OpenStreetMap supplied road and infrastructure data. WorldPop supported population mapping and dasymetric disaggregation, while national statistical sources supplied socio-economic indicators. Indicator redundancy was addressed through blockwise PCA, which preserved conceptual domain structure while reducing collinearity. k-means clustering then identified recurring spatial typologies of vulnerability and hazard, and ordinal logistic spatial-lag (SLX) regression quantified the strength and spatial effects of the relationship between indicators and observed damage, restricted to the observed flood footprint in each region.

The results show that mapped indicators align with flood impact zones to a meaningful extent, although the strength of the relationship differs across indicator domains and countries. Built surface and built volume consistently formed a built-mass component, while broad socio-demographic components captured correlated population, education, employment, income, and household counts. Comparing clusters by damage share identified an *urban core* typology in all four countries. These clusters combined dense road networks, high built mass, concentrated infrastructure, and frequently low vegetation cover.

Road density was the strongest shared indicator. It was elevated in every highest-damage-share urban-core cluster and had a positive, statistically significant association with damage in all four regional regression models. Built mass also recurred across the high-impact typologies and was important in three regional models. Germany differed because built-up areas were concentrated in a wider part of the Ahr Valley that experienced lower flood intensity than the confined upstream reaches.

Case-specific factors outside the spatial model also shaped the observed impacts. Germany's confined valley terrain and documented warning failures contributed to severe damage. Italy's flat and slower-onset flooding was associated with lower peak damage severity despite a large flooded area. These findings show that physical vulnerability patterns require interpretation through local terrain, warning systems, and governance conditions.

Methodologically, the thesis demonstrates a full analytical pipeline, from literature-based indicator selection through dasymetric disaggregation, dimensionality reduction, clustering, and spatial regression, applied consistently across four countries with significantly different data infrastructures. Key limitations include variable inconsistencies across national statistical sources and reliance on infrastructure damage as a proxy for the broader concept of flood impact.

The thesis concludes that mapped vulnerability indicators, especially those describing dense urban infrastructure, can support the identification of high-impact flood typologies across European contexts. Flood risk policy can use this physical urban-core profile to prioritize infrastructure-heavy areas for land-use, structural, and preparedness measures. Socio-demographic and governance dimensions require local calibration for each region. Future work should extend this cross-case validation approach to additional hazard types and regions, incorporate more temporally dynamic socio-economic data, and apply more rigorous sensitivity testing to the clustering and dimensionality reduction choices made here.

Contents

Acknowledgments i

Summary ii

Abbreviations ix

1 Introduction 1
- 1.1 Background . . . 1
- 1.2 Research Question . . . 2
  - 1.2.1 Main Research Question . . . 2
  - 1.2.2 Research Sub-Questions . . . 2
- 1.3 Research Flow . . . 3
- 1.4 Case Selection . . . 3
- 1.5 Relevance to the EPA Program . . . 4
- 1.6 Report Structure . . . 5

2 Literature Review 6
- 2.1 Conceptualizing Flood Vulnerability . . . 6
  - 2.1.1 Definitions of Vulnerability . . . 6
  - 2.1.2 Vulnerability Frameworks . . . 7
  - 2.1.3 Selected Conceptual Framework and Domains . . . 7
- 2.2 Indicator Identification Process . . . 9
  - 2.2.1 Deductive and Inductive Approaches to Indicator Selection . . . 9
  - 2.2.2 Two-phase Literature-based Indicator Identification . . . 9
  - 2.2.3 Cross-Case Data Availability and Indicator Feasibility . . . 10
- 2.3 Literature-Derived Core Indicator Set . . . 10
  - 2.3.1 Core Indicator Set and Expected Effects . . . 10
  - 2.3.2 Rationale for the Retained Indicator Set . . . 10
- 2.4 Conceptualizing and Measuring Flood Impact . . . 11
  - 2.4.1 Dimensions of Flood Impact . . . 11
  - 2.4.2 Infrastructure Damage as a Proxy for Impact . . . 11

3 Study Area, Data, and Indicator Construction 14
- 3.1 Case Studies and Spatial Delineation . . . 14
  - 3.1.1 Regional Units and Spatial Resolution . . . 14
  - 3.1.2 Impact-Based Study Area Delineation . . . 15
  - 3.1.3 Target Grid, Projection, and Population Filter . . . 15
  - 3.1.4 Study Area Delineation and Analytical Samples . . . 15
- 3.2 Data Sources . . . 16
  - 3.2.1 Sources for Hazard and Susceptibility Indicators . . . 16
  - 3.2.2 Copernicus EMS Flood Extent and Damage Data . . . 18
  - 3.2.3 Administrative Boundaries and Spatial Reference Data . . . 19
  - 3.2.4 Temporal Alignment of Data . . . 19
- 3.3 Data Harmonization and Indicator Construction . . . 19
  - 3.3.1 Variable Types and Spatial Representation . . . 19
  - 3.3.2 Dasymetric Mapping and Ancillary Variables . . . 20
  - 3.3.3 Derivation of Hazard and Susceptibility Indicators . . . 20
  - 3.3.4 Operationalized Indicator Set . . . 21
  - 3.3.5 Construction of Flood Impact Variables . . . 21

4 Spatial Analysis Methods 23
- 4.1 Analytical Workflow and Indicator Screening . . . 23
- 4.2 Blockwise Principal Component Analysis . . . 23

4.2.1 Rationale for Blockwise PCA . . . 23
4.2.2 Principal Component Extraction and Retention . . . 24
4.2.3 Correlation-Based Indicator Blocks . . . 24
4.3 Spatial Clustering of Vulnerability Typologies . . . 25
4.3.1 Selection of K-Means Clustering . . . 25
4.3.2 Selection of the Number of Clusters . . . 27
4.3.3 Identification of Impact-Prone Typologies . . . 27
4.4 Spatial Regression of Flood Damage . . . 27
4.4.1 Regression Sample and Outcome Variable . . . 27
4.4.2 Baseline Model and Multicollinearity Screening . . . 28
4.4.3 Spatial Weights and Residual Spatial Dependence . . . 28
4.4.4 Spatial Lag of X Model . . . 29
4.4.5 Hazard-Only Control Model . . . 29

5 Spatial Analysis Results **30**
5.1 Blockwise PCA Results . . . 30
5.1.1 Grouping Variables by Measurement Type . . . 30
5.1.2 PCA Screening and Block Formation . . . 30
5.1.3 PCA Results and Reduced Indicator Set: Germany . . . 31
5.1.4 PCA Results and Reduced Indicator Set: Italy . . . 31
5.1.5 PCA Results and Reduced Indicator Set: Poland . . . 31
5.1.6 PCA Results and Reduced Indicator Set: Spain . . . 31
5.2 Spatial Clustering Results . . . 36
5.2.1 Selection of the Number of Clusters . . . 36
5.2.2 Cluster Typologies and Damage Distribution: Germany . . . 39
5.2.3 Cluster Typologies and Damage Distribution: Italy . . . 39
5.2.4 Cluster Typologies and Damage Distribution: Poland . . . 41
5.2.5 Cluster Typologies and Damage Distribution: Spain . . . 41
5.3 Spatial Regression Results . . . 44
5.3.1 Regression Sample and Model Specification . . . 44
5.3.2 Residual Spatial Autocorrelation Diagnostics . . . 45
5.3.3 Added Explanatory Value of Susceptibility Indicators . . . 45
5.3.4 Direct and Spatially Lagged Effects: Germany . . . 46
5.3.5 Direct and Spatially Lagged Effects: Italy . . . 48
5.3.6 Direct and Spatially Lagged Effects: Poland . . . 50
5.3.7 Direct and Spatially Lagged Effects: Spain . . . 52
5.3.8 Ex-Post Spatial Diagnostics . . . 54
5.4 Summary of Key Findings . . . 54

6 Discussion **55**
6.1 Cross-Case Synthesis of Vulnerability Patterns . . . 55
6.1.1 Indicator Structures Across Case Studies . . . 55
6.1.2 High-Impact Spatial Typologies Across Case Studies . . . 56
6.1.3 Regression-Based Evidence on Damage Associations . . . 59
6.1.4 Convergence and Divergence Between Clustering and Regression . . . 60
6.2 Interpreting the Findings Through Vulnerability Theory . . . 62
6.2.1 Built Environment, Land Cover, and Hazard Amplification . . . 62
6.2.2 Socio-Demographic Vulnerability and Exposure . . . 63
6.2.3 Place-Based and Context-Dependent Vulnerability . . . 63
6.3 Explaining Cross-Case Differences . . . 63
6.3.1 Germany . . . 63
6.3.2 Italy . . . 64
6.3.3 Poland . . . 65
6.3.4 Spain . . . 65
6.4 Implications and Contributions . . . 65
6.4.1 Policy Implications . . . 65
6.4.2 Academic Contribution . . . 66
6.5 Methodological Reflections and Limitations . . . 67

6.6 Future Research . . . 70

7 Conclusion **71**

References **73**

A IRL Framework Component Figures **79**

B Choropleths **82**
B.1 Germany . . . 82
B.2 Italy . . . 86
B.3 Poland . . . 89
B.4 Spain . . . 92

C Spatial Clustering K-Value Diagnosis Raw Values **95**
C.1 Germany . . . 95
C.2 Italy . . . 96
C.3 Poland . . . 97
C.4 Spain . . . 98

D Full Spatial Regression Model Results **99**
D.1 Germany . . . 99
D.2 Italy . . . 101
D.3 Poland . . . 103
D.4 Spain . . . 104

E Full Cross-Region Consistency Results **106**

F Data Validation and Indicator Construction Checks **109**
F.1 General Validation Procedures . . . 109
F.1.1 Spatial Reference and Grid Checks . . . 109
F.1.2 Numerical Screening . . . 109
F.1.3 Dasymetric Allocation Checks . . . 110
F.2 Germany . . . 110
F.2.1 Administrative Identifier and Source-Format Checks . . . 110
F.2.2 German Zensus Data and Disclosure-Control Checks . . . 110
F.2.3 Education Data Allocation . . . 110
F.2.4 Correction of Count-Variable Allocation . . . 110
F.3 Italy . . . 111
F.3.1 Coordinate Reference and Overlay Checks . . . 111
F.3.2 Household-Weighted Income Allocation . . . 111
F.3.3 Income and Poverty Allocation Checks . . . 111
F.4 Poland . . . 111
F.4.1 API Retrieval and Metadata Checks . . . 111
F.4.2 Hierarchy and Derived-Indicator Checks . . . 112
F.4.3 Foreign Population Allocation . . . 112
F.5 Spain . . . 112
F.5.1 Raster and Census-Tract Checks . . . 112
F.5.2 Grid Merge and Duplicate-Column Checks . . . 112
F.5.3 Province-Level Employment Allocation . . . 112
F.6 Hazard, Infrastructure, and Impact Checks . . . 112
F.6.1 Hazard Indicators . . . 112
F.6.2 Infrastructure Indicators . . . 113
F.6.3 Flood-Impact Indicators . . . 113
F.7 Final Screening Before Analysis . . . 113

List of Figures

1.1 Research flow diagram of this thesis. 4

2.1 Integrated Risk Linkages (IRL) framework 8

3.1 Study area delineation for Germany 16
3.2 Study area delineation for Italy 17
3.3 Study area delineation for Poland 17
3.4 Study area delineation for Spain 18

5.1 Spatial clustering map of Germany, cluster profiles, and histogram of damage distribution. . . 38
5.2 Spatial clustering map of Italy, cluster profiles, and histogram of damage distribution. 40
5.3 Spatial clustering map of Poland, cluster profiles, and histogram of damage distribution. . . . 42
5.4 Spatial clustering map of Spain, cluster profiles, and histogram of damage distribution. . . . 43
5.5 Fit comparison of hazard-only model and with susceptibility variables included 46
5.6 Coefficient shift for hazard variables, Germany 46
5.7 Forest plot of the direct and lag coefficients of the variables in Germany's full model ($p < 0.05$) 47
5.8 Coefficient shift for hazard variables, Italy 48
5.9 Forest plot of the direct and lag coefficients of the variables in Italy's full model ($p < 0.05$) . . . 49
5.10 Coefficient shift for hazard variables, Poland 50
5.11 Forest plot of the direct and lag coefficients of the variables in Poland's full model ($p < 0.05$) . 51
5.12 Coefficient shift for hazard variables, Spain 52
5.13 Forest plot of the direct and lag coefficients of the variables in Spain's full model ($p < 0.05$) . . 53

6.1 Share of damaged grids per cluster per region 56
6.2 Typologies of clusters with the highest share of damaged grids per cluster per region 57

A.1 Hazard hierarchy 79
A.2 Susceptibility hierarchy 80
A.3 Resilience hierarchy 81

B.1 Choropleths of hazard indicators for Germany. 82
B.2 Choropleths of physical susceptibility indicators for Germany. 83
B.3 Choropleths of human susceptibility indicators for Germany. 84
B.4 Choropleths of social susceptibility indicators for Germany. 85
B.5 Choropleths of hazard indicators for Italy. 86
B.6 Choropleths of physical susceptibility indicators for Italy. 86
B.7 Choropleths of human susceptibility indicators for Italy. 87
B.8 Choropleths of social susceptibility indicators for Italy. 88
B.9 Choropleths of hazard indicators for Poland. 89
B.10 Choropleths of physical susceptibility indicators for Poland. 89
B.11 Choropleths of human susceptibility indicators for Poland. 90
B.12 Choropleths of social susceptibility indicators for Poland. 91
B.13 Choropleths of hazard indicators for Spain. 92
B.14 Choropleths of physical susceptibility indicators for Spain. 92
B.15 Choropleths of human susceptibility indicators for Spain. 93
B.16 Choropleths of social susceptibility indicators for Spain. 94

C.1 K value plots according to different methods for Germany. 95
C.2 K value plots according to different methods for Italy. 96
C.3 K value plots according to different methods for Poland. 97
C.4 K value plots according to different methods for Spain. 98

List of Tables

2.1 Preliminary indicator set derived from literature. 13

3.1 Final operationalized indicator set 22

5.1 PCA loadings and screening for Germany 32
5.2 PCA loadings and screening for Italy 33
5.3 PCA loadings and screening for Poland 34
5.4 PCA loadings and screening for Spain 35
5.5 Normalized clustering validation indices by number of clusters for Germany. 36
5.6 Normalized clustering validation indices by number of clusters for Italy. 37
5.7 Normalized clustering validation indices by number of clusters for Poland. 37
5.8 Normalized clustering validation indices by number of clusters for Spain. 37
5.9 Damage distribution by cluster in Germany 39
5.10 Damage distribution by cluster in Italy 39
5.11 Damage distribution by cluster in Poland 41
5.12 Damage distribution by cluster in Spain 41
5.13 Variables removed due to VIF multicollinearity, by region 45
5.14 Moran's I on OLS residuals by region 45
5.15 Ordinal SLX model coefficients for Germany (direct and spatially lagged effects) 47
5.16 Ordinal SLX model coefficients for Italy (direct and spatially lagged effects) 50
5.17 Ordinal SLX model coefficients for Poland (direct and spatially lagged effects) 51
5.18 Ordinal SLX model coefficients for Spain (direct and spatially lagged effects) 53
5.19 Likelihood ratio test, non-spatial vs. SLX ordinal logit, by region 54
5.20 Residual spatial autocorrelation before and after the SLX specification 54

6.1 Damage distribution by cluster, all regions 56
6.2 Rank-averaged consensus of indicator importance across regions 59
6.3 Evidence table classification counts by region 60
6.4 Indicators classified as strongly consistent, by region 61
6.5 Indicators classified as conflicting, by region 61

C.1 Raw clustering validation indices by number of clusters, Germany 96
C.2 Raw clustering validation indices by number of clusters, Italy 96
C.3 Raw clustering validation indices by number of clusters, Poland 97
C.4 Raw clustering validation indices by number of clusters, Spain 98

D.1 Model comparison statistics for Germany 99
D.2 Likelihood ratio test, non-spatial vs. SLX ordinal logit, Germany 99
D.3 Moran's I on model residuals, Germany 100
D.4 Ordinal SLX model coefficients — Germany (direct and spatially lagged effects) 100
D.5 Model comparison statistics for Italy 101
D.6 Likelihood ratio test, non-spatial vs. SLX ordinal logit, Italy 101
D.7 Moran's I on model residuals, Italy 101
D.8 Ordinal SLX model coefficients — Italy (direct and spatially lagged effects) 102
D.9 Model comparison statistics for Poland 103
D.10 Likelihood ratio test, non-spatial vs. SLX ordinal logit, Poland 103
D.11 Moran's I on model residuals, Poland 103
D.12 Ordinal SLX model coefficients — Poland (direct and spatially lagged effects) 103
D.13 Model comparison statistics for Spain 104
D.14 Likelihood ratio test, non-spatial vs. SLX ordinal logit, Spain 104
D.15 Moran's I on model residuals, Spain 104

D.16 Ordinal SLX model coefficients — Spain (direct and spatially lagged effects) 105

E.1 Full evidence classification, Germany 106
E.2 Full evidence classification, Italy 107
E.3 Full evidence classification, Poland 107
E.4 Full evidence classification, Spain 108

Abbreviations

Abbreviation	Definition
AIC	Akaike Information Criterion
AOI	Area of Interest
BIC	Bayesian Information Criterion
CI	Critical Infrastructure
COVID-19	Coronavirus Disease 2019
DANA	Depresión Aislada en Niveles Altos (Isolated Depression at High Levels)
DEM	Digital Elevation Model
Destatis	Statistisches Bundesamt (German Federal Statistical Office)
DWD	Deutscher Wetterdienst (German National Weather Service)
EAD	Expected Annual Damages
EMS	Emergency Management Service
EPA	Engineering and Policy Analysis
EU	European Union
GHSL	Global Human Settlement Layer
GUS	Główny Urząd Statystyczny (Polish Central Statistical Office)
GUS BDL	Bank Danych Lokalnych (Local Data Bank)
HAND	Height Above Nearest Drainage
INE	Instituto Nacional de Estadística (Spanish National Statistics Institute)
INKAR	Indikatoren und Karten zur Raum- und Stadtentwicklung (German regional monitoring database)
IPCC	Intergovernmental Panel on Climate Change
IRL	Integrated Risk Linkages
Istat	Istituto Nazionale di Statistica (Italian National Institute of Statistics)
LAU	Local Administrative Unit
LISA	Local Indicators of Spatial Association
LM	Lagrange Multiplier
LR	Likelihood Ratio
MEF	Ministero dell'Economia e delle Finanze (Italian Ministry of Economy and Finance)
MOVE	Methods for the Improvement of Vulnerability Assessment in Europe
NDVI	Normalized Difference Vegetation Index
NUTS	Nomenclature des Unités Territoriales Statistiques (Nomenclature of Territorial Units for Statistics)
OE	Observed Event
OLS	Ordinary Least Squares
OSM	OpenStreetMap
PAR	Pressure and Release
PC	Principal Component
PCA	Principal Component Analysis
SAC	Spatial Autoregressive Combined

Abbreviation	Definition
SAR	Spatial Autoregressive (model)
SDEM	Spatial Durbin Error Model
SDM	Spatial Durbin Model
SEM	Spatial Error Model
SLM	Spatial Lag Model
SLX	Spatial Lag of X (model)
SQ	Sub-Research Question
TU	Technische Universiteit
VIF	Variance Inflation Factor
z22	Zensus 2022 (German census)

1

Introduction

1.1. Background

Globally, floods are responsible for nearly 40 percent of all economic losses resulting from natural disasters (Biswas & Tortajada, 2020). Within Europe, they are the most common natural hazard, claiming the lives of over 4,000 citizens between 1980 and 2023 (European Environment Agency (EEA), 2025). Furthermore, the current state of flood risk in the continent is historically unique, as recent hydrological reconstructions in Europe reveal that the past three decades have been one of the most intense, flood-rich periods in the last 500 years (Blöschl et al., 2020). This intensity is physically represented through a growing spatial footprint of the floods, with the average extent of European floods having already increased by 11.3% from 1951 to 2020 (Fang et al., 2024).

Moving forward, European floods are projected to become highly spatially segmented, with specific regions slated to experience massive expansions in flood extent and frequency (Fang et al., 2025). As these floods move further inland, they reach heavily altered urban environments. Currently, around 52 million people, 12 percent of the EU population, live in floodplains. Concurrently, over 300 million people live in dense urban areas where high levels of soil sealing, caused by impermeable materials such as concrete and asphalt, reduce the environment's natural capacity to withstand the severity of surface flooding (European Environment Agency (EEA), 2025).

In addition to affecting the population directly through fatalities and injuries, these expanding and amplified floodwaters also damage the built environment systematically, with floods accounting for 89% of global Expected Annual Damages (EAD) (Koks et al., 2019). While exposed buildings and facilities fall victim to these in flood events, road networks are particularly vulnerable. Once a flood disrupts road networks, it severs the connectivity of a region, inhibiting further evacuation efforts and isolating impacted households from lifeline resources such as hospitals and emergency shelters. Consequently, evaluating the topological robustness of transport infrastructure alongside general infrastructure damage has become an important consideration in modern flood risk resiliency (Birkmann et al., 2013; Dong et al., 2020; Z. Li et al., 2026; Liang et al., 2026).

However, the severity of infrastructure failures cannot be seen by physical damage alone. Societal factors play a role in understanding flood risk. Damage from floods disproportionately affects marginalized populations. When roads fail and recovery is delayed, lower-income households and socially vulnerable demographics often lack the financial capacity and resources to adapt to prolonged service disruptions, leading to severe, long-term economic ruin (Dong et al., 2020; Houston et al., 2020). Therefore, a region's true vulnerability is dictated by a multitude of factors, ranging from physical environmental exposure, to infrastructural robustness and the underlying socio-economic conditions of the impacted area. This vulnerability is also shaped by a region's capacity to cope with and recover from a flood once it strikes, a dimension referred to throughout this thesis as resilience.

Traditionally, the default policy approach towards mitigating these complex risks relied heavily on physical means, such as constructing higher dikes or floodwalls. Yet, as extreme events continue to overwhelm these structural means, modern policy is being forced to shift from localized flood control toward some form of

integrated flood risk management strategies (Buijs et al., 2020; C. Li et al., 2016). These integrated strategies involve non-structural approaches to flood impacts in addition to conventional structural means, such as spatial planning, insurance, and flood resilient construction, with lowering flood risks that come with the implementations of these means (Dawson et al., 2011; Poussin et al., 2012). However, developing these strategies requires a comprehensive understanding of how different, multidimensional factors spatially interact to determine an effective intervention to prevent disaster risks.

Multidimensional indicator-based vulnerability approaches have been widely applied in a plethora of use cases and angles of analyses in the current literature space (Alabbad & Demir, 2022; Dong et al., 2020; Hendry et al., 2019; Z. Li et al., 2026; Loli et al., 2022; Pallathadka et al., 2022; Roy et al., 2021; Tate et al., 2021). Yet, a common drawback is the lack of empirical validation that comes with these indicators (Moreira et al., 2021). This would effectively limit the reliability in their approach, as the calculated vulnerabilities are not verified to have a satisfactory precision range. Additionally, the scope of their cases is often isolated in single regions, missing the benefits of understanding similarities across flood events in proximal, yet different, circumstances.

This master thesis aims to bridge this gap by proposing a multidimensional approach to flood vulnerability through validation with flood impact data. This research maps and integrates distinct layers of vulnerability indicators spanning socio-economic, physical, and infrastructural factors. Furthermore, because shifting hydrological patterns are producing varying flood dynamics across the continent (Fang et al., 2025), a comparative case study design across multiple recent European flood events is utilized. By cross-comparing these localized spatial layers, this thesis highlights recurring typologies and systemic vulnerabilities between different disasters, providing actionable, data-driven lessons to inform a more flood-resilient future for Europe.

1.2. Research Question

1.2.1. Main Research Question

The core research question for this thesis is:

To what extent do theoretical flood vulnerability indicators align with actual post-disaster impact zones to define spatial typologies across recent European flood events?

This question links literature-based, multi-dimensional vulnerability constructs to empirically observed damage patterns, and asks whether consistent spatial configurations of indicators can be identified across different flood contexts.

1.2.2. Research Sub-Questions

The main research question will be answered through several sub-research questions, detailed below.

SQ 1: Which indicators are identified in academic literature as the critical drivers of flood vulnerability?

Desk research will be done to review and filter indicators of flood vulnerability from the available literature, resulting in a list of variables that will be operationalized in the subsequent research phases. This process follows recent efforts to synthesize flood vulnerability indices and frameworks, which emphasize the need for transparent indicator selection and mapping between conceptual domains and measurable variables (Hamidi et al., 2025; Tabasi et al., 2025). Frameworks and reviews of flood risk assessments provide structured domains of vulnerability that guide the initial backbone of the indicator list. Factor analyses in regional studies are used in an auxiliary manner to identify locally important variables.

SQ 2: Using spatial statistics, to what extent do the mapped vulnerability indicators cluster and correlate with the actual flood impact zones?

The selected indicators from the previous sub-research question are mapped alongside collected empirical spatial data of flood impact maps (from Copernicus EMS). These datasets will be harmonized and unified into a spatial database for each flood event. Quantitative spatial analysis is then applied to this combined database to identify typological combinations of indicators against damaged areas, and to estimate the strength of association between indicators and observed impacts.

Exploratory choropleth mapping and dimensionality reduction are used to reveal univariate spatial patterns and to address multicollinearity among indicators, following common practice in vulnerability index construc-

tion and socio-economic spatial analyses (Cutter et al., 2003; Fekete, 2010; Moragues et al., 2025). Clustering methods support the identification of spatial typologies of vulnerability and hazard, and have been widely adopted in flood risk assessments and urban flooding studies to group locations with similar indicator profiles (Uddin et al., 2019; Xu et al., 2024). Spatial regression models are then used to quantify how much selected indicators and their spatial context contribute to the mapped damage, building on work that integrates spatial dependence into risk and vulnerability modeling (Rüttenauer, 2019). Together, these tools provide complementary perspectives, where clustering highlights recurring combinations of indicators in high-impact areas while spatial regression offers estimates of indicator effects on damage at fine spatial resolution levels.

SQ 3: Based on these spatial correlations, what high-impact vulnerability typologies consistently emerge across case studies?
Statistical commonalities between case studies are analyzed, and possible policy implications are synthesized. The vulnerability typologies identified through clustering and spatial regression in each event are compared to determine whether particular combinations of indicators are consistently associated with high-impact zones. This comparative approach aligns with recent calls for more cross-case, multi-hazard perspectives in vulnerability research that can inform broader risk reduction strategies (Moreira et al., 2021; UNISDR, 2015). The resulting typologies are interpreted with the light of existing theory and case-specific narratives, with attention to how they may guide targeted, place-based interventions.

1.3. Research Flow

Answering the research questions require sequential steps to ensure a coherent information flow across processes. Figure 1.1 attempts to visualize that. Initial problem identification, followed by gap analysis, results in the research questions. Subsequent steps include selecting the relevant case studies for this thesis. The selected case studies will be used to gather the relevant flood impact zones as well as to frame and scope the first sub research question through literature reviews to identify the critical drivers of flood vulnerability.

The resulting list of flood vulnerability drivers will then be operationalized as indicators. The data for these indicators will be collected for each of the study area of the cases. As the collection commences, a database containing the indicator data and the flood impact data will be built and used for the spatial analysis. These spatial analyses are initially sequential through choropleth mapping and dimensionality reduction processes, before proceeding in spatial clustering and spatial regression in a parallel approach. Only then will the third sub question will be answered.

The results of these spatial analyses will be used to answer the third sub question in the form of a cross comparison between the cases. The analysis will be interpretative and explanatory, and reflects on the quantitative output and literature background. The thesis then converges and concludes with conclusions, limitations, and recommendations for future research.

1.4. Case Selection

Four flood events were selected based on two criteria. The first criterion is a minimum threshold of documented fatalities to convey significant human impact. The second aims for geographic and typological diversity across European contexts, to capture variation in flood mechanism, geomorphic setting, and national institution context. The 2021 European floods, the 2023 Emilia-Romagna floods, the 2024 Central European floods, and the 2024 Spanish floods are chosen as the case studies for this thesis. Events with comparable fatality counts, notably the 2023 Bosnia and Herzegovina floods, were excluded on the basis of data availability, as the analysis requires harmonized data consistent with EU data infrastructure.

The 2021 European floods in mid July 2021 affects the Ahr Valley in Germany the most, constituting one of the deadliest riverine flash flood events in post-war Western European history. This flood represents a perfect storm of circumstances around the event. Extreme precipitation exceeding 100 mm within 24 hours over the Ahr river catchment caused a rapid river rise, resulting in 134 fatalities in the Ahr Valley alone and an estimated 33 billion euro damage across Germany (Rhein & Kreibich, 2025). The valley morphology amplified flood velocity and debris transport, contributing to the large number of casualties in the area (Tradowsky et al., 2023). The event exposed systemic failures in early warning systems, where despite existing meteorological forecasts, warnings did not reach or mobilize at-risk populations, a failure attributed to both fragmented institutional responsibilities regarding data sharing and consequential infrastructure failures (Mohr et al., 2022; Thieken et al., 2023). Additionally, social compounding events as an aftermath of the COVID-19 pandemic also

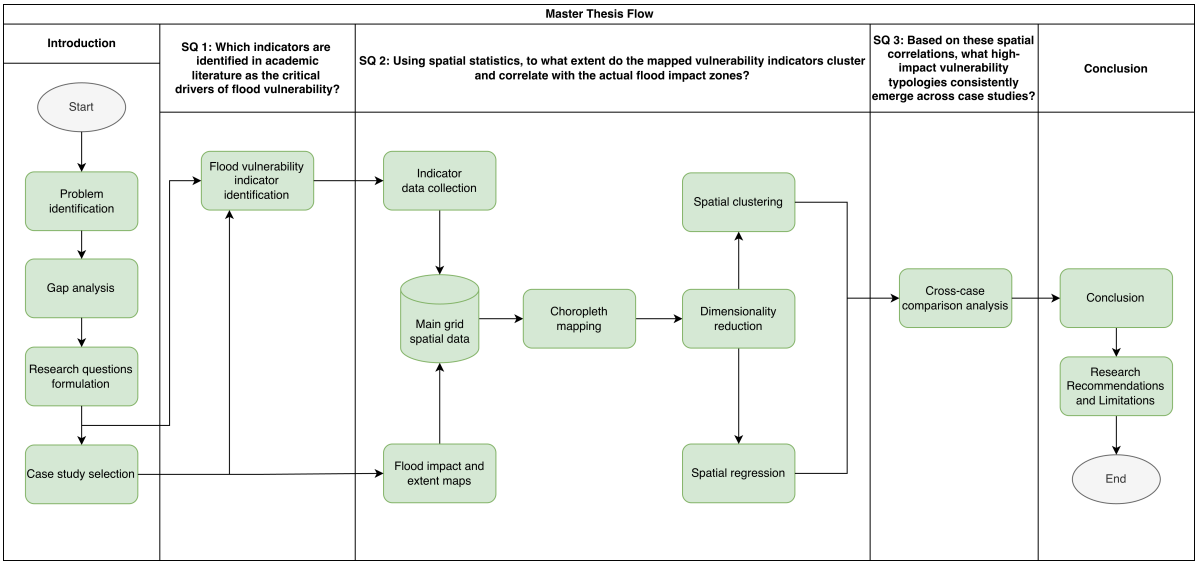


Figure 1.1: Research flow diagram of this thesis.

hinders evacuation efforts through low trust and anti-government sentiment disruptions (Fekete & Sandholz, 2021).

The 2023 Emilia-Romagna floods were a slow-onset multi-river overflow event driven by two successive rainfall occurrences in May 2023 across the Po river network in Italy. Seventeen rivers breached their banks, releasing floodwaters across approximately 500 km squared of flat plains, affecting nearly one million people, with at least 17 fatalities and estimated damages of 8.5 billion euros (D'Angelo & Toth, 2026; Marchi et al., 2025; Valente et al., 2025), and damaged 3000 houses in the Ravenna area (International Federation of Red Cross and Red Crescent Societies, 2023). In contrast to flash flood events, gradual onsets reveal a different vulnerability profile dominated by land-use, with developments of urban and agricultural expansion into floodplain zones reduce natural water retention capacity. This was exacerbated as it was preceded by a drought that dried out the land, followed by another flood several weeks prior, effectively reducing the soil's saturation capacity to absorb water in a short time (Pulvirenti et al., 2024).

The 2024 Central European floods, focused on the Klodzko Valley in southwestern Poland, resulted from sustained and extremely heavy rainfall from Storm Boris across the Sudeten Mountains in September 2024, triggering a rise of the Nysa Klodzka river. The event caused at least 9 fatalities in Poland and severe infrastructure damage across southwestern Poland, which includes 3633 km of roads, wastewater treatment plants, and landfills (Kałmykow-Piwińska & Witkowska, 2026).

The 2024 Spanish floods were triggered by a DANA (Depresión Aislada en Niveles Altos, commonly known as a cold drop) weather system on October 2024, producing a localized extreme rainfall over the lowlands south of Valencia city. The Barranco del Poyo, a normally dry channel, brought a flash flood wave through urbanized areas, resulting in over 250 fatalities (Bekić, 2026) and up to EUR 2.6 billion in repair costs of critical infrastructure damage (Castro-Melgar et al., 2025). The chaotic flood event was further compounded by political fragmentation between the regional Valencian government and the national government, which delayed emergency coordination and public warnings by several hours (Pitarch, 2024).

1.5. Relevance to the EPA Program

This research topic aligns with the MSc Engineering and Policy Analysis (EPA) at TU Delft, which focuses on solving complex problems concerning multiple actors with conflicting interests. Disaster and emergency management is a bona-fide "Grand Challenge", a complex and interconnected (Miller et al., 2025) societal challenge that involves diverse stakeholders, spanning different countries and sectors, with significant impacts to society. Analyzing disaster events through a systemic perspective with statistical tools is consistent with the program's emphasis on system understanding, simulation, and policy evaluation.

This thesis has a primarily quantitative approach through geospatial analysis. This method highlights varia-

tions in the typologies of regions, to provide complex analytical observations of disasters without discounting geographic characteristics. The use of spatial analysis using Python is representative of EPA courses such as programming and spatial data science.

A literature-centric approach comes before the programming, used to assess spatial indicators and frameworks and to piece together the events surrounding each flood. Case reports and academic sources document how early warning and emergency response broke down in some of these events, split across national forecasters, regional authorities, and municipalities. This, together with the quantitative and spatial analysis, helps explain the dynamics behind disaster outcomes and connects the vulnerability patterns to the institutions that turn hazard into damage. The multi-disciplinary nature of this thesis allows exploration of policy, socio-economic factors, and data science united under the EPA umbrella, an appropriate match for real-world complex problem-solving at the center of technology and society.

1.6. Report Structure

The report will be segmented in the following structure. The current Chapter 1 establishes the urgency of this research, research questions, and the case studies. The following Chapter 2 will begin with a literature review, understanding flood vulnerability indicators and the corresponding framework and address the first sub research question. Chapter 3 will explore data sources and construction along with operationalization preparations. Chapter 4 will detail spatial methods used to address the second sub research question, with the results reported in Chapter 5, corresponding to the steps of analysis according to Figure 1.1. This chapter will first explore the case studies independently of each other. Subsequently, Chapter 6 will zoom out and interpret the analysis across the four cases and commence the discussion, answering the third research question with additional contextual non-spatial data and implications on policy and limitations. Lastly, Chapter 7 will close the thesis with conclusions.

2

Literature Review

This chapter explores flood vulnerability indicators in the academic literature, answering the first sub-research question of this thesis. The primary goal is to identify the critical drivers of flood vulnerability that will form the basis for the comparative spatial analysis in the subsequent chapters. To do so, the chapter first outlines the conceptual skeleton of vulnerability and its associated frameworks, and then describes the process by which these frameworks were translated into a structured set of indicators, including explicit refinement steps. The following section will present the preliminary indicator list based on the steps detailed in the preceding section, and will be ready to be operationalized in the following chapter.

2.1. Conceptualizing Flood Vulnerability

Deriving indicators from a concept such as vulnerability requires an understanding of how vulnerability has been defined and broken down in prior research. A substantial body of work in disaster risk, climate change, and social vulnerability has proposed and refined definitions of vulnerability (Adger, 2006; Cutter et al., 2003; McCarthy, 2001; Neil Adger, 1999). A recent review by Hamidi et al. (2025) highlights that these definitions consistently emphasize factors that constrain specific groups' ability to manage risks posed by floods across the phases of preparation, response, and recovery. At the same time, Cutter et al. (2003) emphasized that vulnerability itself carries different connotations depending on the research orientation and perspective, which has direct implications for how it is operationalized in indicator-based analyses.

2.1.1. Definitions of Vulnerability

According to Cutter et al. (2003), vulnerability to environmental hazards simply means the potential for loss, and as losses vary geographically, temporally, and demographically, vulnerability also varies over time and space. Across the reviewed literature, three broad dimensions commonly appear in definitions of vulnerability. These are the exposure to potentially harmful events, the susceptibility or sensitivity of the exposed elements, and the capacity to adapt or cope. As an example, McCarthy (2001) defined vulnerability as a function of a system's exposure to climate change, its sensitivity, and its adaptive capacity. In contrast, social vulnerability research adds the focus of demographic and socio-economic characteristics that forge communities' ability to anticipate, withstand, and recover from hazards (Adger, 2006; Cutter & Finch, 2008; Cutter et al., 2003). In flood-related work, these dimensions often manifest as the physical exposure to inundation, susceptibility of buildings and populations to damage, and the presence or absence of resources that support response and relief.

In this thesis, these recurring dimensions are used as the backbone for organizing indicators. A new vulnerability definition will not be proposed, rather the analysis will build on existing concepts and formulations. Vulnerability is then treated as a multidimensional construct that surfaces from the interaction between hazard, exposure, susceptibility, and resilience.

2.1.2. Vulnerability Frameworks

Conceptual frameworks offer a structured way to link these different dimensions and to specify how the interactions occur. Several systematic reviews of flood vulnerability research were examined to identify commonly used frameworks and their corresponding components (Hamidi et al., 2025; Moreira et al., 2021; Shehzad et al., 2026; Tabasi et al., 2025). These reviews typically describe which frameworks are utilized, how they segment vulnerability into domains, and how they are used to guide indicator selection.

One of the earliest and most widely cited frameworks is the ”Risk Triangle” by Crichton (2001). In this approach, risk is seen as a function of three components, hazard, exposure, and vulnerability, each represented as a side of the triangle. The triangle visualizes the alteration of overall risk if there are changes in any of the sides. The simplicity of this framework made it a foundational tool for mapping flood risk patterns and blazed a trail of more complex frameworks (Tabasi et al., 2025) that seek to further unpack and expand the vulnerability side of the triangle.

The Pressure and Release (PAR) model shifts the focus to the social production of vulnerability, with vulnerability evolving through root causes, dynamic pressures, and unsafe conditions (Blaikie et al., 1994). However, as Turner et al. (2003) argues, this model has limitations for broader flood risk assessment, since it focuses primarily on social conditions and does not adequately address the biophysical vulnerability of ecosystems and infrastructure.

Alongside these research-driven frameworks, policy frameworks also offer perspectives on how vulnerability and risk are framed. The Sendai Framework for Disaster Risk Reduction emphasizes understanding disaster risk in all of its dimensions in exposure, vulnerability, and hazard, further strengthening disaster risk governance, investing in resilience, and enhancing preparedness and recovery (UNISDR, 2015). This framework, while not a technical index framework for analysis, asserts the importance of multi-dimensional, multi-scale risk assessment and provides guidance on which components should be considered when assessing risk and designing indicators.

More recent frameworks combine these threads. The MOVE framework (Methods for the Improvement of Vulnerability Assessment in Europe) combines hazard, exposure, vulnerability, and resilience explicitly into a comprehensive risk assessment approach (Birkmann et al., 2013). It aims to further explore vulnerability’s multi-faceted nature, as it supports assessments across physical, social, ecological, economic, cultural, and institutional aspects. While it has been widely cited as a comprehensive, theory-grounded approach, MOVE’s application often remains at a conceptual domain level and thus requires further work to translate its components into detailed indicators.

2.1.3. Selected Conceptual Framework and Domains

Building on these integrative thinking antecedents, Tabasi et al. (2025) proposed the Integrated Risk Linkages (IRL) framework in their review publication. IRL is a flood-specific structure that emphasizes the interconnectedness of its risk assessment components. In this framework, risk is defined as a combination of hazard and vulnerability. While it is acknowledged that vulnerability has various definitions, IRL maintains the idea of exposure being a component of vulnerability, where it is here considered as physical vulnerability. Physical vulnerability alongside intrinsic vulnerability, from here on referred to as susceptibility, results in overall vulnerability. Additionally, resilience reduces vulnerability, which itself is built by adaptive and coping capacities. The conceptual map of IRL is depicted in Figure 2.1.

Tabasi et al. (2025) developed IRL after reviewing a broad set of flood risk assessment frameworks and noting two recurring gaps. The first gap is many frameworks treat vulnerability either as a single, aggregated component or focus predominantly on social conditions without explicitly distinguishing how exposure, susceptibility, and resilience interact in flood settings. The second gap revolves around the implicitness of the links between conceptual components such as hazard, susceptibility, and resilience, making indicator derivation and subsequent operationalization fragmented and difficult to compare across studies. IRL addresses these gaps by making the relationships between these components explicit and through the proposal of hierarchical structures of criteria for each component that can be adapted to different study areas.

In the hazard component, pictured in Figure A.1, IRL starts with a decision branch of whether physical-based flood mapping is applicable. If hydrodynamic modeling or detailed flood characteristics are available, hazard is quantified using data such as flood depth, velocity, and duration. If that data is not feasible, the framework reframes hazard quantification through proxy using area characteristics. The first aspect of area characteris-

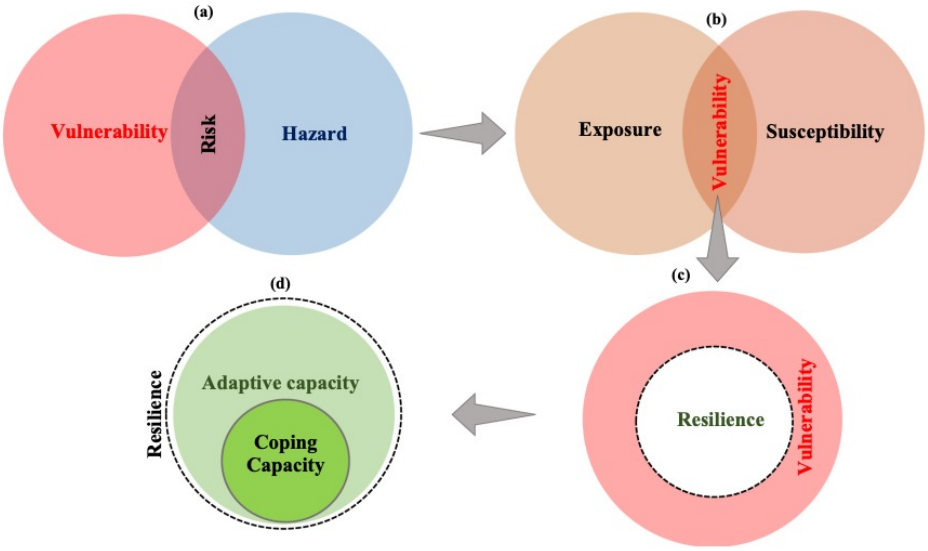


Figure 2.1: Integrated Risk Linkages (IRL) framework (Tabasi et al., 2025): a. Risk as a combination of vulnerability and hazard; b. Vulnerability is shaped by the intersection of exposure and susceptibility; c. Contribution of resilience in reducing vulnerability; d. Resilience consists of adaptive and coping capacities

tics, topographic condition, considers the physical features of the terrain such as slope and curvature. The second, physiographic condition, highlights geographical features of a region that helps in identifying prone areas to flooding such as land cover and distance to channel or river. This dual path allows the hazard side of the framework to be tailored to the level of data and modeling capacity available in a given case.

For susceptibility, IRL organizes criteria around the characteristics of exposed elements that influence their damage potential during floods. These include social (such as income, education, and employment), human (such as population density and sensitive groups), physical (such as building and infrastructure characteristics), and managerial (such as crisis management and policy implementation) aspects, detailed in Figure A.3. Tabasi acknowledged the difficulty in properly differentiating the criteria of vulnerability and susceptibility, along with susceptibility and exposure, as they overlap substantially in the literature. For this reason, the IRL hierarchy treats exposure and intrinsic vulnerability jointly as susceptibility in the operational structuers, while keeping vulnerability as a higher-level concept expressed through the intersection of susceptibility and resilience in the conceptual diagram. This choice aims to tackle one of the gaps that birthed IRL in the first place, a pragmatic decision to avoid double-counting similar criteria under multiple labels when building indicator sets, and to keep the hierarchical lists focused on measurable properties rather than on abstract vulnerability definitions.

Resilience in IRL is defined through coping and adaptive capacities. The resilience hierarchy, depicted in Figure A.3, distinguishes between the aspects of available resources (such as search and rescue, medical treatment, and psychosocial support) and management and planning (such as response and relief programs, task organization, and the use of lessons from past events). Tabasi et al. (2025) utilize both scientific literature and guidelines from crisis management organizations and the Sendai Framework, thus making resilience more operational while ensuring consistency with policy frameworks.

A distinguishing feature of IRL is its explicit adaptability. The hierarchical criteria lists for hazard, susceptibility, and resilience are not intended to be applied in full in every study. Instead, the framework encourages users to select subsets of criteria according to data availability, study objectives, and the scale of analyses, and to build alternative risk configurations with different levels of detail. In this thesis, IRL is therefore used as the guiding framework for structuring vulnerability domains, while the indicator selection in later sections and chapters draws selectively from its criteria hierarchies and from other literature, rather than exhausting the full catalog proposed by Tabasi et al. (2025). Hazard-side criteria from IRL are included primarily as contextual variables to describe the spatial distribution and intensity of the flood processes, and to be used as controls in subsequent spatial analyses. Resilience criteria, however, are not converted into spatially explicit indicators in this thesis due to data limitations and scale considerations. These are instead treated as part of the broader

interpretative context when discussing vulnerability patterns and typologies.

The full hierarchical criteria lists for hazard, susceptibility, and resilience that IRL proposes are provided in Appendix A rather than reproduced here in full. Table 2.1, presented later in this chapter, applies this hierarchy directly to the selected indicator set through its sub-component column, showing how each retained indicator maps onto the IRL structure introduced above.

2.2. Indicator Identification Process

In vulnerability studies, indicator selection processes are essential to drive research forward. Having established the conceptual framework and domains, this section describes the process by which vulnerability indicators were identified and refined for the comparative flood events considered in this thesis. Two complementary operationalization approaches are commonly distinguished, they are deductive and inductive.

2.2.1. Deductive and Inductive Approaches to Indicator Selection

A deductive strategy moves from general conceptual ideas and frameworks to specific indicator definitions. In this approach, the starting point is the chosen vulnerability framework and its domains. Indicators are then selected to represent each domain based on theory, prior empirical studies and data availability. An inductive strategy moves in the opposite direction, that it begins with a large set of observed indicators and uses statistical methods such as principal component analysis (PCA) to identify latent structures and groupings. These emergent components can then be interpreted as vulnerability dimensions and used to refine frameworks and indicator sets.

Inductive approaches are often preferred in single-region studies, as they adapt indicator groupings to local data structures and reveal context-specific vulnerability patterns (Hamidi et al., 2025). However, in comparative, multi-country settings, purely inductive strategies are challenging because differences in data types, quality and availability make cross-country comparability difficult. For this reason, this thesis adopts a hybrid approach. A deductively derived indicator set is first constructed that is conceptually consistent and comparable across the European flood events studied. Subsequently, inductive analyses such as PCA are applied within each case to explore how these indicators cluster and load locally, thereby capturing context-specific nuances without sacrificing comparability.

2.2.2. Two-phase Literature-based Indicator Identification

Indicator identification in this thesis follows two phases. The first phase is framework-led and literature-based. Recent systematic and scoping review papers on flood vulnerability indices and frameworks are used as starting points, as they already synthesize indicators and domains used across a wide range of studies (Hamidi et al., 2025; Moreira et al., 2021; Shehzad et al., 2026; Tabasi et al., 2025). These papers were identified through Scopus searches using combinations of terms ”flood” AND ”vulnerability” AND ”indicator*” AND (”index*” OR ”framework*”), restricted to publications after 2021, document type as Review, English-language publications, and unrestricted by region in their review. From these reviews, the thesis traces cited framework and index papers through snowballing and extracts indicators explicitly linked to flood vulnerability or risk, organizing them according to the IRL-informed domains described previously. Particular attention is paid to indicators that appear frequently across different studies and regions, and to those identified as central drivers of social or physical vulnerability in prior work. Additionally, the definition and expected effect on vulnerability are derived from snowballing the review papers.

The second phase refines this initial, cross-case indicator set using targeted, case-study-specific literature. For each of the four case study regions (Germany, Italy, Poland, and Spain), indicator-based flood vulnerability assessments are identified, with priority given to studies employing PCA or other multivariate methods. These studies were located using tailored search combinations of ”flood vulnerability” with country or region names and terms such as ”indicator*”, ”index*”, and (”principal component analysis” OR ”PCA”). From these studies, indicators with high loadings on principal components or repeated importance in local vulnerability indices are noted and compared with the foundational framework indicator list. In addition, event documentation and grey literature on the specific floods are consulted to highlight locally significant factors, such as land-use in Emilia-Romagna (Pulvirenti et al., 2024), road network damage in Valencia (Castro-Melgar et al., 2025), or the elderly population in the Ahr Valley (Rhein & Kreibich, 2025). These insights are used to confirm and, where necessary, introduce indicators that capture particular dynamics of each event. This combined approach allows indicators that are empirically influential in local contexts to be retained or elevated in the final list.

In parallel, recent reviews of social vulnerability to floods are consulted to identify indicators that are conceptually important yet under-represented in existing studies (Hamidi et al., 2025). Examples include health status, preparedness, social cohesion and certain dimensions of gender and minority status. These under-represented indicators are considered for inclusion to address gaps, even when the underlying data are not spatially explicit. In such cases, closely related indicators from the IRL framework or from locally derived indicator sets are used as proxies in the spatial analysis, while the original under-represented variables are retained in the discussion and interpretation results. This approach ensures that the indicator set does not focus solely on more readily available socio-economic and demographic variables, and that less visible dimensions of vulnerability do not dissipate in the analytical narrative even when they cannot be mapped directly.

2.2.3. Cross-Case Data Availability and Indicator Feasibility

Because the indicators identified in this chapter are subsequently operationalized as spatial variables in Chapter 3, data availability across all four flood events acts as a practical filter on the final indicator list. Indicators are retained in the core set only if suitable, comparable data sources can be identified for each case study, whether through census data, administrative datasets, remote sensing products or other geospatial sources. Indicators that are conceptually strong but lack consistent data for one or more events are either documented and excluded from the comparative analysis or, where possible, substituted with another variable that is theoretically similar and is available across all regions.

2.3. Literature-Derived Core Indicator Set

The outcome of the conceptual and operational steps described above is a structured taxonomy of flood vulnerability indicators derived from the literature. Indicators are grouped into domains and sub-domains consistent with the IRL framework, and each indicator is associated with a definition, typical measurement, and literature sources from which the indicator is selected and its expected effect is sourced. This taxonomy acts as the bridge between indicators from theory and data for the subsequent spatial analysis.

2.3.1. Core Indicator Set and Expected Effects

Table 2.1 lists the preliminaty indicators identified through the two-phase process, specifying for each its component, indicator name, typical measurement and unit, expected effect on vulnerability, and main literature sources. Indicators are organized in a hierarchy based on the IRL framework. At the highest level, Components reflect if the variable belongs to the hazard hierarchy or the susceptibility hierarchy. Within susceptibility, indicators are also defined to which aspect of susceptibility they belong. At the lowest level, individual indicators are named and subsequently defined to measurable quantities, such as percentage of population aged 65+, unemployment rate, road density, or distance to river.

2.3.2. Rationale for the Retained Indicator Set

The indicators in Table 2.1 were selected based on their recurrence in the literature, their empirical association with flood impacts, and their suitability for spatial operationalization in the four case study events. Hazard indicators, such as elevation, slope, distance to river and NDVI, describe the physical setting that shapes flood exposure and intensity. Susceptibility–physical indicators capture the characteristics of the built environment and infrastructure that influence damage potential, while susceptibility–social and –human indicators represent the socio-economic and demographic dimensions that affect coping capacity and the consequences of flooding for different groups.

The expected effect on vulnerability reported for each indicator summarizes how increases in the indicator value are hypothesized to influence flood vulnerability, informed by the cited frameworks and empirical studies. The publications depicted are a combination of justification for depiction, being either part of phase one or two of the indicator identification, and the expected effect toward vulnerability. The plurality of the sources are due to some review papers do not present the justification necessary for each indicator and rather only report on the frequency of the indicators, thus snowballing is necessary from said papers to the actual indicator study pertaining to the indicator mentioned so that the reasons are possible to be articulated.

In region-specific studies that employ PCA or factor analysis, indicators with high absolute loadings on well-interpreted components are treated as strong candidates for inclusion in the vulnerability indicator set. High loadings indicate that a variable contributes substantially to a latent dimension (for example, socio-economic disadvantage, demographic fragility) and thus captures an important aspect of local vulnerability structure.

However, PCA loadings are used in a complementary way alongside conceptual justification, as they inform prioritization among closely related indicators and the design of composite indices, but they are not interpreted as direct measures of association with flood impacts. The relationship between selected indicators and observed damage is evaluated separately in the spatial analyses.

Table 2.1 is deliberately not exhaustive, and two further considerations shaped which indicators were carried forward. First, indicators with strong, largely uncontested empirical support across the reviewed literature, such as literacy rate, were deprioritized in favor of indicators where evidence remains more limited, contested, or context-dependent, following the observation in several reviewed papers (Hamidi et al., 2025; Moreira et al., 2021) that well-established indicators are persistently reconfirmed rather than meaningfully re-tested, while a comparative, cross-country design such as this one is better positioned to add evidence on indicators whose role is less settled. Second, an initial sense of cross-country data plausibility, whether a given indicator could realistically be sourced for all four case studies, already informed which candidates were retained at this stage rather than left for exclusion during operationalization. Table 2.1 should therefore be read as a literature-grounded core set shaped by both theoretical relevance and anticipated feasibility, and the fuller, more granular indicator set actually operationalized in Chapter 3 builds on this core through the country-specific refinement process described above.

2.4. Conceptualizing and Measuring Flood Impact

Having established the indicator set used to represent flood vulnerability, this section turns to the outcome those indicators are validated against, the observed impact of the flood events themselves. Defining what ”impact” means, and what a given measurement of it can and cannot capture, is necessary before the indicator-impact relationship investigated in the subsequent chapters can be properly interpreted.

2.4.1. Dimensions of Flood Impact

Flood impact is not a single, uniformly measured quantity in the literature. Reviews of flood consequences typically distinguish several overlapping dimensions, including human impact, such as fatalities, injuries, and displacement (Doocy et al., 2013); economic impact, covering both direct losses to property and infrastructure and indirect losses from service disruption (Koks et al., 2019); infrastructural or physical impact, damage to buildings, transport networks, and utilities (Diakakis et al., 2020); and environmental impact, effects on ecosystems, agriculture, and water quality (Q. Yu et al., 2022). These dimensions are related but not interchangeable, a flood that causes extensive structural damage does not necessarily produce a comparable human or economic cost, and the reverse also holds, so the choice of which dimension to measure meaningfully shapes what conclusions can be drawn about vulnerability.

This thesis focuses on the infrastructural dimension, operationalized as building and infrastructure damage. This choice is made primarily on data availability grounds. Human impact data, such as casualty or displacement figures at fine spatial resolution, and economic loss data, are rarely available in a form that is both spatially explicit and consistently reported across national boundaries, whereas infrastructure damage assessments derived from remote sensing are produced through a comparable methodology for each of the four case study events, discussed further in Chapter 3.

2.4.2. Infrastructure Damage as a Proxy for Impact

Using infrastructure damage as the sole impact measure carries an implicit assumption, that the spatial pattern of structural damage is a reasonable proxy for the broader concept of flood impact referred to in the initial gap analysis. Infrastructure damage is a plausible proxy for several reasons. It is directly observable and comparably measured across countries, unlike survey-based or emergency-service-based impact measures, which vary substantially in coverage and methodology between national systems (Fekete et al., 2025; Kruspe et al., 2021; Moreira et al., 2021). It also captures a dimension of impact with a clear physical link to the built-environment and hazard indicators used elsewhere in this thesis, since structural damage is a direct consequence of water depth, velocity, and duration interacting with the built environment, in a way that is more difficult to establish for indirect economic loss or long-term social disruption. Flood severity classification schemes developed elsewhere similarly treat damage to the built environment as a distinct and load-bearing category within a broader impact taxonomy, rather than as an incomplete substitute for it (Diakakis et al., 2020).

At the same time, infrastructure damage does not capture the full range of what floods affect. It says nothing

directly about loss of life, injury, or psychological impact, nor about indirect economic consequences such as lost income or business interruption, both of which are widely treated as important, sometimes dominant, components of overall flood impact in the literature (Doocy et al., 2013; Q. Yu et al., 2022). It also cannot distinguish flood impact from the vulnerability conditions investigated as its explanatory variables, since a heavily built environment is both more likely to sustain damage and more likely to be assessed by remote sensing in the first place, an issue discussed further as a data limitation in Chapter 6. Infrastructure damage is therefore treated throughout this thesis as a partial, physically grounded proxy for flood impact, appropriate for the adopted comparative, cross-country design, rather than as a complete representation of impact in a comprehensive and exhaustive sense.

Table 2.1: Preliminary indicator set derived from literature.

Component	Sub-component	Indicator	Expected effect on vulnerability	Sources
Hazard	Physiographic condition	Normalized difference vegetation index (NDVI)	Lower vegetation cover increase exposure	(Pulvirenti et al., 2024; Tabasi et al., 2025; Taramelli et al., 2022)
Hazard	Physiographic condition	Distance to nearest river	Shorter distance increase flood exposure and damage	(Rincón et al., 2018; Tabasi et al., 2025; Taromideh et al., 2022)
Hazard	Physiographic condition	Height above nearest drainage (HAND)	A vertical version of distance to nearest river, higher HAND reduce flood exposure	(Purwanto et al., 2025; Rincón et al., 2018)
Hazard	Topographic condition	Elevation	Higher elevation reduces flood depth and potential damage	(Tabasi et al., 2025; Taromideh et al., 2022)
Hazard	Topographic condition	Slope	Steeper slopes lead to faster runoff and can increase flood hazard	(Tabasi et al., 2025; Taromideh et al., 2022)
Susceptibility–Physical	Transportation network	Road density	Higher density increases exposed assets, potential network disruption, and increase impervious surfaces	(Dong et al., 2020; Moreira et al., 2021; Taramelli et al., 2022; J. Yu et al., 2023)
Susceptibility–Physical	Urban facilities	Distance to nearest critical infrastructure (CI)	Greater distance may reduce emergency response capacity and increase vulnerability. CI is defined as hospitals, fire stations, and police stations	(Dong et al., 2020)
Susceptibility–Social	Income and economic capacity	% households below poverty line	Higher values expected to increase vulnerability due to reduced coping capacity	(Cutter et al., 2003; Houston et al., 2020)
Susceptibility–Social	Income and economic capacity	Income per household	Higher values expected to decrease vulnerability due to higher coping capacity and possible better zoning positioning	(Cutter et al., 2003; Hamidi et al., 2025)
Susceptibility–Social	Employment	Unemployment rate	Higher values expected to increase vulnerability due to lower coping capacity and lack of insurance	(Fekete, 2010; Moreira et al., 2021)
Susceptibility–Social	Employment	Women unemployment rate	Women may be more vulnerable due to family care responsibilities, higher values expected to increase vulnerability	(Cutter et al., 2003; Fekete, 2010; Hamidi et al., 2025)
Susceptibility–Social	Employment / social cohesion	Foreign unemployment rate	Representation of social cohesion, higher values expected to increase vulnerability	(Fekete, 2010; Hamidi et al., 2025)
Susceptibility–Human	Population density	Population density	Higher values increase exposed population and potential casualties	(Fekete, 2010; Hamidi et al., 2025; Moreira et al., 2021; Tabasi et al., 2025)
Susceptibility–Human	Population density	Persons per household	Higher values increase exposed population and potential casualties	(Fekete, 2010; Moreira et al., 2021)
Susceptibility–Human	Sensitive population	Elderly rate	Higher values expected to increase vulnerability due to mobility and health constraints	(Fekete, 2010; Hamidi et al., 2025; Moragues et al., 2025)

3

Study Area, Data, and Indicator Construction

This chapter describes the study areas, data sources, and database construction used to operationalize the indicators, derived from literature in the previous chapter. The focus is on how flood hazard, susceptibility, and impact variables are assembled and harmonized across the four European flood events.

3.1. Case Studies and Spatial Delineation

The study area for this thesis is built upon several constraints. This section details the deliberations that went into determining the scope of the spatial analysis within the selected case studies.

3.1.1. Regional Units and Spatial Resolution

The spatial analysis covers four recent European flood events introduced in Chapter 1, with each event affecting different parts of its respective region. To ensure a uniform methodological approach across countries in the European Union, Eurostat's NUTS (Nomenclature des Unités territoriales statistiques, Nomenclature of territorial units for statistics) system is used, as is often applied in socio-economic analyses in the region (Eurostat, 2024). The NUTS system segments countries into three hierarchical levels based on population, with NUTS 1 being the highest level and NUTS 3 the smallest segmentation. The data collection perspective and constraints are therefore viewed from a NUTS-level perspective.

The case selection encompasses the 2021 European floods in Ahr Valley, 2023 Emilia-Romagna floods in Italy, the 2024 Central European floods in southwestern Poland, and the 2024 Spanish floods in Valencia. As some events cover wider inundated areas than others, a uniform NUTS level is selected for consistency. Each event spans multiple NUTS 3 regions in each country, otherwise known as provinces in Italy and Spain, districts in Germany, and subregions in Poland. Among these, one NUTS 3 region is selected per event based on Copernicus activations, selecting the region with the highest documented impact. The final chosen NUTS-3 level regions are the Ahrweiler district in Germany, the Ravenna province in Italy, the Walbrzyski subregion in Poland, and the Valencia province in Spain. These NUTS 3 regions form the initial frame for data collection. However, due to subsequent processing of these regions and for ease of documentation, the segmentation of the case studies in this analysis will refer to them as their respective countries, which frames these study areas such as "The Germany Case" or "The Spain Case".

Within each NUTS 3 region, Local Administrative Units (LAU, municipalities) are used as the primary administrative units for socio-economic and census-based data. This choice is based on both data availability and the need to capture intra-regional heterogeneity in the vulnerability indicators. However, native spatial resolutions differ across countries and variables. Some indicators are available at municipality level, others at higher levels such as NUTS 2, and a few at finer resolutions such as census tracts, postcodes, or raster grids. These differences motivate the use of spatial disaggregation techniques, such as dasymetric mapping, and gridded representations to achieve a consistent analysis scale.

3.1.2. Impact-Based Study Area Delineation

Copernicus Emergency Management Service (EMS) grading products provide Areas of Interest (AOIs). AOIs are geometric polygons defined according to Service Request Forms and Copernicus guidelines, which favor populated places, avoid overlapping AOIs, enforce a minimum area of 10 km^2, and generally limit individual AOIs to single countries in border regions (Copernicus, 2024). AOIs delineate where detailed flood extent and damage mapping has been carried out.

Municipalities that intersect any grading AOI for a given event are identified and form the core impact-driven area. To avoid artificial boundaries around AOIs and to capture nearby municipalities that may share similar vulnerability conditions, a convex hull around impacted municipalities is used as an extension, and selected buffer municipalities are added. The convex hull provides the smallest convex polygon that encapsulates the set of impacted municipalities, resulting in a simple and contiguous boundary that is reproducible across countries. Alternative approaches based on arbitrary distance buffers, administrative adjacency rings, or alpha-shapes either require additional tuning parameters or can produce fragmented buffer regions, making cross-country comparison less transparent. This resulting study area is defined as AOI-intersecting and buffer municipalities within the selected NUTS 3 region.

3.1.3. Target Grid, Projection, and Population Filter

For each event, a target raster grid with 100 m resolution is defined within the study area boundary established above. This grid serves as the common spatial reference for hazard, susceptibility, and impact variables. All raster and vector data are projected to a common equal-area projection to support area-preserving comparisons across regions. This thesis uses the ESRI:54009 projection for cross-country comparison, as it preserves relative area across the continent, which is particularly important for indicator densities and subsequent area-based weighting procedures such as dasymetric mapping. Pre-existing rasters are clipped to the study area and resampled to the 100 m grid in later steps, as described in subsequent sections. The choice of 100 m resolution considers both computational feasibility and the need to capture local variation in infrastructure and population.

Because vulnerability studies typically focus on populated segments of a study area rather than uninhabited land (Cutter & Finch, 2008; Fekete, 2010; Moreira et al., 2021), the grid is further restricted to populated cells only. WorldPop population data, described in more detail in Section 3.2.1, is used for this filter since it provides a consistent raster surface across all four countries, minimizing bias that could arise from using country-specific population sources with differing definitions or resolutions.

This populated grid is in turn used to define two distinct analytical samples, since clustering and regression ask different questions of the data. Spatial clustering uses the full populated grid within the study area boundary, since its aim is to characterize the general vulnerability structure of the region regardless of whether a given cell was ultimately flooded. Spatial regression instead uses only the subset of the populated grid that falls within the observed flood event footprint, since its aim is to isolate the relationship between vulnerability indicators and flood damage specifically among cells that were actually exposed to flooding; including unflooded cells in this sample would otherwise conflate the physical determinants of flood occurrence with the socio-economic determinants of differential impact given exposure. This distinction, and its consequences for sample size and interpretation, is elaborated further in Chapter 4. Subsequent analysis may also shrink the focus to only the AOIs within a region to center on areas with documented damage.

3.1.4. Study Area Delineation and Analytical Samples

Figure 3.1 illustrates the resulting study area delineation for Germany, drawing together the administrative, impact-driven, and grid-based boundaries defined above. Panel (a) situates the selected NUTS 3 region within its NUTS 2 context, establishing the broader administrative hierarchy from which the case study region is drawn. Panel (b) shows the flood-affected core municipalities, the buffer municipalities added through the convex hull, the flood AOI, and the NUTS 3 boundary together, illustrating how the final study area boundary is constructed from these overlapping delineations. Panels (c) and (d) then show the two populated-grid samples introduced above, both outlined using the combined boundary of the core and buffer municipalities shown in panel (b) instead of the full NUTS 3 extent, so that the boundary drawn in the bottom row matches the study area actually defined in panel (b). Panel (c) shows the full populated grid, the sample used for spatial clustering. Panel (d) restricts this to populated cells within the observed flood footprint, the sample used for spatial regression.

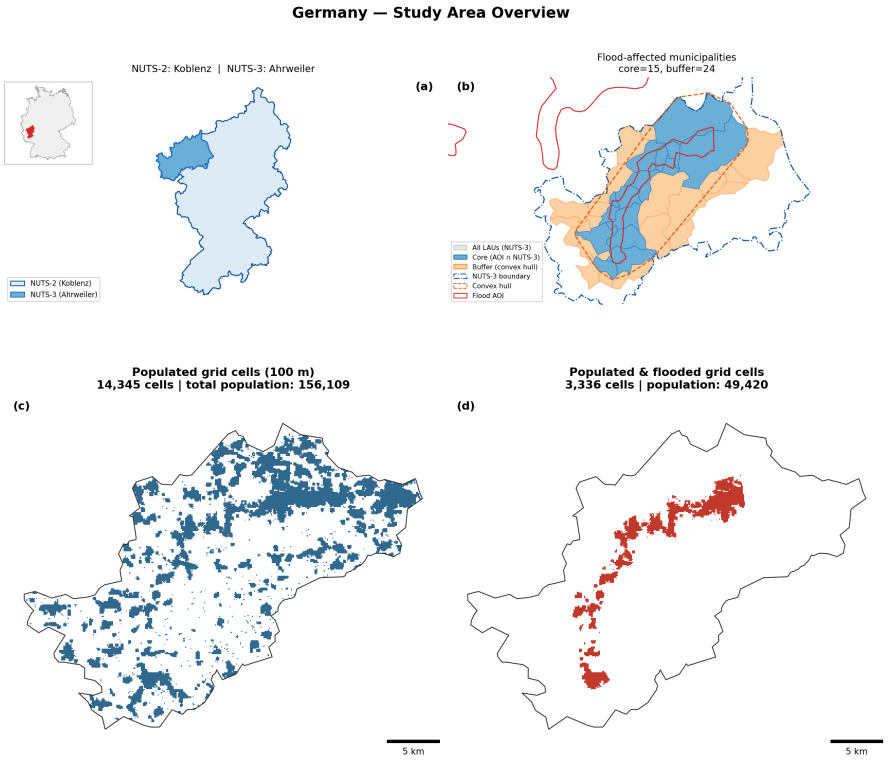


Figure 3.1: Study area delineation for Germany. (a) NUTS-2 region with the selected NUTS-3 subregion highlighted; (b) flood-affected core municipalities, buffer municipalities, flood AOI, and NUTS-3 boundary; (c) populated 100 m grid cells within the combined core and buffer boundary; (d) populated grid cells within the observed flood footprint.

The same four-panel structure is applied to the remaining three case studies, shown in Figures 3.2, 3.3, and 3.4. Each figure follows the identical panel layout described above, so only country-specific summary values are noted in the captions.

3.2. Data Sources

3.2.1. Sources for Hazard and Susceptibility Indicators

Indicators used in this thesis are sourced from a combination of global, pan-European, and national datasets. Hazard-related indicators are sourced primarily from Copernicus satellite products. Elevation and NDVI are taken directly from Copernicus Digital Elevation Model (DEM) (European Space Agency, 2022) and Sentinel-2 satellite data (Copernicus Land Monitoring Service, 2021), respectively. Indicators with relation to rivers such as HAND or distance to river are calculated or otherwise calibrated with EU-Hydro river data (European Environment Agency (EEA), 2019). The derivation and construction will be explained in the subsequent subsections.

Physical susceptibility data, related to road network and critical infrastructure, are sourced from OpenStreetMap (OSM), as it offers comprehensive mapping of infrastructure features (OpenStreetMap contributors, 2017). Additionally, built environment data is sourced from Copernicus Global Human Settlement (GHS) data (Pesaresi et al., 2024), as they provide both surface (GHS-Built-S) and volume (GHS-Built-V) of the built environment. These products provide information on building presence and estimated built volume at grid level, which is useful for describing urban structure in a fine spatial resolution.

Population and age-structure data are represented using WorldPop 100 m gridded datasets. WorldPop integrates national census and survey data, UN population estimates, and geospatial covariates to produce both unconstrained and constrained products. Unconstrained products distribute population across administrative units using spatial covariates, while constrained products additionally restrict population to building footprints and other built environments. Given the focus on infrastructure and built-up areas in flood impacts, the constrained WorldPop products are used as the baseline for population-related indicators.

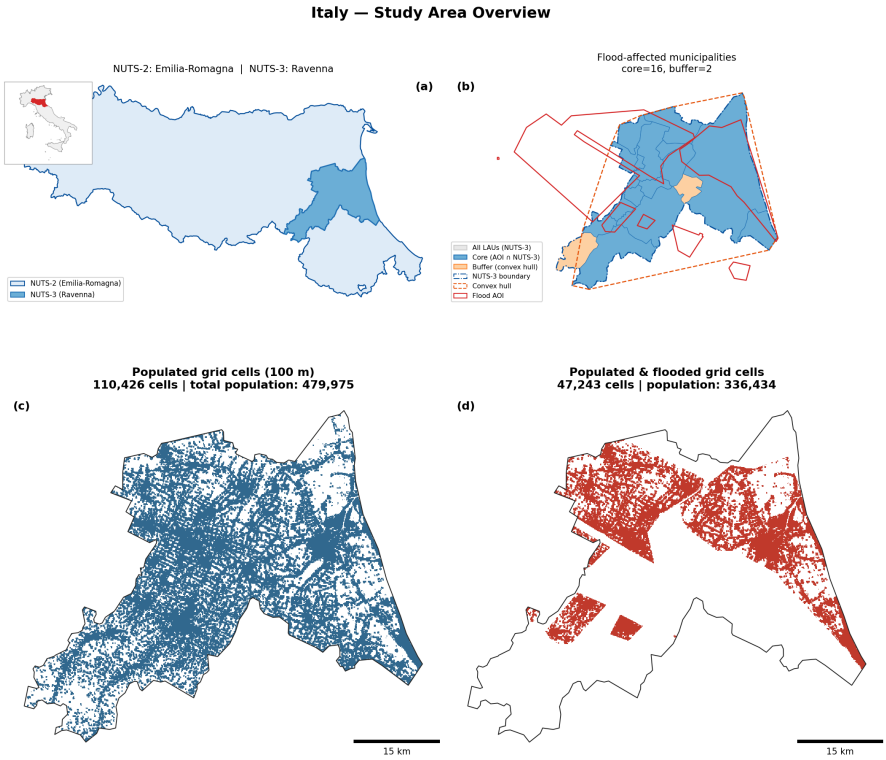


Figure 3.2: Study area delineation for Italy, following the same panel structure as Figure 3.1.

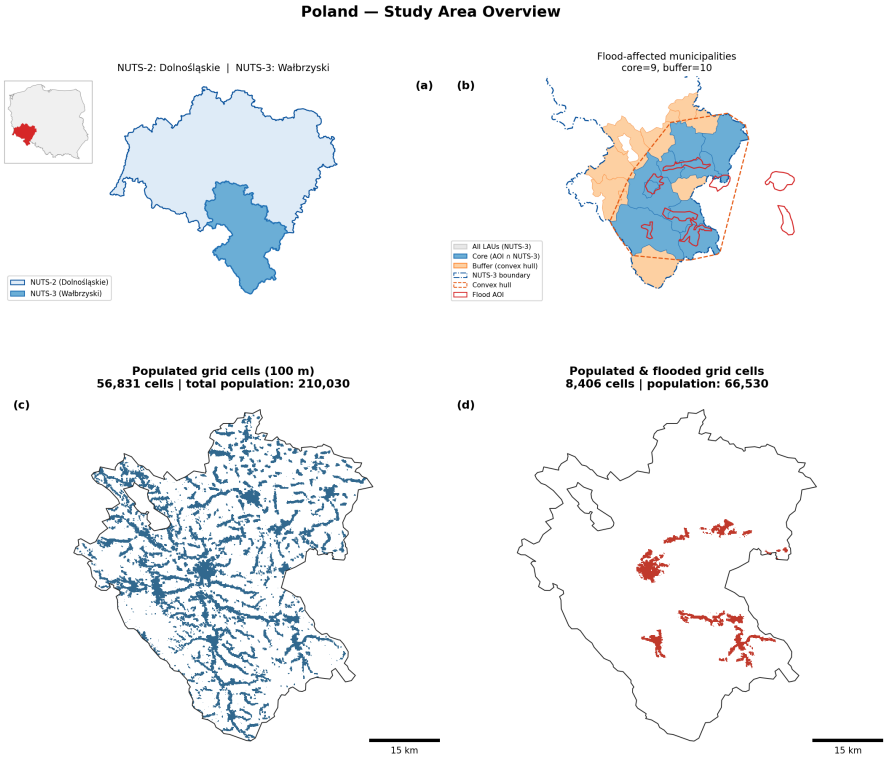


Figure 3.3: Study area delineation for Poland, following the same panel structure as Figure 3.1.

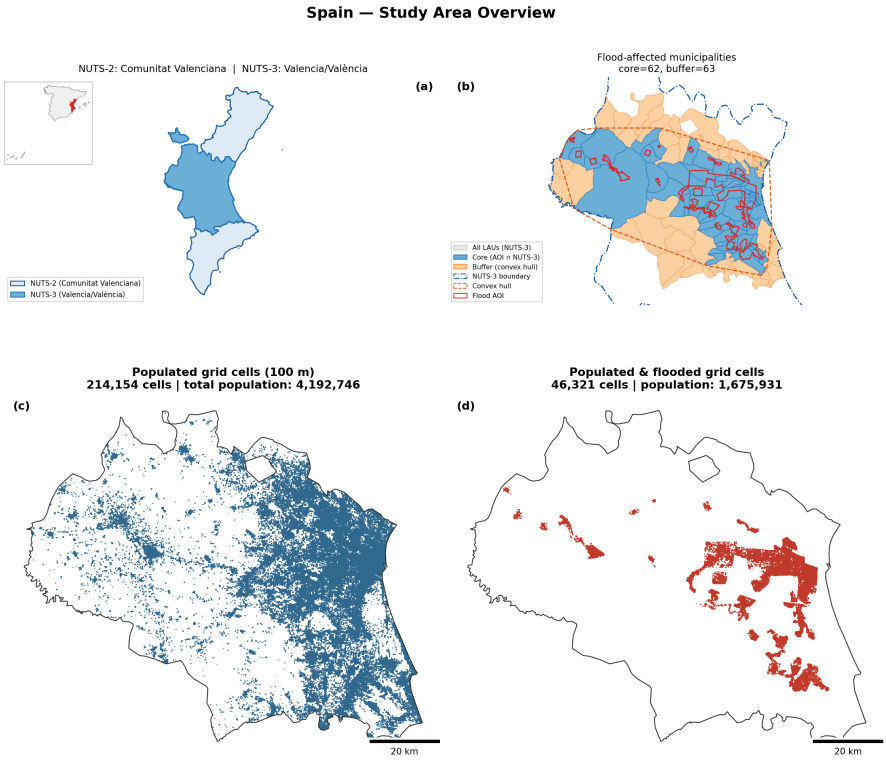


Figure 3.4: Study area delineation for Spain, following the same panel structure as Figure 3.1.

Most socio-economic and demographic indicators within the susceptibility component are derived from national censuses and statistical offices, which are INE (Instituto Nacional de Estadística, National Statistics Institute) for Spain, Destatis (Statistisches Bundesamt, Federal Statistical Office) for Germany, Istat (Istituto nazionale di statistica, National Institute of Statistics) for Italy, and GUS (Główny Urząd Statystyczny, Central Statistical Office) for Poland. As a result, the native spatial resolution and conceptual definitions of indicators vary between countries. The database that is used for these data are the IneAtlas for Spain (García Guzmán, 2026), Zensus 2022 (z22) for Germany (Lieth, 2026), GUS BDL (Bank Danych Lokalnych, Local Data Bank) for Poland (Statistics Poland, 2026), and Istat 2021 census for Italy (Istat, 2026).

Income data present specific challenges. Household-level income is rarely available directly in census releases, often due to privacy constraints, so additional sources are used. In Italy, an open data platform called Zornade aggregates information from Istat and Italy's MEF (Ministero dell'Economia e delle Finanze, Ministry of Economy and Finance), providing income variables in spatial formats. In Germany, the BBSR (Bundesinstitut für Bau-, Stadt- und Raumforschung, Federal Institute for Research on Building, Urban Affairs and Spatial Development) publishes the INKAR atlas (Indikatoren und Karten zur Raum- und Stadtentwicklung, Indicators and Maps for Spatial and Urban Development) which consolidates indicators from regional statistical offices and other providers, including income and labor market data at regional scales. Poland and Spain both provide income-related variables within their national statistical systems, though the concepts and units differ.

A preliminary inspection of the available indicators reveals noticeable differences in spatial resolution and units. For example, poverty rates in Poland are initially available at NUTS 2 level, while other socio-economic variables are reported at municipality or sub-municipal scales. These differences are addressed through intensive/extensive transformations and dasymetric mapping explained in subsequent sections.

3.2.2. Copernicus EMS Flood Extent and Damage Data

Flood impact data are sourced from Copernicus EMS activations for each event. Each activation includes delineation and grading products for relevant AOIs. Delineation products map flood extent, while grading products add classifications of observed damage to buildings, facilities and transport infrastructure. Grading products necessarily contain the extent information, but not all AOIs have grading layers if damage was minimal or unobserved. For this thesis, only AOIs with grading products are considered.

Grading datasets contain several thematic layers that consist of Area of Interest, Built-Up, Facilities, Observed Event A and P, and Transportation. Area of Interest defines the polygonal AOI as explained in the previous sections. Built-Up represents assessed building damage using point features located at building centroids. Facilities layers capture critical facilities in two forms, polygon features (A) represent large installations, and line features (L) represent linear infrastructure such as pipelines, electricity lines, and cables. Observed Event polygons delineate inundated areas, while point features represent discrete events. Transportation layers include transport-related polygons (for example, ports, airports) and lines (roads, railways).

The damage is assessed using satellite-derived remote sensing (European Commission, Joint Research Centre, 2020). The damage grading is segmented into classes which are No visible damage, Possibly damaged, Damaged, and Destroyed. These grading system of the thematic layers forms the basis for constructing impact variables in Section 3.3.5.

3.2.3. Administrative Boundaries and Spatial Reference Data

Administrative boundary data for NUTS and LAU units are obtained from Eurostat GISCO and national GIS portals. Most indicator datasets are distributed with associated geometries such as municipality, census tracts, or postcodes, while others provide only attribute information and require joining to external boundary layers by codes. All boundary datasets are projected to the common analysis projection and joined to the indicator dataset that has yet to have geometries.

3.2.4. Temporal Alignment of Data

The different sources of data in this thesis come from different reference years across indicators and countries for some. Where multiple vintages exist of the same resolution, the selection prioritizes the most recent data that still predate the respective flood events, to approximate pre-event vulnerability conditions.

In Germany, the 2022 census releases are preferred over older datasets such as the 2011 census, as they provide more up-to-date socio-economic and demographic information closer to the 2021 Ahr Valley floods. For Italy, the data consistently refers to the 2021 censuses. In Spain and Poland, different variables are drawn from 2021 and 2024 statistical releases, depending on when specific indicators (for example, poverty, income, labor market) are available in their finest spatial resolution form.

Administrative boundary layers are chosen to correspond to the reference years of the underlying data (for example, 2021 census variables are matched to 2021 boundaries, 2024 indicators to 2024 boundaries) and are then projected to the common analysis projection and intersected with the target grids. For defining the study area, the latest boundary limits that are prior to each flood event are used, so that vulnerability indicators are interpreted relative to the actual boundaries that existed when the floods occurred.

3.3. Data Harmonization and Indicator Construction

3.3.1. Variable Types and Spatial Representation

Susceptibility indicators taken from literature and data sources can be broadly classified as intensive variables (rates, proportions, densities), extensive variables (counts, totals) and denominators (population, households, area). Extensive variables can be redistributed across finer grids using dasymetric mapping, whereas intensive variables are typically treated as uniform within their source units. When extensive variables are attached to heterogeneous administrative units, their values may partly reflect differences in unit size as opposed to differences in underlying conditions, which can distort clustering and dimensionality reduction if such counts are used directly as inputs. This distinction remains relevant after disaggregation, but its interpretation changes once variables are expressed on a regular equal-area grid. On the 100 m grid, counts such as population or buildings per cell can be interpreted as local concentrations because each cell has the same spatial area. This makes them more suitable for comparative spatial analysis, including clustering and dimensionality reduction, than counts attached to irregular administrative units, where variation may partly reflect differences in unit size instead of underlying local conditions (Huang et al., 2020; Scheider & Huisjes, 2018).

In several cases, when the data is not granular enough, rate-based indicators from national statistics are converted into extensive form through multiplication with the appropriate denominators. For example, unemployment rates are transformed into counts of unemployed persons per unit, and poverty rates into counts of persons below poverty thresholds. These extensive indicators are then redistributed across the 100 m grid using ancillary data. When both forms are available in fine spatial formats, intensive variables are retained

for interpreting vulnerability patterns, as spatial analysis methods such as PCA are sensitive to values (Rufat, 2012), while extensive forms support spatial disaggregation. After disaggregation to the equal-area grid, count variables are also retained where relevant as measures of local exposure intensity. Denominators are stored to maintain transparency and support potential recomputation of rates at different aggregation levels.

3.3.2. Dasymetric Mapping and Ancillary Variables

Dasymetric mapping is used to disaggregate coarse socio-economic indicators to the 100 m grid. Previous studies highlight the advantages of dasymetric mapping over simple areal interpolation (Amadio et al., 2018; Bonnevie et al., 2024; Moos et al., 2021), especially when building footprints and land-use data are available as ancillary information, as they help confine population and socio-economic attributes to residential structures and urban blocks rather than spreading them across farmland and roads.

As previously mentioned, variables are segmented into intensive and extensive variables. Disaggregation is applied to extensive variables such as the number of people below poverty line, the number of unemployed, while intensive variables (for example, poverty rate, unemployment rate) are treated as uniform within their source polygons. This thesis adopts the WorldPop top-down constrained products as ancillary data. These products already incorporate building footprints, nighttime lights, and other covariates to distribute population at 100 m resolution, providing a spatially refined representation of where people reside. Extensive socio-economic indicators are redistributed across grid cells in proportion to WorldPop population counts, under the assumption that socio-economic attributes broadly follow population distribution at this scale.

Detailed validation procedures for the harmonized grid datasets are provided in Appendix F.

3.3.3. Derivation of Hazard and Susceptibility Indicators

Hazard Indicators

Hazard indicators are constructed from DEM, satellite-based vegetation products, Copernicus flood layers and river or drainage networks. Elevation is taken from DEM data and resampled to the 100 m target grid. Slope is derived from the resampled DEM using standard gradient operators. Height Above Nearest Drainage (HAND) is computed from the DEM by delineating flow directions and accumulation, identifying drainage lines, and then calculating the vertical difference between each grid cell and its nearest drainage cell. The HAND thresholds are checked against EU-Hydro river networks to ensure that the resulting drainage pattern is consistent with mapped rivers. NDVI describes vegetation and surface characteristics that influence runoff and infiltration, and is derived from Sentinel-2 imagery and resampled to the target grid. Distance to river is calculated from grid-cell centroids to the nearest drainage or river line from the EU-Hydro database.

Physical Susceptibility Indicators

Physical susceptibility indicators describe the built environment and infrastructure. Road density is computed as total road length per km^2 within grid cells or aggregation units. Distance to primary road is derived from OSM tags such as `motorway`, `trunk`, `primary` and their associated links, capturing proximity to major transport corridors. Distance to nearest critical infrastructure is calculated from grid centroids to the closest facility tagged as hospitals, clinics, fire departments, police stations or ambulance stations. Building footprint density from GHS-Built-S and GHS-Built-V provides additional measures of structural concentration.

Social and Human Susceptibility Indicators

Social susceptibility indicators encompass poverty, income, unemployment and household characteristics. Poverty counts and rates, income per household, total and subgroup unemployment, education levels and household composition indicators are harmonized conceptually across countries and, where necessary, disaggregated to the grid. Human susceptibility indicators focus on population density, persons per household and age structure, including elderly and youth shares and dependency ratios, constructed from census and WorldPop data.

Income and poverty indicators differ across countries in terms of underlying concepts and units. Mean income variables typically capture average disposable income at household or person level, while median indicators in some cases refer to labor earnings or taxable income instead of full household income. Poverty measures range from shares of social assistance recipients to shares of taxpayers below a fixed taxable threshold, or shares of individuals with equivalised net income below 60% of the national median. These indicators are interpreted as approximate, country-specific proxies for economic resources and hardship rather than fully

harmonized measures, and they are treated as capturing relative economic capacity and deprivation within each case study.

When constructing the indicators, the initial list derived from the literature is adjusted to reflect what can be measured with the available data. Some indicators cannot be implemented as originally defined because the required variables are missing, restricted or only available for a subset of countries. In these situations, the indicator definition is preserved at a conceptual level, but operationalization relies on a proxy that is available across all case study regions. A typical example is the replacement of “number of unemployed foreign residents” with “number of foreign residents” where unemployment by nationality is not consistently reported. These substitutions are treated as approximations and are made explicit in the final indicator table.

3.3.4. Operationalized Indicator Set

After harmonization and construction, the final indicator table consolidates hazard and susceptibility variables that are operationalized as 100 m grid-level indicators across all case studies. Each indicator is listed with its component (hazard or susceptibility domain), short name, measurement unit, expected effect on vulnerability, and key sources. This table provides the direct link between the conceptual indicators identified in the previous chapter and the geospatial variables used in the spatial analysis methods in the next chapter.

3.3.5. Construction of Flood Impact Variables

Impact variables are derived from Copernicus EMS grading layers. As mentioned in the previous subsections, the classes of damage grading that Copernicus uses span No visible damage, Possibly damaged, Damaged, and Destroyed. While most of them are related to the severity of the destruction observed, Possibly damaged acts as an exception, as it refers to cases where the confidence level of the interpretation is slightly lower due to issues such as image quality (European Commission, Joint Research Centre, 2020). However, this thesis proceeds with the assumption of an ordinal scale among these grades. As such, damage grades are coded as 1 (possibly damaged), 2 (damaged), and 3 (destroyed).

The graded structure used by Copernicus is consistent with how damage severity is represented elsewhere in the flood impact literature. Severity scales developed for classifying built-environment impacts, for instance, are explicitly constructed as ordered classes running from minor to catastrophic, instead of an unordered set of categories or a directly measured continuous quantity, precisely because damage severity is judged relative to a known, ranked progression of physical states (Diakakis et al., 2020). Treating the combined damage measure used in this thesis as ordinal, in preference to a simple count or a binary presence measure, preserves this ranked structure and is consistent with prior impact-based approaches in the vulnerability literature (Houston et al., 2020).

A combined damage intensity indicator per 100 m grid cell, combined_dmg_num, is constructed by summing the maximum ordinal damage grades observed for built-up areas, facilities, and transport, reflecting the combined severity of physical impacts on structures and infrastructure within each cell, resulting in a range of 0 for non-damaged and 9 when all three infrastructure types are destroyed. This process is reflective of existing impact-based research within the flood vulnerability sphere (Houston et al., 2020). Additionally, combined_dmg_num treats NaN or unreported damage, including no visible damage, as zero under the assumption that areas without reported damage are undamaged.

Additional impact variables are defined to support alternative analyses and visualizations. combined_dmg_binary identifies whether any damage is present in a grid cell and combined_dmg_raw preserves original NaN values from Copernicus. For clustering and regression, combined_dmg_num is also categorized into ”none”, “low”, and “high” damage brackets in a combined_dmg_num_bracket variable based on natural breaks, using the Jenks method, providing a simplified representation of impact intensity. This bracket column splits the damage between 0 as none, 1-2 as low, and 3 and above as high.

Copernicus EMS grading products offer systematically interpreted, event-specific information on observed physical damage to buildings and infrastructure. While they do not capture all dimensions of flood impact, such as spatially detailed economic loss, affected population, or long-term social consequences, they provide consistent, spatially explicit damage assessments across the case studies. Using combined damage indicators at 100 m resolution therefore provides a pragmatic proxy for direct physical flood impacts that is suitable for evaluating literature-derived vulnerability indicators in the spatial analysis chapters.

Table 3.1: Final operationalized indicator set, expanded from Table 2.1, including extensive/intensive variants of applicable indicators. Country-specific abbreviations are DE = Germany, IT = Italy, PL = Poland, ES = Spain.

Component	Indicator (intensive / extensive)	Variable name	Data sources (country)	Additional notes (substitution / justification)
Hazard	NDVI (I)	ndvi	Copernicus NDVI 2021	-
Hazard	Elevation (masl) (I)	dem_m	Copernicus DEM 2011	-
Hazard	Slope (I)	slope	Copernicus DEM 2011	-
Hazard	Distance to nearest river (I)	dist_river_m	Copernicus DEM 2011, EU-Hydro (2020)	-
Hazard	HAND (I)	hand_m	Copernicus DEM 2011, EU-Hydro (2020)	-
Susceptibility–Physical	Building footprint volume (E)	built_volume	Copernicus GHSL (GHS-BUILT-V)	As proxy for population density and for dasymetric mapping (Hidayah et al., 2021)
Susceptibility–Physical	Building footprint surface (E)	built_surface	Copernicus GHSL (GHS-BUILT-S)	As proxy for population density (Hidayah et al., 2021)
Susceptibility–Physical	Road density (I)	road_density_m_per_km2	OpenStreetMap / OSMnx (pre-flood query)	-
Susceptibility–Physical	Distance to nearest arterial/primary road (I)	dist_nearest_primary_road_m	OpenStreetMap / OSMnx (pre-flood query)	As proxy for accessibility from rural or remote areas (European Commission, Joint Research Centre, 2023)
Susceptibility–Physical	Distance to nearest CI (I)	dist_nearest_critical_infra_m	OpenStreetMap / OSMnx (pre-flood query)	Includes hospitals, fire departments, police stations
Susceptibility–Human	Persons per household (I)	persons_per_household	z22 2022 (DE), Istat 2021 (IT), GUS BDL 2021 (PL), IneAtlas 2021 (ES)	Used as count-based companion to household-size indicators; to gain spatial granularity
Susceptibility–Human	Number of foreigners over population (I)	foreign_share	z22 2022 (DE), Istat 2021 (IT), GUS BDL 2021 (PL), IneAtlas 2021 (ES)	Substitute foreign unemployment rate (Fekete, 2010; Hamidi et al., 2025)
Susceptibility–Human	Number of foreigners (E)	foreign_total	z22 2022 (DE), Istat 2021 (IT), GUS BDL 2021 (PL), IneAtlas 2021 (ES)	Substitute foreign unemployment rate (Fekete, 2010; Hamidi et al., 2025); to gain granularity
Susceptibility–Human	Women over population (I)	women_per_pop	INKAR 2021 (DE), Istat 2021 (IT), GUS BDL 2021 (PL), IneAtlas 2021 (ES)	Substitute for female unemployment rate (Cutter et al., 2003; Fekete, 2010; Hamidi et al., 2025)
Susceptibility–Human	Women count (E)	women_count	INKAR 2021 (DE), Istat 2021 (IT), GUS BDL 2021 (PL), IneAtlas 2021 (ES)	To gain spatial granularity for gender composition
Susceptibility–Human	Dependency rate (I)	age_dependency_rate	WorldPop 2020 (DE), 2022 (IT), 2023 (PL, ES)	Combines elderly and youth rate in one indicator (Fekete, 2010; Hamidi et al., 2025; Moragues et al., 2025)
Susceptibility–Human	Elderly rate (65+ over population) (I)	elderly_rate	WorldPop 2020 (DE), 2022 (IT), 2023 (PL, ES)	-
Susceptibility–Human	Elderly count (65+ years) (E)	age_65_plus	WorldPop 2020 (DE), 2022 (IT), 2023 (PL, ES)	To gain spatial granularity
Susceptibility–Human	Youth rate (<15 over population) (I)	youth_rate	WorldPop 2020 (DE), 2022 (IT), 2023 (PL, ES)	Substitute for people with special needs
Susceptibility–Human	Youth count (<15 years) (E)	age_under_15	WorldPop 2020 (DE), 2022 (IT), 2023 (PL, ES)	To gain spatial granularity
Susceptibility–Social	Income per household (I)	income_mean_hh	INKAR 2021 (DE), MEF/Zornade 2021 (IT), GUS BDL 2021 (PL), IneAtlas 2023 (ES)	-
Susceptibility–Social	Income total (E)	income_total	INKAR 2021 (DE), MEF/Zornade 2021 (IT), GUS BDL 2021 (PL), IneAtlas 2023 (ES)	To gain spatial granularity
Susceptibility–Social	Number of people below poverty line (E)	poverty_count	INKAR 2021 / z22 2022 (DE), MEF/Zornade 2021 (IT), GUS BDL 2024 (PL), IneAtlas 2023 (ES)	Substitute for poverty rate where the rate is too coarse
Susceptibility–Social	Employed people over population (I)	employment_rate_total	INKAR 2021 (DE), Istat 2021 (IT), GUS BDL 2021 (PL), IneAtlas 2021 (ES)	Substitute for unemployment rate
Susceptibility–Social	Employed people (E)	employed_persons_total	INKAR 2021 (DE), Istat 2021 (IT), GUS BDL 2021 (PL), IneAtlas 2021 (ES)	To gain spatial granularity
Susceptibility–Social	Low education (count, lower than lower secondary) (E)	edu_low_comp_count	z22 2022 (DE), Istat 2021 (IT), GUS BDL 2024 (PL), IneAtlas 2023 (ES)	Proxy for illiteracy (Moreira et al., 2021; Tabasi et al., 2025)
Susceptibility–Social	Single-person households (E)	hh_1_person_count	z22 2022 (DE), MEF/Zornade 2021 (IT), GUS BDL 2021 (PL), IneAtlas 2023 (ES)	Proxy for social isolation, often underrepresented (Hamidi et al., 2025)
Susceptibility–Social	High education (count, tertiary) (E)	edu_high_comp_count	z22 2022 (DE), Istat 2021 (IT), GUS BDL 2024 (PL), IneAtlas 2021 (ES)	Adds an education dimension to vulnerability (Fekete, 2010; Hamidi et al., 2025)

4

Spatial Analysis Methods

This chapter describes the spatial analysis methods used to examine the relationship between the vulnerability indicators constructed in the previous chapter and the observed flood impacts. The same sequence is applied to each case study region. The analyses are conducted separately for each region, which means that the number and composition of the kept indicators differs across countries, and this shapes the specific list of variables that enters each subsequent step.

4.1. Analytical Workflow and Indicator Screening

The analytical workflow begins with dimensionality reduction to address redundancy among indicators, then identifies spatial typologies through spatial clustering, and finally estimates the relationship between selected indicators and flood damage through spatial regression. Before this sequence begins, each indicator is screened for meaningful spatial variation. Variables that show little variation across the study area, or that are too sparse to provide interpretable spatial patterns, indicated by a share of non-null, non-zero grid cells below a chosen threshold, are flagged for removal or reformulation. This screening step does not determine indicator relevance on its own, but it helps ensure that only variables capable of contributing meaningfully to clustering and regression are carried forward. Screening was informed by choropleth mapping of each indicator, provided in full in Appendix B; the resulting screened indicator set is reported in Chapter 5.

This sequence is chosen because each method answers a different analytical requisite. Dimensionality reduction limits overlap between closely related indicators. Clustering identifies recurring combinations of conditions in space, while regression estimates the strength and direction of relationships with observed impacts. All analyses are implemented in Python through Jupyter Notebooks, which provide a transparent and reproducible environment for data processing, model estimation, and visual inspection of intermediate outputs.

4.2. Blockwise Principal Component Analysis

Dimensionality reduction is applied before typology construction and regression modeling. Since the indicator set is assembled from multiple sources and conceptual domains, several variables are expected to measure closely related processes. Leaving all of these variables unchanged would risk redundancy, reduce interpretability, and potentially introduce multicollinearity in the later stages of the analysis.

4.2.1. Rationale for Blockwise PCA

Principal Component Analysis (PCA) is used to reduce the number of variables, but this comes with a constraint. A global PCA would compress the full dataset into a small number of principal components (PCs), which would make it difficult to preserve the specific conceptual content of the vulnerability domains. Since the aim of the thesis is to identify spatial typologies of vulnerability rather than to replace the full indicator system with a few abstract axes, PCA is required to maintain some level of granularity in the resulting indicators.

4.2.2. Principal Component Extraction and Retention

Given a set of standardized indicators $Z = \{z_1, z_2, \ldots, z_p\}$, each with zero mean and unit variance, PCA finds a set of orthogonal linear combinations of these variables, the principal components, that successively capture the maximum remaining variance in the data (Jolliffe & Cadima, 2016). Formally, this is solved through the eigendecomposition of the correlation matrix R of Z

$$Rv_i = \lambda_i v_i$$

where v_i is the i-th eigenvector and λ_i its corresponding eigenvalue. Each principal component is then constructed as $PC_i = Zv_i$, a linear combination of the original variables weighted by the eigenvector, and the i-th component explains a share of the total variance equal to $\lambda_i / \sum_{j=1}^{p} \lambda_j$. Components are ordered so that PC_1 explains the most variance, PC_2 the second most subject to being uncorrelated with PC_1, and so on. In practice, only enough components are retained to explain a chosen share of total variance, so that the smallest set of components satisfying

$$\sum_{i=1}^{m} \lambda_i \Big/ \sum_{i=1}^{p} \lambda_i \geq \tau$$

is kept, where τ is a chosen variance threshold and $m \leq p$ is the resulting number of retained components. This thesis uses $\tau = 0.8$, so that retained components jointly explain at least 80% of the variance within each block.

There are two possible ways to implement PCA under this variance-retention constraint. The first, adopted by Tate et al. (2025) in constructing social vulnerability profiles, computes a zero-order correlation matrix within thematic groups of indicators, defined in that study as components such as hazard or human susceptibility, and then runs PCA on the remaining indicators, retaining a fixed number of PCs (seven in their case) for clustering. The second option uses clustering as the primary determinant of which variables enter PCA. In this approach, variables are first grouped into blocks, which are then passed into the PCA algorithm. Blocks can be defined either by proximity in the spatial-temporal space, often used in image processing (Nishino et al., 2005), or by correlation, as in Park et al. (2020) for multi-omics data.

The approach chosen here combines these ideas. The indicator set is initially split into previously-defined components to ensure a fair representation of vulnerability. Given the relatively low number of indicators, this split is simplified to hazard and susceptibility, rather than more detailed categories such as physical, social, and human susceptibility. Following Rufat (2012), who notes that PCA performs better on rate variables than on raw counts, the components are further divided into extensive and intensive variables. Although extensive variables have already been transformed to an area-based grid resolution, remaining differences in scale may still affect PCA behavior, so this additional split is introduced before applying blockwise PCA.

4.2.3. Correlation-Based Indicator Blocks

The block-formation step is a variable-grouping procedure where pairwise association between indicators is assessed using Spearman's rank correlation coefficient, which measures the strength and direction of monotonic relationships based on ranked values. This is appropriate for the indicator set because several variables are skewed, sparse, or derived from counts and therefore may not satisfy the assumptions associated with Pearson correlation. Each pair of indicators z_i and z_j is assigned a dissimilarity

$$d(z_i, z_j) = 1 - |\rho_{ij}|$$

where ρ_{ij} is Spearman's rank correlation coefficient. Variables are grouped into a block when their absolute rank correlation exceeds the selected threshold, $|\rho_{ij}| \geq \rho^*$. This thesis uses $\rho^* = 0.9$. PCA is then applied to the standardized original variable values within each resulting block. Variables that do not belong to a correlated block are retained as singletons. The reduced dataset is then carried forward to clustering and regression.

4.3. Spatial Clustering of Vulnerability Typologies

Spatial clustering is used to identify recurring indicator typologies in space. This spatial analysis is used to identify to what extent flood vulnerability characteristics cluster with actual flood impact zones. The purpose of this step is to group grid cells that share similar combinations of susceptibility and hazard characteristics and to examine whether particular types of clusters are more often associated with observed flood damage. In this way, spatial clustering supports the identification of place-based vulnerability profiles rather than only variable-by-variable relationships. The clustering procedure is applied to the reduced dataset obtained from the previous stage, and the resulting typologies are visualized spatially. The selected indicators and principal components are standardized to zero mean and unit variance before being used as input for the clustering algorithm, so that no single variable dominates the distance calculation due to differences in scale.

4.3.1. Selection of K-Means Clustering

Clustering algorithms themselves can take several forms. Saxena et al. (2017) distinguishes two methods of clustering, which are hierarchical clustering and partitional clustering. Given a set of standardized grid cell observations $X = \{x_1, x_2, \ldots, x_n\}$, where each $x_i \in \mathbb{R}^p$ represents a grid cell described by p indicators, both methods aim to partition X into a set of k clusters $C = \{C_1, C_2, \ldots, C_k\}$, such that observations within a cluster are more similar to each other than to observations in other clusters. The two methods differ in how this partition is actually constructed.

Hierarchical clustering builds clusters in a stepwise, agglomerative or divisive fashion. For an agglomerative approach, it begins with each observation as its own cluster and successively merges the two closest clusters until a single cluster remains, producing a dendrogram. A divisive approach reverses this process. All observations initially belong to a single cluster, which is then divided into progressively smaller clusters. These processes require a linkage criterion to define the distance between clusters. A common choice, and the one used in the typology literature this thesis draws on (Rufat, 2012; Tate et al., 2025), is Ward's method, an agglomerative hierarchical clustering which merges the pair of clusters C_i and C_j that minimizes the resulting increase in the total within-cluster sum of squares

$$\Delta(C_i, C_j) = \sum_{x \in C_i \cup C_j} \|x - \bar{c}_{ij}\|^2 - \sum_{x \in C_i} \|x - \bar{c}_i\|^2 - \sum_{x \in C_j} \|x - \bar{c}_j\|^2$$

where $\bar{c}_i$, $\bar{c}_j$, and $\bar{c}_{ij}$ are the centroids (or the arithmetic mean of the points in the cluster) of C_i, C_j, and their union, respectively (Murtagh & Legendre, 2014). Ward's method aims for low within-cluster variability and high between-cluster variability at each merge, and it does not require a predefined k to run, since the dendrogram can be cut at any level to yield a different number of clusters after the process. However, this flexibility comes at a computational cost (Yin et al., 2026). Agglomerative hierarchical clustering requires computing and updating a full pairwise distance matrix across all n observations, giving a time complexity of $O(n^2 \log n)$ and a memory complexity of $O(n^2)$ for typical implementations. This becomes prohibitive at the grid resolution and case study extents used in this thesis, where the number of observations ranges from several hundred to over ten thousand cells per region.

By contrast, partition-based clustering directly divides the data into a preset number of clusters acting as cluster centroids, and therefore requires the number of clusters, k, to be specified before running the algorithm. K-means, the partition-based method used here, seeks the assignment of observations to clusters that minimizes the total within-cluster sum of squares

$$\arg\min_{C} \sum_{i=1}^{k} \sum_{x \in C_i} \|x - \mu_i\|^2$$

where μ_i is the centroid of cluster C_i. This is solved iteratively through Lloyd's algorithm (Lloyd, 1982). Cluster centroids are initialized, each observation is assigned to its nearest centroid, centroids are recomputed as the mean of their assigned observations, and this process repeats until assignments stabilize. Each iteration has a time complexity of $O(nkp)$, which is substantially cheaper than hierarchical clustering's pairwise distance computation and makes k-means manageable at the scale of the grid-based dataset used in this thesis. The trade-off is that k-means requires k to be specified in advance, and its Euclidean distance objective assumes

clusters are roughly spherical and similarly sized, an assumption hierarchical clustering with Ward's method also shares but that neither method fully escapes (Saxena et al., 2017).

Given this computational constraint, the thesis proceeds with partition-based k-means clustering rather than hierarchical clustering, following common practice in vulnerability typology work at similar sample sizes where the cost of pairwise hierarchical methods becomes difficult to justify.

Beyond k-means, other partition-based methods exist and are worth considering briefly. K-medoids, also known as Partitioning Around Medoids (PAM), follows a similar logic to k-means but replaces the mean-based centroid with a medoid, an actual observation from the dataset chosen to minimize total distance to the other members of its cluster (Kaufman & Rousseeuw, 1990). This makes k-medoids more robust to outliers, since a mean can be pulled away from the bulk of a cluster by a single extreme observation, while a medoid always remains a genuine data point. This thesis keeps outliers in the indicator set instead of removing them. An unusually high value on a susceptibility or hazard indicator often marks the kind of extreme condition the typology is meant to capture, so trimming it away would blunt the analysis instead of cleaning it up. K-medoids' resistance to outliers therefore offers little practical benefit, since those extreme values are being kept on purpose. K-medoids also requires evaluating pairwise distances across all candidate medoids at each iteration, giving it a computational cost closer to hierarchical clustering than to k-means, which reintroduces the same scalability concern raised above.

Gaussian Mixture Models (GMM) offer a different kind of flexibility. Rather than assigning each observation to exactly one cluster, GMM treats the data as generated from a mixture of Gaussian distributions and assigns each observation a probability of belonging to each cluster, fitted through the Expectation-Maximization algorithm (Reynolds, 2009). This relaxes the assumption that clusters are spherical and similarly sized, since each Gaussian component has its own covariance structure. Since the indicators used in this thesis are standardized before clustering, the added flexibility of GMM is less critical than it would be for raw, differently-scaled variables, and the additional complexity of fitting and validating a mixture model was judged not to be proportionate to the benefit for this application.

Given these trade-offs, k-means remains the most suitable partition-based method for this thesis, as a balance of computational feasibility and a standardized input space to reduce the impact of its underlying spherical-cluster assumption.

Since k is not determined internally by k-means, it has to be tuned externally. This thesis uses four complementary diagnostics combined into a single composite ranking.

The first is the elbow or inertia method, which examines the within-cluster sum of squares as a function of k and looks for the point where additional clusters stop reducing this value meaningfully. The second is the silhouette score (Rousseeuw, 1987), which for each observation x compares its mean distance to other points in its own cluster, $a(x)$, against its mean distance to points in the next-nearest cluster, $b(x)$

$$s(x) = \frac{b(x) - a(x)}{\max\{a(x), b(x)\}}$$

where $s(x) \in [-1, 1]$, with values closer to 1 indicating that x is well matched to its own cluster and poorly matched to neighboring clusters. Averaged across all observations, the silhouette score gives a single measure of cluster cohesion and separation for a given k.

The third and fourth diagnostics are the Calinski-Harabasz index (Caliński & Harabasz, 1974) and the Davies-Bouldin index (Davies & Bouldin, 1979), both of which summarize cluster quality across the entire partition rather than per observation. The Calinski-Harabasz index compares between-cluster dispersion to within-cluster dispersion

$$CH(k) = \frac{\mathrm{tr}(B_k)}{\mathrm{tr}(W_k)} \cdot \frac{n - k}{k - 1}$$

where $\mathrm{tr}(B_k)$ is the trace of the between-cluster dispersion matrix, $\mathrm{tr}(W_k)$ is the trace of the within-cluster dispersion matrix, and n is the total number of observations. Higher values indicate clusters that are dense

and well separated, so the value of k that maximizes $CH(k)$ is preferred. The Davies-Bouldin index instead measures, for each cluster C_i, the worst-case similarity to any other cluster

$$DB(k) = \frac{1}{k} \sum_{i=1}^{k} \max_{j \neq i} \left(\frac{\sigma_i + \sigma_j}{d(\mu_i, \mu_j)} \right)$$

where σ_i is the average distance of points in C_i to their centroid μ_i, and $d(\mu_i, \mu_j)$ is the distance between the centroids of clusters C_i and C_j. Lower values indicate more compact, well-separated clusters, so the value of k that minimizes $DB(k)$ is preferred.

4.3.2. Selection of the Number of Clusters

Because the elbow method, silhouette score, Calinski-Harabasz index, and Davies-Bouldin index can each favor a different value of k, this thesis follows practice similar to consensus-based cluster validation tools such as NbClust (Charrad et al., 2014), which combine multiple internal validation indices rather than relying on a single one. The elbow method is treated separately from the remaining three diagnostics in the composite score below, since the inertia decreases monotonically with k and therefore has no true optimum to be rescaled, it instead serves as an initial qualitative check on the plausible range of k before the composite score is computed. The silhouette, Calinski-Harabasz, and Davies-Bouldin scores are each rescaled to a common 0 to 1 range across the tested values of k, with the Davies-Bouldin scale inverted so that higher values consistently indicate better performance across all three indices. These rescaled scores are then averaged into a single composite score for each k, and the value of k with the highest composite score is selected. This reduces the risk of choosing k based on a single diagnostic that happens to favor an atypical or unstable partition.

4.3.3. Identification of Impact-Prone Typologies

The resulting clusters represent different combinations of conditions within the study area. These typologies are then compared against the mapped damage variables by overlaying the cluster map with flood impact outcomes. Particular attention is paid to clusters that contain a relatively high concentration of damaged cells, since these provide a first indication of which vulnerability typologies align with impact-prone areas.

4.4. Spatial Regression of Flood Damage

Spatial regression is used to estimate the relationship between the selected indicators and the observed flood damage variable. This step addresses the extent to which specific vulnerability and hazard indicators are associated with the spatial distribution of impacts. Regression is appropriate because it allows the joint evaluation of multiple independent variables against a dependent variable, while preserving the direction and magnitude of the estimated relationships (Tanni et al., 2020). In a spatial context, however, the assumptions of standard regression may be violated because nearby observations are often more similar than distant ones. This concern is consistent with Tobler's first law of geography, which states that everything is related to everything else, but near things are more related than distant things (Tobler, 1970).

4.4.1. Regression Sample and Outcome Variable

The regression analysis was restricted to the observed-event (OE) sample rather than the full area of interest (AOI). While the AOI provides broader spatial coverage, it includes a substantial number of grid cells that were never inundated during the flood event, meaning any observed correlation between vulnerability indicators and damage in that sample would conflate two distinct processes, either the physical determinants of flood occurrence itself (captured largely by the hazard-block indicators, such as elevation, slope, and distance to river) and the socio-economic determinants of differential impact given exposure. Since the guiding subresearch question concerns the extent to which mapped vulnerability indicators correlate with actual flood impact, the analysis sample was restricted to grid cells within the observed flood event footprint. Within this sample, zero-damage cells represent locations that were exposed to flooding but had no recorded damage. They do not combine unexposed cells with exposed but undamaged cells. This restriction isolates the vulnerability–impact relationship from the confounding influence of hazard exposure and ensures that estimated associations reflect differential vulnerability rather than spatial variation in flood occurrence.

Initially, the target dependent variable was the combined_dmg_num that sums all damage columns. Consid-

ering the constraints of the impact variables values, which contain many zeros, valued as positive and having small integers, exploration to other regression methods is warranted. Ordinal logit, Poisson, and Hurdle models are considered.

Poisson regression is a natural candidate for non-negative integer outcomes, but the dependent variable is not a true event count. It is a composite damage score derived by summing Copernicus damage grades across three infrastructure categories, making a count-data framework a poor conceptual fit. Hurdle models were also tested, but Poland's model failed to converge due to a non-invertible Hessian, and the two-part structure implies a separate mechanism generating zeros, which is difficult to justify when zeros simply indicate no recorded damage. Negative binomial regression was tested alongside Poisson as a check on overdispersion, but dispersion values were low enough across all regions that neither offered a meaningful advantage over the simpler Poisson specification, and the conceptual fit problem described above remained decisive.

Ordinal logistic regression is therefore used by shifting from combined_dmg_num to combined_dmg_num_bracket, thus using the damage scores as three ordered brackets, none (0), low (scores 1-2), and high (scores 3+). These thresholds are applied uniformly across all four countries. The proportional-odds model respects the ordered nature of damage severity and avoids distributional assumptions. For an outcome with J ordered categories, the model estimates the cumulative log-odds of the outcome falling at or below category j as

$$\log\left(\frac{P(y \leq j)}{P(y > j)}\right) = \alpha_j - X\beta$$

for $j = 1, \ldots, J-1$, where α_j is a category-specific intercept, or cut point, and β is the vector of coefficients shared across all category thresholds (McCullagh, 1980). This shared-coefficient structure, known as the proportional-odds assumption, means each predictor is assumed to have the same effect on the odds of moving to a higher damage category regardless of which threshold is being crossed.

4.4.2. Baseline Model and Multicollinearity Screening

The regression pipeline begins with a non-spatial Ordinary Least Squares (OLS) model fitted to the full indicator set, of the general form

$$y = X\beta + \varepsilon$$

where y is the observed damage outcome, X is the matrix of selected indicators, β is the vector of coefficients to be estimated, and ε is the error term. This baseline model provides a reference against which the added explanatory value of spatial structure can later be assessed.

Multicollinearity is then assessed using the Variance Inflation Factor (VIF), calculated for each indicator k as

$$VIF_k = \frac{1}{1 - R_k^2}$$

where R_k^2 is the coefficient of determination obtained from regressing indicator k on all remaining indicators in the model (O'Brien, 2007). A high VIF_k indicates that indicator k is well explained by a linear combination of the other predictors, meaning its own coefficient estimate becomes unstable and difficult to interpret. Indicators exceeding a chosen VIF threshold are removed before the pipeline can proceed, since retaining highly collinear predictors inflates the variance of the coefficient estimates and can destabilize the model, in some cases preventing it from converging at all. This underlines the importance of managing multicollinearity before regression, and is one reason PCA is applied as a preceding step. The VIF threshold used throughout this thesis is 5.

4.4.3. Spatial Weights and Residual Spatial Dependence

The spatial weights matrix W is constructed using a k-nearest-neighbors criterion, where each grid cell is connected to its eight nearest neighbors based on the Euclidean distance between cell centroids (Rey & Anselin, 2009). A k-nearest-neighbors criterion is used rather than contiguity-based weights (for example, queen or rook adjacency) because it guarantees a fixed, non-zero number of neighbors for every observation regardless of local grid irregularities, such as gaps at the edge of the populated grid or along the boundary of the

flood footprint, where a contiguity-based approach could otherwise leave some cells with few or no neighbors. The resulting weights matrix is row-standardized, so that each row of W sums to one and the spatial lag of a variable represents the average value among a cell's k nearest neighbors rather than their raw sum.

Whether spatial regression is actually needed can be assessed ex-ante, where it justifies the need for a spatial model before running one, by testing the residuals of the initial OLS model for spatial autocorrelation using Moran's I (Moran, 1950)

$$I = \frac{n}{\sum_i \sum_j w_{ij}} \cdot \frac{\sum_i \sum_j w_{ij}(e_i - \bar{e})(e_j - \bar{e})}{\sum_i (e_i - \bar{e})^2}$$

4.4.4. Spatial Lag of X Model

Several spatial regression specifications are available, depending on where the spatial dependence is assumed to lie (Rüttenauer, 2019). Spatial autoregressive models (SAR or SLM) introduce a spatial lag of the dependent variable. Spatial error models (SEM) locate the dependence in the error term. Spatial lag of X models (SLX) introduce spatially lagged covariates instead. More complex combinations of these structures are also possible, including spatial autoregressive combined (SAC), spatial Durbin model (SDM), spatial Durbin error model (SDEM), and the general nesting specification (GNS).

Determining which model to use can be done in two ways. The first is through the use of Lagrange multiplier (LM) tests for lag and error, with the higher LM value determining the model to use. However, Rüttenauer (2019) argues that theoretical considerations should drive the model selection by identifying which sources of spatial dependence are plausible in the empirical setting. As a result, rather than relying on LM test comparisons, this thesis follows the theory-driven approach.

Because the research question focuses on the relationship between local vulnerability indicators, neighboring vulnerability conditions, and observed damage, the Spatial Lag of X (SLX) model is selected as the primary spatial specification. SLX is considered because it estimates the effect of neighboring covariates directly, which is relevant in a flood context where nearby socio-economic and infrastructural conditions may influence local impacts. Monte Carlo evidence suggests that SLX can yield accurate direct effects and relatively less biased indirect effects under several realistic conditions (Rüttenauer, 2019).

The general form of the selected model is given below

$$y = X\beta + WX\theta + \varepsilon$$

for the SLX specification, where WX represents the spatial lag of the covariates and θ their associated coefficients. Combined with the ordinal specification described above, the covariates X include both the direct indicator values and their spatial lags WX, so that the full model estimates the effect of both local and neighboring conditions on the ordered probability of observing low or high flood damage.

4.4.5. Hazard-Only Control Model

Finally, a hazard-only control model is estimated to assess whether the inclusion of vulnerability indicators improves explanatory performance relative to hazard conditions alone. This is used to test whether vulnerability indicators meaningfully improve model fit relative to hazard variables alone.

5

Spatial Analysis Results

This chapter directly addresses SQ 2, using blockwise PCA, spatial clustering, and spatial regression to assess the extent to which the mapped vulnerability indicators cluster and correlate with the observed flood impact zones across the four case studies. The same sequence of methods, described in the previous chapter, is applied to each case study region. Results are organized by analytical step, with separate subsections for Germany, Italy, Poland, and Spain. This structure presents the case-specific outputs before the cross-case synthesis developed in the Discussion chapter.

Each indicator was visually screened via choropleth mapping prior to dimensionality reduction to confirm meaningful spatial variation and flag any that appeared uniform or too sparse for interpretation. The full set of choropleths for all indicators and regions is provided in Appendix B for reference.

5.1. Blockwise PCA Results

Blockwise Principal Component Analysis (PCA) is used to reduce redundancy among closely related indicators while preserving the conceptual content of the vulnerability domains. This section reports the correlation structures, the resulting components, and the reduced indicator sets for each region.

5.1.1. Grouping Variables by Measurement Type

The initial plan was to execute the blockwise PCA per framework component segmentation, which splits variables into hazard, physical susceptibility, human susceptibility, and social susceptibility. However, a prior global blockwise PCA run, where variables are not segmented into components, reveals that extensive variables often cluster together regardless of component segmentation. This prompted a comparison of alternative variable-grouping specifications.

Two blockwise PCA specifications were evaluated. The first iteration splits the variables to components and subsequently into intensive and extensive. The second iteration only splits them based on intensive and extensive variables. The resulting PCs reveal that extensive and intensive variables cluster across components. For this reason, this thesis proceeds with the latter iteration, where variables are initially separated into intensive (int) and extensive (ext) before executing the blockwise PCA.

5.1.2. PCA Screening and Block Formation

The specification of this process is as follows. After filtering to only populated grids, variables with more than 50% null values are removed to maintain sample size. Two parameters are tuned to ensure the variability of the final variable list, the PC variance threshold and the correlation threshold. The PC variance threshold is kept at 0.8, and the correlation threshold (rho) is at 0.9. Previous runs utilized 0.7 and 0.8 thresholds respectively, and this resulted in a more heavily reduced indicator set with limited remaining variation. However, this is a limitation as these initial values are based on common practice for both specifications, and a proper sensitivity analysis might improve the selection. For ease of reading, this section presents only the retained variable blocks whose pairwise correlations meet the selected threshold of $|\rho| \geq 0.9$. The corresponding correlations are statistically significant, and PCA loadings are rounded to two decimal places.

5.1.3. PCA Results and Reduced Indicator Set: Germany

For German indicators, blockwise PCA generated three principal components. The first PC combines two intensive variables, age_dependency_rate and elderly_rate, with positive loadings, forming the elderly_dependency_pc variable. Subsequent PCs occur in the extensive variables, with built_surface and built_volume combined into one built_mass PC, while several extensive variables coagulate into another PC consisting of the counts of the elderly, the young, both high and low education completion, employed people, and women, forming the sociodemographic_mass_pc variable. The detailed loading values in Table 5.1a show that each PC has an almost uniform positive loading across its variables, indicating that these components behave simply as aggregates of age structure, built mass, and socio-demographic volume without any contrasts between individual indicators.

The final list of indicators for Germany is shown in Table 5.1b. The removed variables depicted in the table did not pass the 50% non-null threshold. From this view it is clear that all remaining extensive variables are combined into principal components, while most intensive variables are retained as singletons.

5.1.4. PCA Results and Reduced Indicator Set: Italy

The indicators for Italy show a different pattern compared to Germany, particularly with a lack of intensive variable clustering and a clearer separation between the extensive variables. The first extensive PC combines built surface and built volume with identical positive loadings, and is interpreted as a built_mass_pc component. The second extensive PC groups age structure with income and poverty, with age_65_plus, age_under_15, income_total, and poverty_count all loading around 0.50, forming the age_income_poverty_pc variable. A third extensive PC aggregates women_count, edu_low_comp_count, and employed_persons_total with similar positive loadings around 0.58, shaping the women_labor_education_pc component. In a pattern similar to Germany's, the nearly uniform, positive loadings in Table 5.2a indicate that each Italian component behaves as an approximately equally weighted composite of the contributing indicators, rather than representing a contrast between individual variables.

The final indicator set for Italy is summarized in Table 5.2b. All intensive variables, covering hazard, physical, and human susceptibility, are retained as singletons. Extensive indicators, in contrast, are mostly combined into the three previously described principal components. Only a few extensive variables (foreign_total, hh_1_person_count, edu_high_comp_count) remain as separate singletons.

5.1.5. PCA Results and Reduced Indicator Set: Poland

The correlation of Polish indicators reveals three main groups of strongly related variables. The first intensive PC combines income_mean_hh and persons_per_household with equal positive loadings, forming the household_income_size_pc component. The first extensive PC groups built_surface and built_volume with identical loadings, again forming a built_mass_pc component similar to Germany and Italy. A second extensive PC brings together a wider set of demographic and socio-economic counts, with age_65_plus, age_under_15, edu_high_comp_count, edu_low_comp_count, employed_persons_total, hh_1_person_count, income_total, poverty_count, and women_count all loading in a narrow range around 0.32–0.34. This pattern is largely similar to Germany's, suggesting a broad population and human-capital magnitude component rather than separate age or poverty axes, and labeled as a sociodemographic_mass_pc. The almost uniform, positive loadings in Table 5.3a therefore indicate that the Polish PCs act as simple aggregates of household socioeconomic status, built mass, and overall demographic–labor volume.

The final indicator set for Poland is summarized in Table 5.3b. Intensive variables, with the exception of income_mean_hh and persons_per_household, are retained as singletons. The inverse is true for extensive indicators, where almost every indicator is combined into the built_mass PC and the broad demographic–labor PC described above, while foreign_total remains as a separate singleton.

5.1.6. PCA Results and Reduced Indicator Set: Spain

The correlation for the Spanish indicators reveals the same main groups as Germany. The first intensive PC combines age_dependency_rate and elderly_rate with identical positive loadings of 0.71, so this component summarizes the joint variation of these two aging indicators, forming the elderly_dependency_pc. The first extensive PC again groups built_surface and built_volume with equal loadings of 0.71, forming a built_mass_pc component. A second extensive PC combines a wider set of socio-demographic counts, with age_65_plus, age_under_15, edu_high_comp_count, edu_low_comp_count, employed_persons_total, foreign_total, hh_-

Table 5.1: PCA loadings and screening for Germany

(a) PCA loadings by block and principal component

variable	intensive (int)	extensive (ext)	
	block 1 pc1 elderly_dependency_pc	block 1 pc1 built_mass_pc	block 2 pc1 sociodemographic_mass_pc
age_dependency_rate	0.71		
elderly_rate	0.71		
built_surface		0.71	
built_volume		0.71	
age_65_plus			0.39
age_under_15			0.40
edu_high_comp_count			0.42
edu_low_comp_count			0.41
employed_persons_total			0.42
women_count			0.42

(b) Screening and feature construction

type	component	variable	action
int	h_sus	age_dependency_rate	PCA elderly_dependency_pc
int	h_sus	elderly_rate	PCA elderly_dependency_pc
int	hazard	ndvi	singleton
int	hazard	dem_m	singleton
int	hazard	slope	singleton
int	hazard	dist_river_m	singleton
int	hazard	hand_m	singleton
int	p_sus	road_density_m_per_km2	singleton
int	p_sus	dist_nearest_primary_road_m	singleton
int	p_sus	dist_nearest_critical_infra_m	singleton
int	h_sus	women_per_pop	singleton
int	h_sus	youth_rate	singleton
int	s_sus	income_mean_hh	singleton
int	s_sus	employment_rate_total	singleton
int	h_sus	persons_per_household	removed (low non-null)
int	h_sus	foreign_share	removed (low non-null)
ext	p_sus	built_surface	PCA built_mass_pc
ext	p_sus	built_volume	PCA built_mass_pc
ext	h_sus	age_65_plus	PCA sociodemographic_mass_pc
ext	h_sus	age_under_15	PCA sociodemographic_mass_pc
ext	h_sus	women_count	PCA sociodemographic_mass_pc
ext	s_sus	edu_high_comp_count	PCA sociodemographic_mass_pc
ext	s_sus	edu_low_comp_count	PCA sociodemographic_mass_pc
ext	s_sus	employed_persons_total	PCA sociodemographic_mass_pc
ext	h_sus	foreign_total	removed (low non-null)
ext	s_sus	income_total	removed (low non-null)
ext	s_sus	poverty_count	removed (low non-null)
ext	s_sus	hh_1_person_count	removed (low non-null)

Table 5.2: PCA loadings and screening for Italy

(a) PCA loadings by block and principal component

variable	extensive (ext)		
	block 1 pc1 built_mass_pc	**block 2 pc1 age_income_poverty_pc**	**block 3 pc1 women_labor_education_pc**
built_surface	0.71		
built_volume	0.71		
age_65_plus		0.50	
age_under_15		0.50	
income_total		0.50	
poverty_count		0.50	
edu_low_comp_count			0.58
employed_persons_total			0.58
women_count			0.58

(b) Screening and feature construction

type	component	variable	action
int	hazard	ndvi	singleton
int	hazard	dem_m	singleton
int	hazard	slope	singleton
int	hazard	dist_river_m	singleton
int	hazard	hand_m	singleton
int	p_sus	road_density_m_per_km2	singleton
int	p_sus	dist_nearest_primary_road_m	singleton
int	p_sus	dist_nearest_critical_infra_m	singleton
int	h_sus	persons_per_household	singleton
int	h_sus	age_dependency_rate	singleton
int	h_sus	elderly_rate	singleton
int	h_sus	youth_rate	singleton
int	h_sus	foreign_share	singleton
int	h_sus	women_per_pop	singleton
int	s_sus	income_mean_hh	singleton
int	s_sus	employment_rate_total	singleton
ext	p_sus	built_surface	PCA built_mass_pc
ext	p_sus	built_volume	PCA built_mass_pc
ext	h_sus	age_65_plus	PCA age_income_poverty_pc
ext	h_sus	age_under_15	PCA age_income_poverty_pc
ext	s_sus	income_total	PCA age_income_poverty_pc
ext	s_sus	poverty_count	PCA age_income_poverty_pc
ext	h_sus	women_count	PCA women_labor_education_pc
ext	s_sus	edu_low_comp_count	PCA women_labor_education_pc
ext	s_sus	employed_persons_total	PCA women_labor_education_pc
ext	h_sus	foreign_total	singleton
ext	s_sus	hh_1_person_count	singleton
ext	s_sus	edu_high_comp_count	singleton

Table 5.3: PCA loadings and screening for Poland

(a) PCA loadings by block and principal component

variable	intensive (int)	extensive (ext)	
	block 1 pc1 household_income_size_pc	block 1 pc1 built_mass_pc	block 2 pc1 sociodemographic_mass_pc
income_mean_hh	0.71		
persons_per_household	0.71		
built_surface		0.71	
built_volume		0.71	
age_65_plus			0.32
age_under_15			0.32
edu_high_comp_count			0.34
edu_low_comp_count			0.34
employed_persons_total			0.34
hh_1_person_count			0.34
income_total			0.34
poverty_count			0.34
women_count			0.34

(b) Screening and feature construction

type	component	variable	action
int	h_sus	persons_per_household	PCA household_income_size_pc
int	s_sus	income_mean_hh	PCA household_income_size_pc
int	hazard	ndvi	singleton
int	hazard	dem_m	singleton
int	hazard	slope	singleton
int	hazard	dist_river_m	singleton
int	hazard	hand_m	singleton
int	p_sus	road_density_m_per_km2	singleton
int	p_sus	dist_nearest_primary_road_m	singleton
int	p_sus	dist_nearest_critical_infra_m	singleton
int	h_sus	age_dependency_rate	singleton
int	h_sus	elderly_rate	singleton
int	h_sus	youth_rate	singleton
int	h_sus	women_per_pop	singleton
int	h_sus	foreign_share	singleton
int	s_sus	employment_rate_total	singleton
ext	p_sus	built_surface	PCA built_mass_pc
ext	p_sus	built_volume	PCA built_mass_pc
ext	h_sus	age_65_plus	PCA sociodemographic_mass_pc
ext	h_sus	age_under_15	PCA sociodemographic_mass_pc
ext	h_sus	women_count	PCA sociodemographic_mass_pc
ext	s_sus	edu_high_comp_count	PCA sociodemographic_mass_pc
ext	s_sus	edu_low_comp_count	PCA sociodemographic_mass_pc
ext	s_sus	employed_persons_total	PCA sociodemographic_mass_pc
ext	s_sus	hh_1_person_count	PCA sociodemographic_mass_pc
ext	s_sus	income_total	PCA sociodemographic_mass_pc
ext	s_sus	poverty_count	PCA sociodemographic_mass_pc
ext	h_sus	foreign_total	singleton

Table 5.4: PCA loadings and screening for Spain

(a) PCA loadings by block and principal component

variable	intensive (int)	extensive (ext)	
	block 1 pc1 elderly_dependency_pc	block 1 pc1 built_mass_pc	block 2 pc1 sociodemographic_mass_pc
age_dependency_rate	0.71		
elderly_rate	0.71		
built_surface		0.71	
built_volume		0.71	
age_65_plus			0.32
age_under_15			0.31
edu_high_comp_count			0.32
edu_low_comp_count			0.31
employed_persons_total			0.34
foreign_total			0.31
hh_1_person_count			0.34
income_total			0.30
poverty_count			0.27
women_count			0.34

(b) Screening and feature construction

type	component	variable	action
int	h_sus	age_dependency_rate	PCA elderly_dependency_pc
int	h_sus	elderly_rate	PCA elderly_dependency_pc
int	hazard	ndvi	singleton
int	hazard	dem_m	singleton
int	hazard	slope	singleton
int	hazard	dist_river_m	singleton
int	hazard	hand_m	singleton
int	p_sus	road_density_m_per_km2	singleton
int	p_sus	dist_nearest_primary_road_m	singleton
int	p_sus	dist_nearest_critical_infra_m	singleton
int	h_sus	persons_per_household	singleton
int	h_sus	youth_rate	singleton
int	h_sus	women_per_pop	singleton
int	h_sus	foreign_share	singleton
int	s_sus	income_mean_hh	singleton
int	s_sus	employment_rate_total	singleton
ext	p_sus	built_surface	PCA built_mass_pc
ext	p_sus	built_volume	PCA built_mass_pc
ext	h_sus	age_65_plus	PCA sociodemographic_mass_pc
ext	h_sus	age_under_15	PCA sociodemographic_mass_pc
ext	h_sus	foreign_total	PCA sociodemographic_mass_pc
ext	h_sus	women_count	PCA sociodemographic_mass_pc
ext	s_sus	edu_high_comp_count	PCA sociodemographic_mass_pc
ext	s_sus	edu_low_comp_count	PCA sociodemographic_mass_pc
ext	s_sus	employed_persons_total	PCA sociodemographic_mass_pc
ext	s_sus	hh_1_person_count	PCA sociodemographic_mass_pc
ext	s_sus	income_total	PCA sociodemographic_mass_pc
ext	s_sus	poverty_count	PCA sociodemographic_mass_pc

1_person_count, income_total, poverty_count, and women_count all loading between about 0.27 and 0.34, forming a broad sociodemographic_mass_pc variable. The nearly uniform, positive values in Table 5.4a indicate that these Spanish components act as an equally weighted composite of dependency, built mass, and broad demographic-labor volume within their respective blocks.

The final indicator set for Spain is given in Table 5.4b. Similar to Germany and Poland, all intensive variables are kept as singletons, except for age_dependency_rate and elderly_rate, which enter through the intensive PC. Extensive indicators are combined into the built-mass PC (built_surface and built_volume) and the socio-demographic PC that aggregates age, education, employment, foreign_total, hh_1_person_count, income_total, poverty_count, and women_count. In Spain, therefore, all extensive variables are represented through principal components, while the hazard and most intensive socio-demographic indicators remain in a form that is straightforward to interpret in the spatial regression.

5.2. Spatial Clustering Results

Spatial clustering is used to identify recurring combinations of vulnerability conditions in the reduced indicator space. This section presents the cluster specifications and profiles, and how the damaged grids are distributed among them. The damage is classified using the combined_dmg_num_bracket variable, which groups combined_dmg_num variables into none, low, and high, with none having no damage, low ranging from 1-2 (representing Copernicus' possibly damaged and damaged gradings), and high representing 3 and above, either destroyed infrastructure or more than one damaged infrastructure category.

5.2.1. Selection of the Number of Clusters

Following the composite scoring procedure described in Chapter 4, the optimal number of clusters is determined separately for each region. Three of the four regions converge on a composite-optimal $k = 3$, while Italy instead converges clearly on $k = 2$, with its composite scores at $k = 2$ substantially higher than any alternative. The normalized validation indices used to select k are reported in the tables below, with the selected value shaded. The corresponding inertia, silhouette, Calinski–Harabasz, and Davies–Bouldin diagnostic plots, together with the raw non-normalized values across the full tested range of k, are provided in Appendix C.

Germany

Inertia decreases monotonically with k and does not show a sharp bend, so it offers little guidance beyond ruling out very small values of k. Silhouette scores peak at $k = 3$ and decline steadily afterward, while Calinski-Harabasz also peaks at $k = 3$ before falling off. Davies-Bouldin instead favors somewhat larger values of k, reaching its best (lowest) raw value around $k = 8$, though this comes at the cost of much weaker silhouette and Calinski-Harabasz scores at that point. The composite score reconciles this disagreement in favor of $k = 3$, which achieves the strongest silhouette and Calinski-Harabasz normalized scores while remaining reasonably competitive on Davies-Bouldin.

Table 5.5: Normalized clustering validation indices by number of clusters for Germany.

k	silhouette	calinski_harabasz	davies_bouldin	normalized_average
2	0.588	0.998	0.000	0.529
3	**1.000**	**1.000**	**0.744**	**0.915**
4	0.513	0.791	0.976	0.760
5	0.532	0.544	0.580	0.552
6	0.232	0.391	0.631	0.418
7	0.217	0.269	0.683	0.390
8	0.192	0.169	1.000	0.454
9	0.088	0.079	0.943	0.370
10	0.000	0.000	0.731	0.244

Italy

Italy shows the clearest signal of the four regions. Silhouette, Calinski-Harabasz, and Davies-Bouldin all reach their best value at $k = 2$, and the gap to the next-best candidate is large across all three indices. This agreement is reflected directly in the composite score, which reaches its maximum of 1.000 at $k = 2$ and drops

sharply for every larger k tested. Unlike the other three regions, no reconciliation between conflicting indices is needed here, all three diagnostics point to the same, low value of k.

Table 5.6: Normalized clustering validation indices by number of clusters for Italy.

k	silhouette	calinski_harabasz	davies_bouldin	normalized_average
2	**1.000**	**1.000**	**1.000**	**1.000**
3	0.141	0.632	0.244	0.339
4	0.194	0.539	0.373	0.369
5	0.214	0.419	0.409	0.347
6	0.037	0.333	0.040	0.137
7	0.046	0.214	0.151	0.137
8	0.005	0.127	0.015	0.049
9	0.000	0.058	0.068	0.042
10	0.020	0.000	0.000	0.007

Poland

Silhouette and Davies-Bouldin both favor $k = 3$, while Calinski-Harabasz peaks slightly earlier at $k = 2$ before declining. This is a smaller disagreement than in Germany, since Calinski-Harabasz's score at $k = 3$ (0.604) remains the second-highest value on that index rather than a distant alternative. The composite score resolves this in favor of $k = 3$, driven primarily by its strong, near-maximal silhouette and Davies-Bouldin scores at that point.

Table 5.7: Normalized clustering validation indices by number of clusters for Poland.

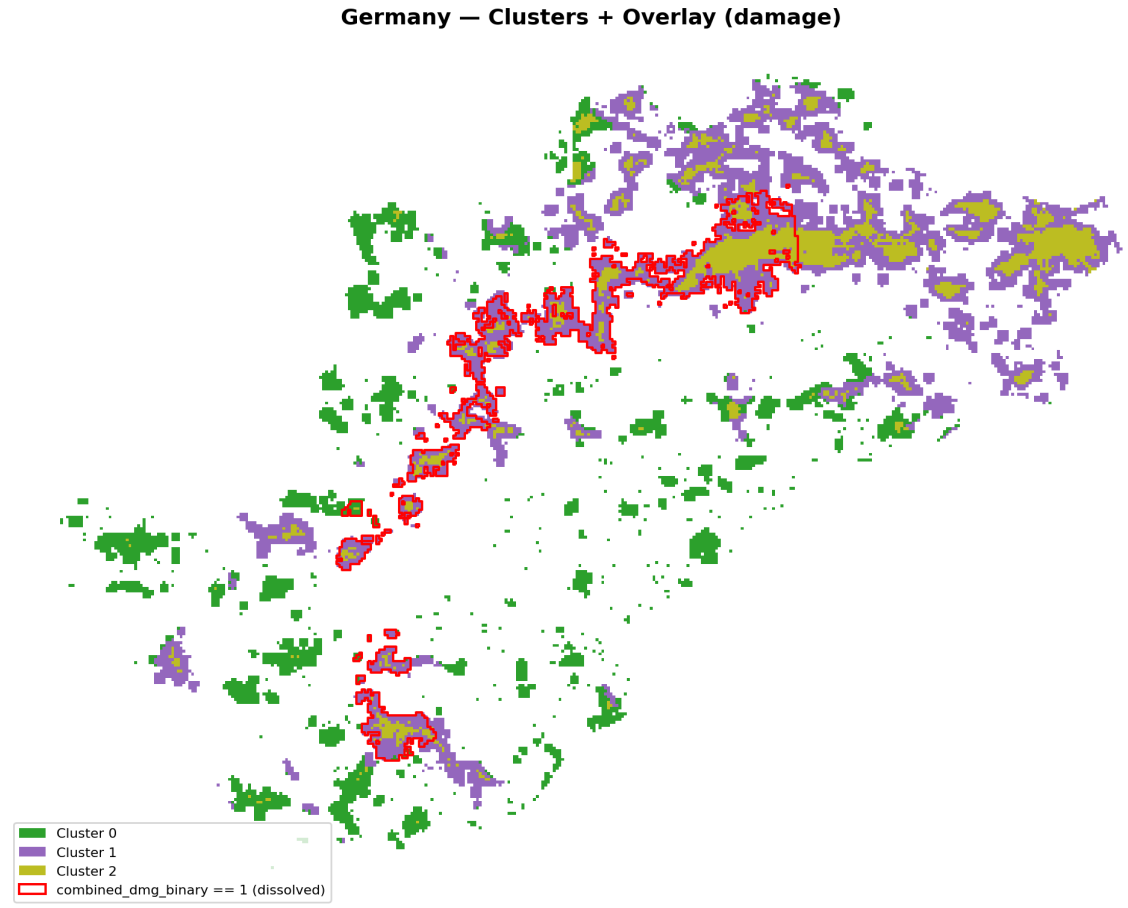
k	silhouette	calinski_harabasz	davies_bouldin	normalized_average
2	0.926	1.000	0.000	0.642
3	**1.000**	**0.604**	**0.892**	**0.832**
4	0.544	0.563	0.982	0.696
5	0.512	0.422	0.808	0.581
6	0.451	0.296	0.934	0.560
7	0.058	0.234	0.818	0.370
8	0.000	0.141	0.975	0.372
9	0.013	0.068	1.000	0.360
10	0.136	0.000	0.936	0.357

Spain

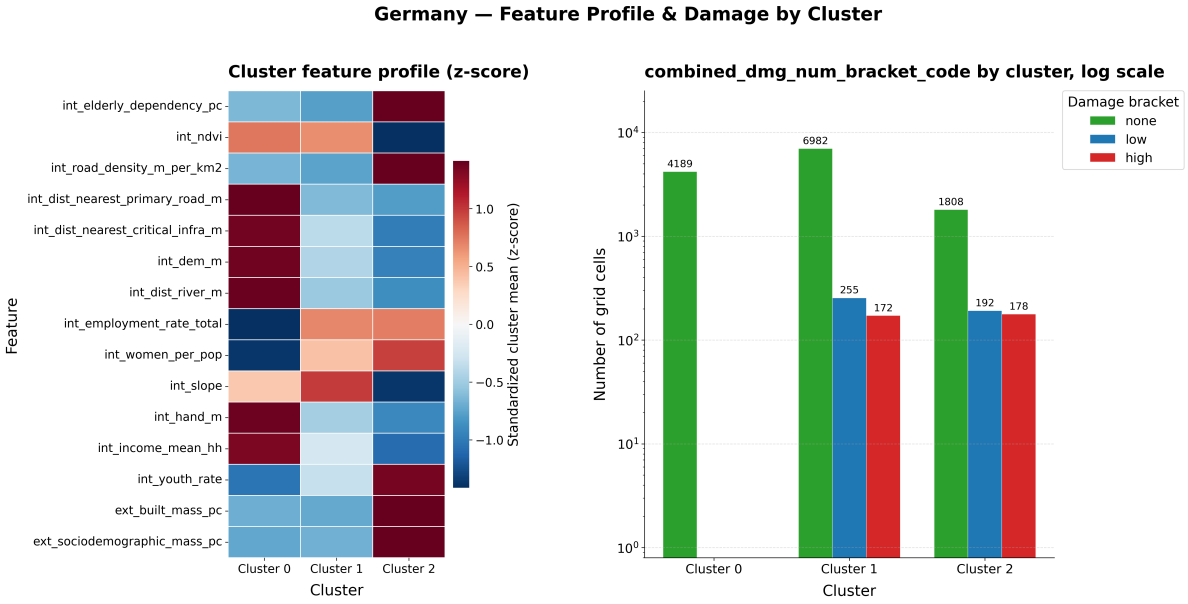
As in Poland, silhouette favors $k = 3$ while Calinski-Harabasz peaks slightly earlier at $k = 2$. Davies-Bouldin behaves less predictably here, its best raw value falls at $k = 10$, but this comes alongside weak silhouette and Calinski-Harabasz scores at that point, so its influence on the composite score is limited by the other two indices. The composite score peaks at $k = 3$, driven by its maximal silhouette score and a comparatively strong Calinski-Harabasz value relative to the remaining candidates.

Table 5.8: Normalized clustering validation indices by number of clusters for Spain.

k	silhouette	calinski_harabasz	davies_bouldin	normalized_average
2	0.760	1.000	0.000	0.587
3	**1.000**	**0.772**	**0.493**	**0.755**
4	0.236	0.576	0.501	0.438
5	0.326	0.361	0.813	0.500
6	0.000	0.226	0.521	0.249
7	0.440	0.158	0.759	0.452
8	0.490	0.100	0.899	0.496
9	0.452	0.049	0.972	0.491
10	0.314	0.000	1.000	0.438



(a) Cluster map with damage overlay



(b) Cluster feature profiles and damage distribution by cluster

Figure 5.1: Spatial clustering map of Germany, cluster profiles, and histogram of damage distribution.

Table 5.9: Damage distribution by cluster in Germany

Cluster	No dmg	Low dmg	High dmg	Total grids	Any-dmg (%)	High-dmg (%)
Rural Upscale Periphery	4189	0	0	4189	0.00	0.00
River Valley Slopes	6982	255	172	7409	5.76	2.32
Urban Core	1808	192	178	2178	16.99	8.17

5.2.2. Cluster Typologies and Damage Distribution: Germany

For Germany, the three clustering typologies are mapped over populated areas in the study area in Figure 5.1a, and with areas experiencing damage shown within the red line. The cluster profiles and the corresponding damage grid distributions in Figure 5.1b are described below.

Cluster 0, mainly present in the rural parts of the study area, has higher standardized values (z-scores) for distance to the nearest primary road, distance to the nearest critical infrastructure, distance to river, elevation, HAND, and average household income than the other clusters. NDVI is also the highest in this cluster, although less pronounced than the other variables. In contrast, it has the lowest values for employment rate, women per population, youth rate, and the extensive sociodemographic mass PC. This cluster contains 4,189 cells and no observed damage of either grade. It is labeled the ”rural upscale periphery” cluster.

Cluster 1 has mostly intermediate z-scores compared with the other two clusters. Slope is strongly positive, consistent with its grids being located along river valleys in the cluster map. Its main negative profile drivers are the aging and dependency PC, road density, and, to a lesser extent, the built-mass PC. This cluster contains 7,409 cells, the largest of the three, and 255 low-damage and 172 high-damage grids, giving an any-damage share of 5.76% and a high-damage share of 2.32%. In the map, the grids in this cluster tend to border those in Cluster 2, wrapping around them along the outskirts. This cluster is labeled the ”river valley slopes” cluster.

Cluster 2 has higher standardized means (z-scores) for the aging and dependency PC, road density, youth rate, both the built-mass and the socio-demographic mass PCs, and slightly higher values for women per population. Its strongest negative values are for NDVI, slope, distance to the nearest critical infrastructure, elevation, HAND, and average household income. Distance to the nearest primary road and distance to river also show negative values, although less pronounced. Cluster 2 contains only 2,178 cells but 192 low-damage and 178 high-damage grids, giving an any-damage share of 16.99% and a high-damage share of 8.17%, the highest of the three. In the map, grids in this cluster are concentrated near urban centers in the Ahrweiler district. This cluster is labeled the ”urban core” cluster.

Cluster 1 therefore holds the largest absolute number of damaged grids, while Cluster 2 holds the highest concentration of damage relative to its size.

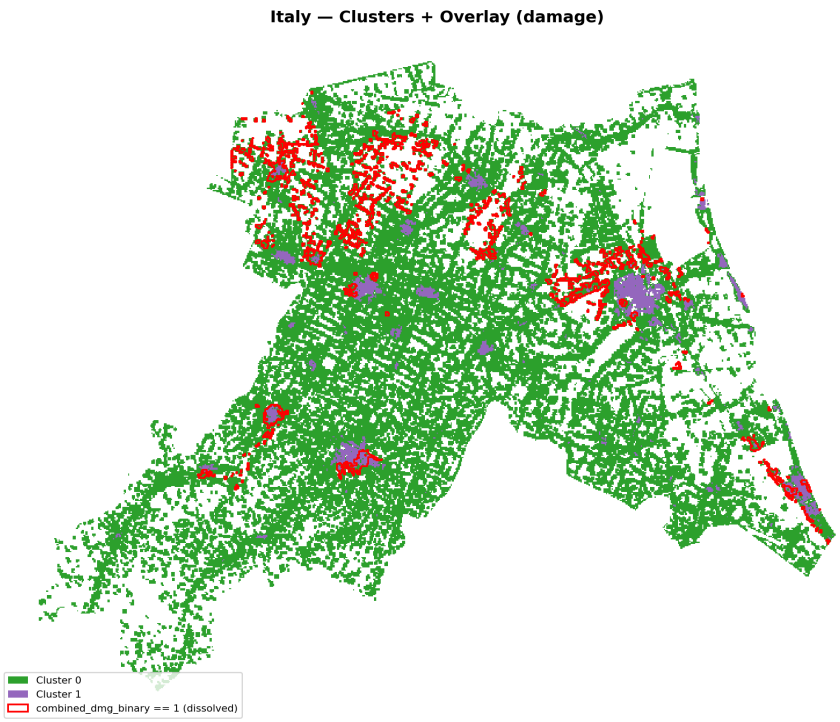
5.2.3. Cluster Typologies and Damage Distribution: Italy

Table 5.10: Damage distribution by cluster in Italy

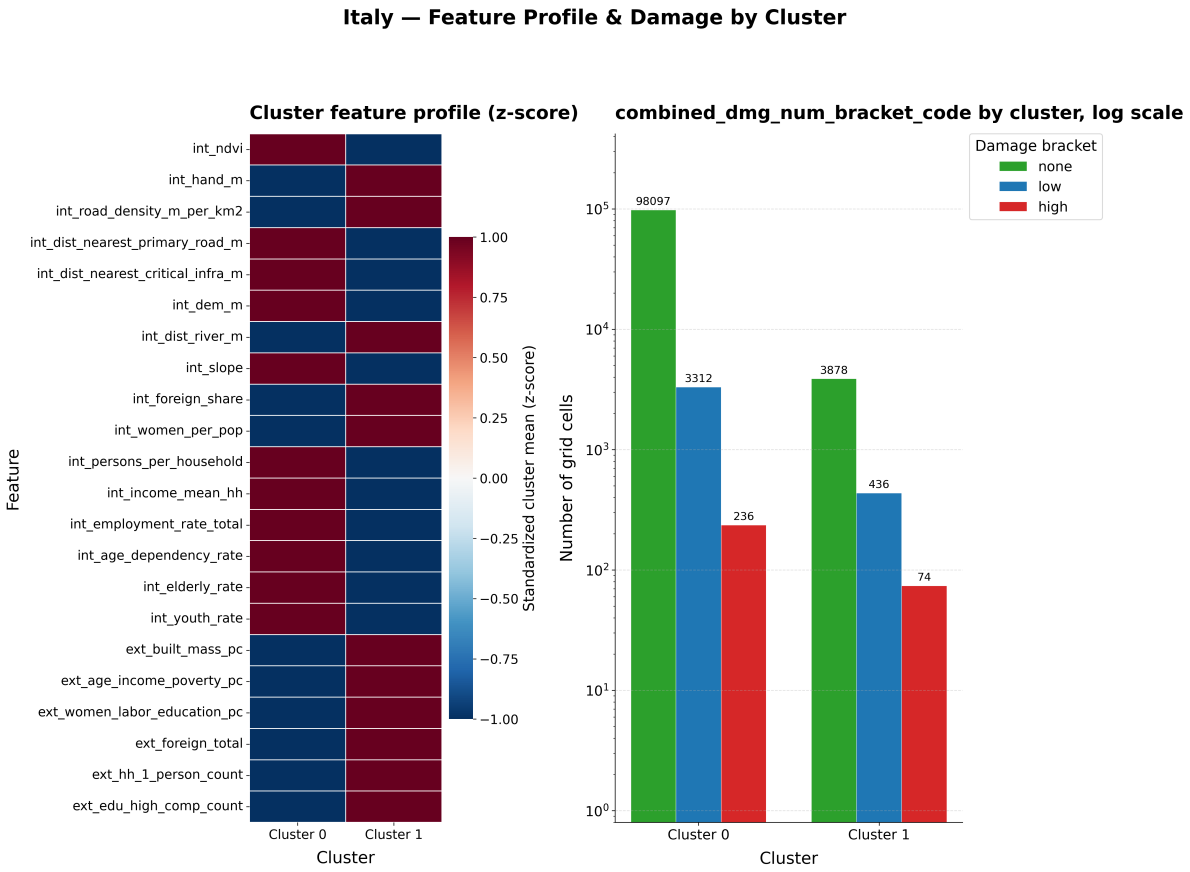
Cluster	No dmg	Low dmg	High dmg	Total grids	Any-dmg (%)	High-dmg (%)
Rural Periphery	98097	3312	236	101645	3.49	0.23
Urban Core	3878	436	74	4388	11.62	1.69

Italy’s two clusters immediately manifest as urban centers and outskirts, mapped in Figure 5.2a, with the Ravenna city proper in the big dot slightly on the right. The cluster profiles as well as the damaged grids are described below based on Figure 5.2b. Due to there being only two clusters, comparisons focus mainly on which variables show a positive standardized z-score for one cluster relative to the other.

Cluster 0, labeled the ”rural periphery” cluster, covers most of the study area and contains 101,645 cells. It is concentrated in rural areas outside the main population centers, with high values for NDVI, distance to nearest primary road, distance to nearest critical infrastructure, elevation, slope, persons per household, average household income, employment rate, age dependency rate, elderly rate, and youth rate. Population-related extensive variables are low. This cluster contains the largest absolute number of damaged cells, with 3,312 low-damage and 236 high-damage grids, corresponding to an any-damage share of 3.49% and a high-damage share of 0.23%.



(a) Cluster map with damage overlay



(b) Cluster feature profiles and damage distribution by cluster

Figure 5.2: Spatial clustering map of Italy, cluster profiles, and histogram of damage distribution.

Cluster 1 is concentrated in Ravenna and the other populated centers within the study area. It shows the opposite profile to Cluster 0, with higher standardized values for the built-mass PC, the age-income-poverty PC, the women-labor-education PC, foreign population count, single-person household count, and higher education count. Road density and proximity to primary roads and critical infrastructure are also elevated, while NDVI and distance to river are lower. This cluster contains only 4,388 cells, far fewer than Cluster 0, but its 436 low-damage and 74 high-damage grids correspond to an any-damage share of 11.62% and a high-damage share of 1.69%, both well above Cluster 0's. This cluster is labeled the "urban core" cluster.

Cluster 0 therefore holds the largest absolute number of damaged grids, while Cluster 1 holds the highest concentration of damage relative to its size.

5.2.4. Cluster Typologies and Damage Distribution: Poland

Table 5.11: Damage distribution by cluster in Poland

Cluster	No dmg	Low dmg	High dmg	Total grids	Any-dmg (%)	High-dmg (%)
Rural Periphery	21142	337	154	21633	2.27	0.71
Suburban Family Belt	32151	106	13	32270	0.37	0.04
Urban Core	2011	135	16	2162	6.98	0.74

In Poland, the clusters are spread across the study area, pictured in Figure 5.3a. Cluster 0 forms an outer band around Cluster 2. Cluster 1 is more widely distributed along road networks. Cluster 2 is concentrated in cities and population centers, with the city of Klodzko near the center of the cluster map. The profile descriptions based on Figure 5.3b are given below.

Cluster 0 has a high standardized cluster mean (z-score) for distance to the nearest primary road, distance to the nearest critical infrastructure, distance to river, HAND, and, to a lesser extent, NDVI, elevation, and slope. Employment rate has a strongly negative profile in this cluster. It contains 21,633 cells, the largest absolute number of damaged grids among the three Polish clusters, with 337 low-damage and 154 high-damage grids, an any-damage share of 2.27% and a high-damage share of 0.71%. This cluster is labeled the "rural periphery" cluster.

Cluster 1 has a high mean z-score for the income and persons-per-household PC, employment rate, and youth rate. It has strongly negative scores for women per population, foreign share, age dependency, and elderly rate. This is the largest Polish cluster by grid count, with 32,270 cells, yet it contains the fewest damaged grids, 106 low-damage and 13 high-damage, giving the lowest any-damage share of the three clusters at 0.37% and a high-damage share of 0.04%. This cluster is labeled the "suburban family belt" cluster.

Cluster 2 has a high score for road density, women per population, and the extensive variables, and a moderately high score for foreign share. It is the smallest Polish cluster, with 2,162 cells, but has the highest damage concentration of the three, with 135 low-damage and 16 high-damage grids corresponding to an any-damage share of 6.98% and a high-damage share of 0.74%. This cluster is labeled the "urban core" cluster.

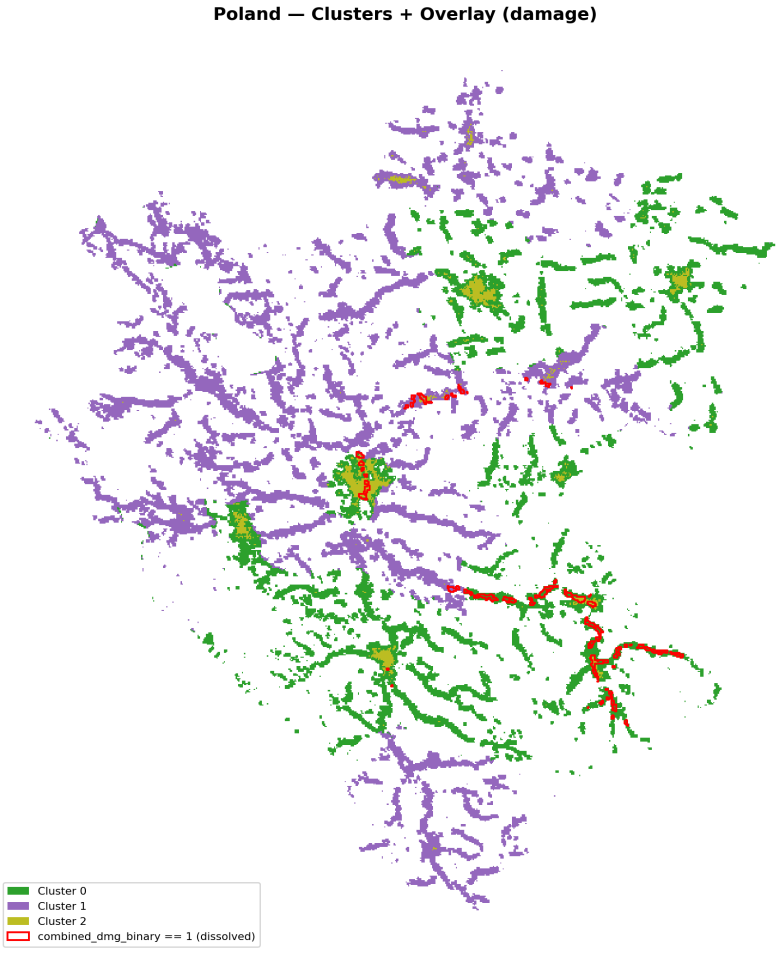
Cluster 0 therefore holds the largest absolute number of damaged grids, while Cluster 2 holds the highest concentration of damage relative to its size.

5.2.5. Cluster Typologies and Damage Distribution: Spain

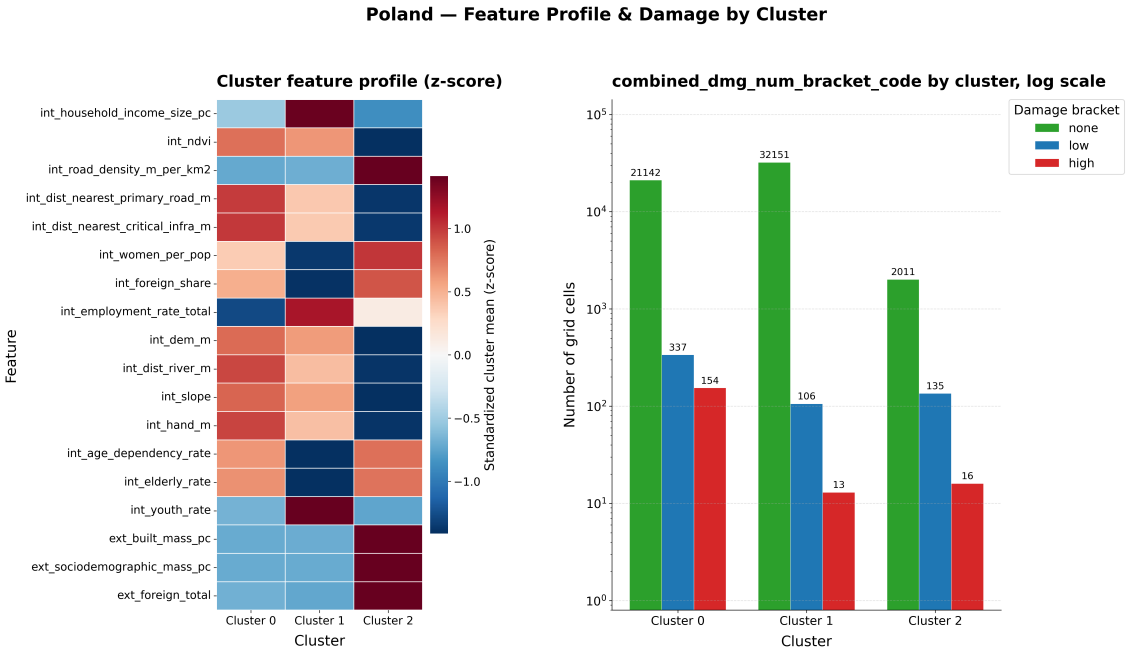
Table 5.12: Damage distribution by cluster in Spain

Cluster	No dmg	Low dmg	High dmg	Total grids	Any-dmg (%)	High-dmg (%)
Rural Elderly Periphery	51744	150	110	52004	0.50	0.21
Employed Residential Belt	115062	3156	816	119034	3.34	0.69
Urban Core	15105	1621	612	17338	12.88	3.53

In Spain, the clusters are distributed across the study area, with Cluster 0 and Cluster 1 forming widespread patterns and Cluster 2 concentrated around urban centers and along the main damage corridor. The cluster map in Figure 5.4a shows damaged grids overlaying these clusters, and the profiles and damage counts are summarized in Figure 5.4b.

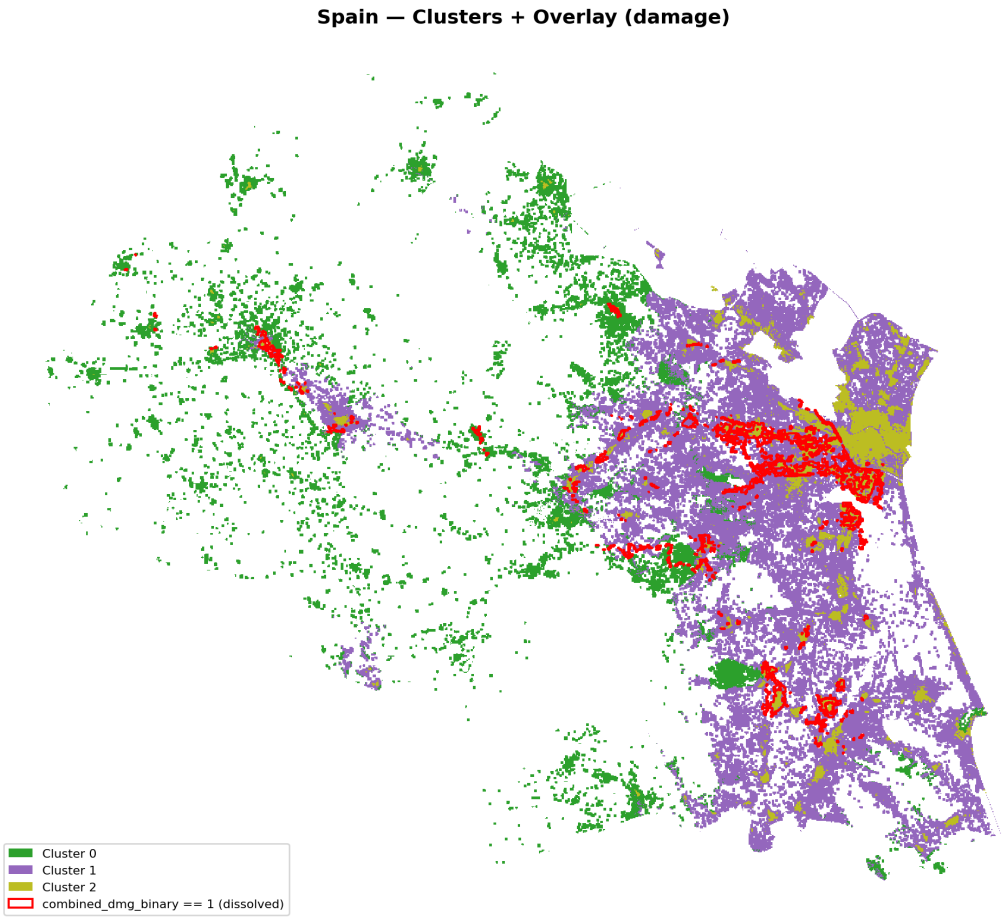


(a) Cluster map with damage overlay

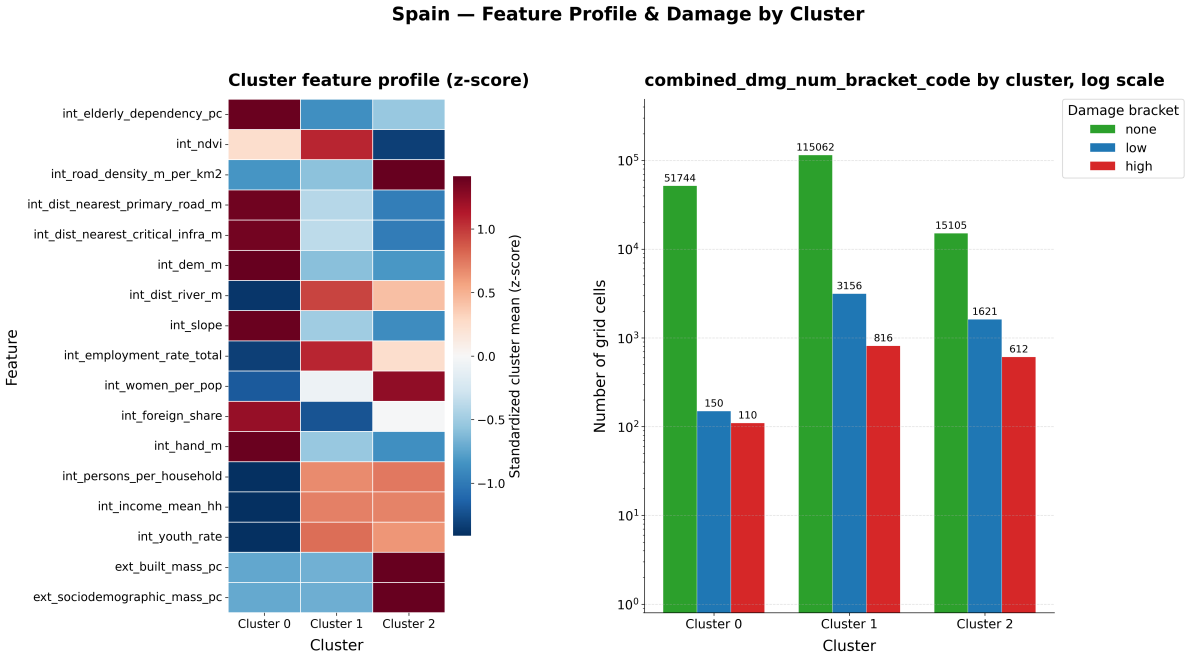


(b) Cluster feature profiles and damage distribution by cluster

Figure 5.3: Spatial clustering map of Poland, cluster profiles, and histogram of damage distribution.



(a) Cluster map with damage overlay



(b) Cluster feature profiles and damage distribution by cluster

Figure 5.4: Spatial clustering map of Spain, cluster profiles, and histogram of damage distribution.

Cluster 0 has relatively high standardized means (z-scores) for the aging and dependency PC, distance to the nearest primary road, distance to the nearest critical infrastructure, elevation, slope, foreign share, and HAND. Distance to river is strongly negative relative to the study-area mean, along with employment rate, women per population, persons per household, mean household income, and youth rate. This cluster contains 52,004 cells, with 150 low-damage and 110 high-damage grids, an any-damage share of 0.50% and a high-damage share of 0.21%. This cluster is labeled the ”rural elderly periphery” cluster.

Cluster 1 has higher z-scores for NDVI, distance to river, employment rate, and a slightly higher score on youth rate, while having negative values on aging and dependency PC and foreign share. It is the largest Spanish cluster, with 119,034 cells, and contains the largest absolute number of damaged grids of the three, with 3,156 low-damage and 816 high-damage grids, an any-damage share of 3.34% and a high-damage share of 0.69%. This cluster is labeled the ”employed residential belt” cluster.

Cluster 2 has high z-scores for road density, women per population, and both extensive PCs, and lower values for NDVI, distance to river and critical infrastructure, elevation, slope, and HAND. It also shows slightly higher persons per household than Cluster 1. This is the smallest Spanish cluster, with 17,338 cells, yet it has by far the highest damage concentration, with 1,621 low-damage and 612 high-damage grids corresponding to an any-damage share of 12.88% and a high-damage share of 3.53%. This cluster is labeled the ”urban core” cluster.

Cluster 1 therefore holds the largest absolute number of damaged grids, while Cluster 2 holds the highest concentration of damage relative to its size.

5.3. Spatial Regression Results

Spatial regression is used to quantify the relationships between selected indicators and observed flood damage, taking spatial dependence into account. This section first summarizes model specification choices and then reports region-specific results.

5.3.1. Regression Sample and Model Specification

Spatial regression is estimated only for populated grid cells within the observed-event footprint, identified by `grid_within_oe = True`. Restricting the sample to inundated cells separates variation in flood damage conditional on exposure from the physical determinants of flood occurrence itself. The regression therefore examines whether vulnerability indicators help explain why some exposed cells record greater damage than others. Additionally, the samples used in the spatial regression will decrease due to this initial filtering.

For each region, Ordinary Least Squares (OLS) regression is done using the reduced set of indicators along with the chosen dependent variable, the bracketed damage variable combined_dmg_num_bracket_code. Variance Inflation Factors (VIFs) are inspected to diagnose multicollinearity and guide further variable selection, following the procedure and threshold described in Chapter 4.

The set of variables removed at this stage differs by region, reflecting differences in each region’s underlying correlation structure. In Germany, the only variable pruned is int_youth_rate, alongside int_elderly_dependency_pc as the other collinear pair. In Italy, three variables are removed: ext_hh_1_person_count, ext_women_labor_education_pc, and int_age_dependency_rate. Poland requires the most extensive pruning, with int_women_per_pop, int_household_income_size_pc, int_employment_rate_total, int_dem_m, int_foreign_share, int_youth_rate, and int_elderly_rate all removed. Spain requires the least, with only int_youth_rate excluded. Table 5.13 summarizes the variables removed per region.

As the research question in mind focuses on the vulnerability indicators, the SLX is the selected model. SLX is considered because it estimates the effect of neighboring covariates directly, which is relevant in a flood context where nearby socio-economic and infrastructural conditions may influence local impacts. Monte Carlo evidence suggests that SLX can yield accurate direct effects and relatively less biased indirect effects under several realistic conditions (Rüttenauer, 2019).

Table 5.13: Variables removed due to VIF multicollinearity, by region

Region	Variables removed
Germany	int_youth_rate
Italy	ext_hh_1_person_count, ext_women_labor_education_pc, int_age_dependency_rate
Poland	int_women_per_pop, int_household_income_size_pc, int_employment_rate_total, int_dem_m, int_foreign_share, int_youth_rate, int_elderly_rate
Spain	int_youth_rate

5.3.2. Residual Spatial Autocorrelation Diagnostics

Before proceeding to a spatial specification, Moran's I is calculated on the residuals of the non-spatial OLS model for each region, following the ex-ante diagnostic described in Chapter 4. In every region, residual spatial autocorrelation is statistically significant, confirming that the OLS specification fails to account for spatial structure in the data and that a spatial model is warranted.

Table 5.14: Moran's I on OLS residuals by region

Region	Moran's I	z_{sim}	p_{sim}
Germany	0.252	14.37	0.0025***
Italy	0.248	50.83	0.0025***
Poland	0.222	15.63	0.0025***
Spain	0.341	68.83	0.0025***

Note: $^{***}p < 0.01$.

Table 5.14 reports Moran's I on the OLS residuals for each region, with 399 permutations each. All four regions show positive, statistically significant spatial autocorrelation, confirming that the non-spatial OLS specification fails to account for spatial structure in the data. The permutation-based p-value reaches its minimum attainable value (1/400 permutations) in every region, so the standardized z_{sim} statistic is reported alongside it to distinguish relative strength across regions. Spain shows the strongest residual spatial autocorrelation ($I = 0.341$, $z_{sim} = 68.8$), while Germany shows the weakest, though still highly significant ($I = 0.252$, $z_{sim} = 14.4$). In every case, this confirms that a spatial regression specification is warranted rather than optional.

5.3.3. Added Explanatory Value of Susceptibility Indicators

Having established that spatial modeling is necessary, the contribution of susceptibility indicators is assessed by comparing a hazard-only baseline against the full model incorporating built environment, demographic, and socio-economic indicators alongside hazard variables. Figure 5.5 shows that the full model achieves a lower Akaike Information Criterion (AIC) than the hazard-only specification in every region, with the improvement most pronounced in Italy. This provides direct evidence that susceptibility conditions contribute meaningfully to explaining flood damage beyond physical hazard exposure alone, addressing part of SQ2 before the region-specific coefficient results are examined in detail.

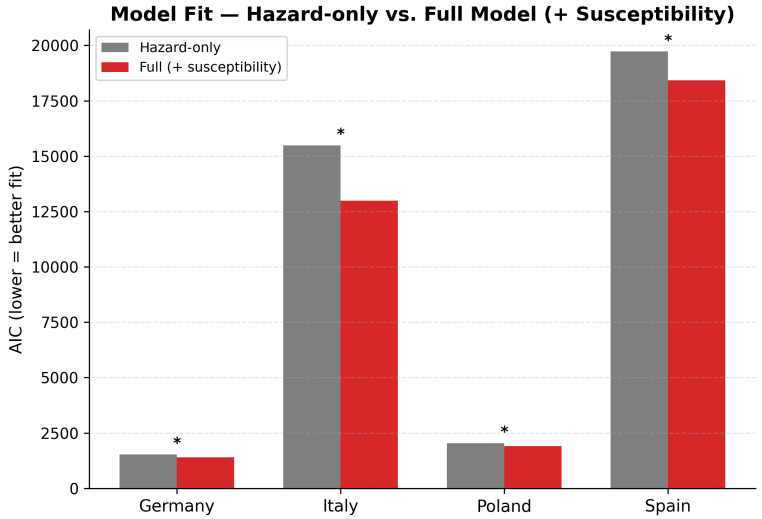


Figure 5.5: Fit comparison of hazard-only model and with susceptibility variables included

5.3.4. Direct and Spatially Lagged Effects: Germany

Section 5.3.3 showed that the full model, including susceptibility indicators, fits Germany's data better than a hazard-only baseline. To understand what drives this improvement, Figure 5.6 compares how each hazard variable's coefficient shifts between the hazard-only and full specifications, revealing which hazard effects are robust to the inclusion of susceptibility conditions and which are partly absorbed by them. Only slope remains statistically significant in both runs. Its direct coefficient is negative, becoming slightly less negative in the full model, while its spatially lagged coefficient is positive and increases to above 1.5 in the full model. NDVI, by contrast, is significant in the hazard-only specification but becomes statistically insignificant once susceptibility indicators are included, its coefficient moving closer to zero, suggesting that some of NDVI's apparent hazard effect in the reduced model reflects susceptibility conditions it happens to correlate with rather than vegetation cover itself. The remaining hazard controls show no statistical significance in either specification.

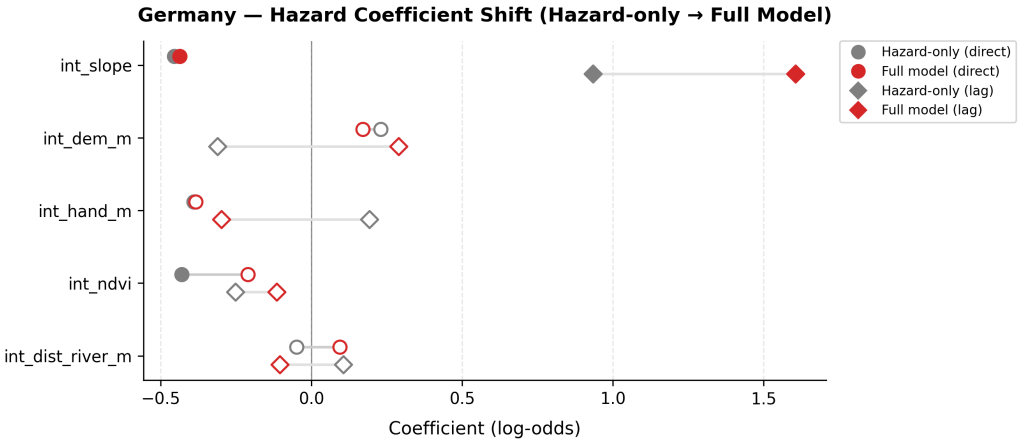


Figure 5.6: Coefficient shift for hazard variables between the hazard-only and full model for Germany ($p < 0.05$)

With this mechanism established, Table 5.15 and Figure 5.7 report the complete set of direct and spatially lagged effects from the full model, including both hazard and susceptibility indicators together.

As for the full model SLX run, whose coefficients and significance are reported in Table 5.15 and visualized in Figure 5.7, the statistically significant results are as follows. Distance to nearest critical infrastructure exhibits high absolute values for both direct and spatially lagged coefficients, albeit in different polarities, with the direct coefficient negatively correlated (-3.468, $p < 0.001$) and the spatial lag positively correlated (3.815, p

Table 5.15: Ordinal SLX model coefficients for Germany (direct and spatially lagged effects)

	Direct		Spatial Lag (WX)	
Variable	Coef.	p	Coef.	p
Intensive Variables				
int_elderly_dependency_pc	0.254	0.002***	0.843	<0.001***
int_ndvi	-0.211	0.071*	-0.116	0.672
int_road_density_m_per_km2	0.419	<0.001***	-0.265	0.242
int_dist_nearest_primary_road_m	-0.128	0.681	-0.057	0.882
int_dist_nearest_critical_infra_m	-3.468	<0.001***	3.815	<0.001***
int_dem_m	0.171	0.880	0.289	0.801
int_dist_river_m	0.094	0.501	-0.105	0.625
int_employment_rate_total	-0.328	0.643	0.299	0.677
int_women_per_pop	0.813	0.598	-1.402	0.365
int_slope	-0.437	0.007***	1.605	<0.001***
int_hand_m	-0.385	0.235	-0.299	0.466
int_income_mean_hh	0.814	0.677	-0.611	0.755
Extensive Variables				
ext_built_mass_pc	-0.328	0.049**	-1.448	<0.001***
ext_sociodemographic_mass_pc	0.916	<0.001***	2.238	<0.001***

Note: $^{*}p < 0.10$, $^{**}p < 0.05$, $^{***}p < 0.01$. Standard errors and z-statistics for all coefficients are reported in Appendix D.

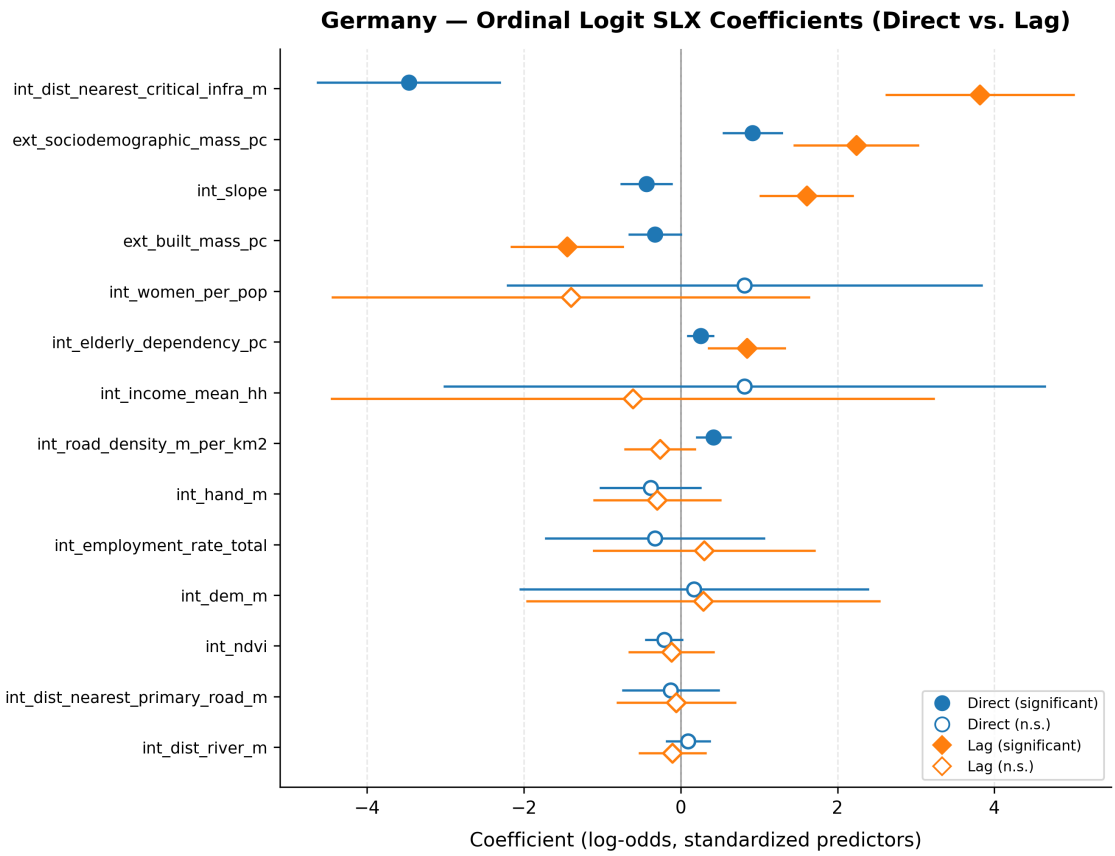


Figure 5.7: Forest plot of the direct and lag coefficients of the variables in Germany's full model (p < 0.05)

< 0.001). A similar, less pronounced pattern emerges in the slope variable, whose direct effect is negative (-0.437, p < 0.01) and spatial lag positive (1.605, p < 0.001). The socio-demographic mass PC has both positive coefficients for direct (0.916, p < 0.001) and lag effects (2.238, p < 0.001), the same can be said for the aging and dependency intensive PC on a smaller scale (0.254 direct, 0.843 lag, both p < 0.01). The remaining two variables are both direct effects, the negatively correlated built-mass PC (-0.328, p < 0.05) and the positively correlated road density (0.419, p < 0.001).

5.3.5. Direct and Spatially Lagged Effects: Italy

Building on the fit comparison in Section 5.3.3, Figure 5.8 traces how each hazard coefficient shifts once susceptibility indicators enter the model, showing where the improvement in fit is coming from. The direct coefficient for distance to nearest river becomes statistically significant and more negatively correlated once susceptibility indicators are introduced, and its spatial lag also becomes significant, though with the opposite, positive polarity. NDVI's direct effect stays significant in both runs and grows larger in magnitude, while its spatially lagged effect loses significance in the full model. Slope shows the reverse pattern to NDVI, its spatial lag becomes significant only once susceptibility is added, while its direct effect stays insignificant throughout. The remaining hazard controls show no statistical significance in either run.

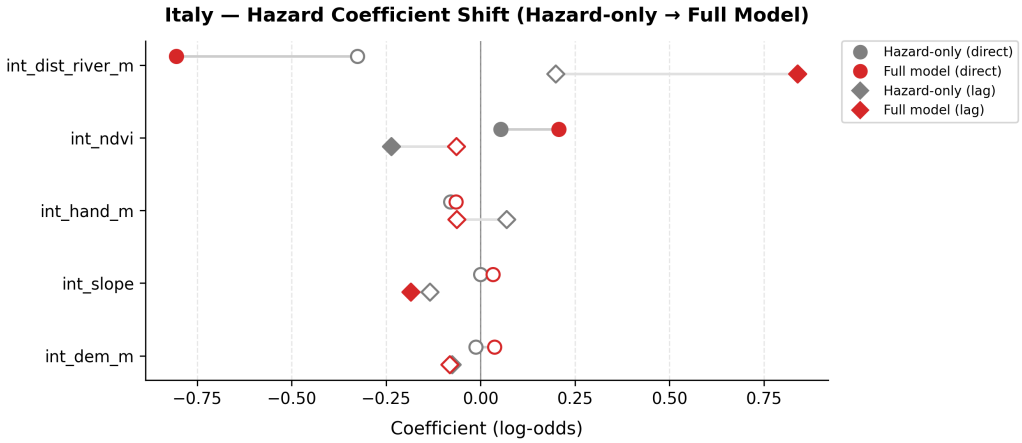


Figure 5.8: Coefficient shift for hazard variables between the hazard-only and full model for Italy (p < 0.05)

With this pattern established, Table 5.16 and Figure 5.9 report the full set of direct and spatially lagged effects, hazard and susceptibility indicators together.

For Italy, several hazard and susceptibility variables are significantly associated with the ordered damage outcome, reported in full in Table 5.16. As previously mentioned, distance to river has a different polarity between its direct and lag coefficients, with its direct being negative (-0.780, p < 0.05) and its lagged being positive (0.789, p < 0.05), a pattern it shares with number of people with higher education, to a lesser extent (-0.241 direct, 0.519 lag, both p < 0.001). Other positively correlated variables include, in descending coefficients, the direct coefficients of built-mass PC (0.680, p < 0.001), road density (0.462, p < 0.001), and NDVI (0.207, p < 0.001). The negatively correlated variables are the spatial lag of number of foreigners (-0.275, p < 0.01), slope (-0.197, p < 0.05), and persons per household (-0.185, p < 0.01), as well as the direct correlation of foreign share (-0.107, p < 0.05) and women per population (-0.098, p < 0.05).

Several patterns appear in Table 5.16 and the accompanying forest plot in Figure 5.9. While distance to river and number of people with high education are both statistically significant for their spatial lags and direct effects, most do not. Six variables (built-mass PC, road density, socio-demographic mass PC, NDVI, foreign share, and women per population) are only significant in their direct effects, while three variables (number of foreigners, slope, and persons per household) are only significant in their spatial effects.

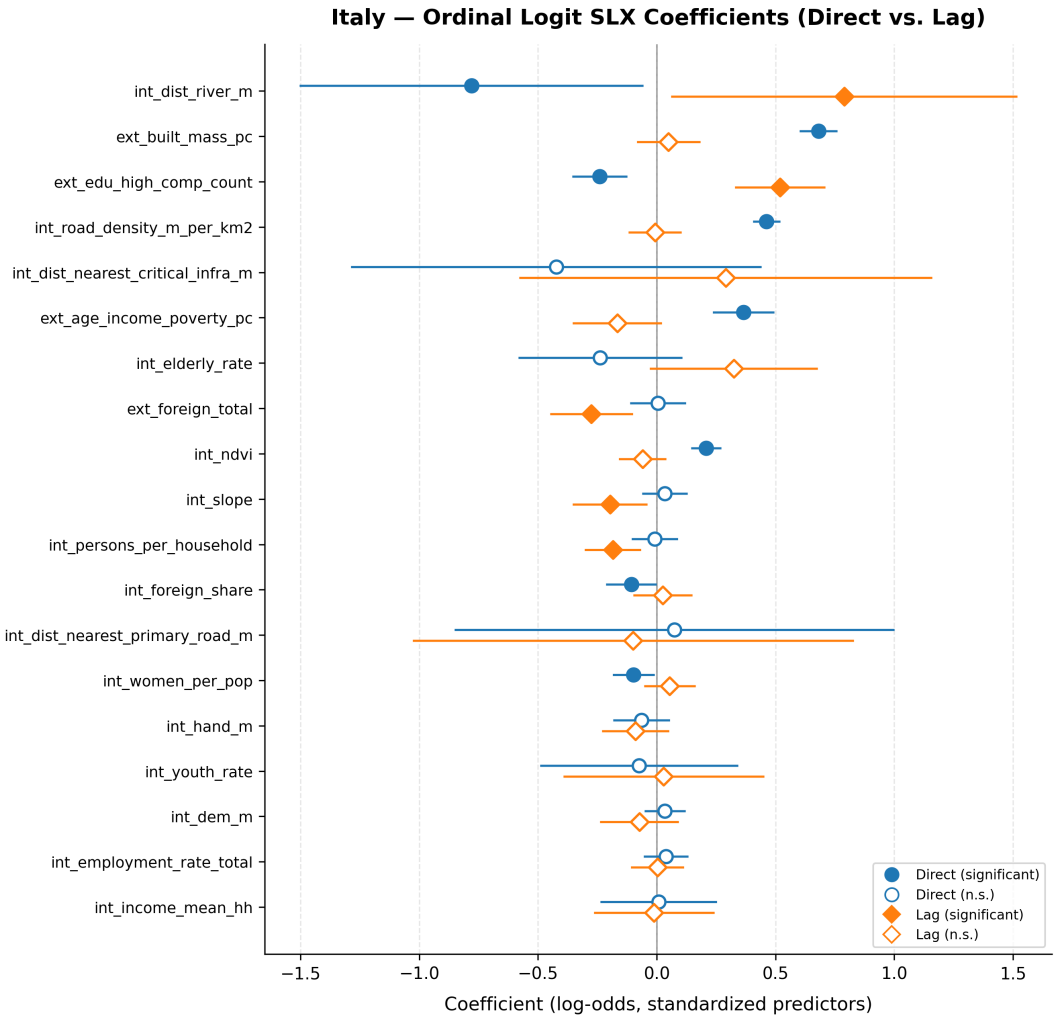


Figure 5.9: Forest plot of the direct and lag coefficients of the variables in Italy's full model ($p < 0.05$)

Table 5.16: Ordinal SLX model coefficients for Italy (direct and spatially lagged effects)

	Direct		Spatial Lag (WX)	
Variable	Coef.	p	Coef.	p
Intensive Variables				
int_ndvi	0.207	<0.001***	-0.060	0.220
int_hand_m	-0.064	0.278	-0.090	0.201
int_road_density_m_per_km2	0.462	<0.001***	-0.007	0.894
int_dist_nearest_primary_road_m	0.074	0.874	-0.100	0.832
int_dist_nearest_critical_infra_m	-0.424	0.334	0.290	0.511
int_dem_m	0.034	0.415	-0.074	0.371
int_dist_river_m	-0.780	0.034**	0.789	0.033**
int_slope	0.033	0.476	-0.197	0.011**
int_foreign_share	-0.107	0.040**	0.025	0.683
int_women_per_pop	-0.098	0.022**	0.054	0.309
int_persons_per_household	-0.008	0.858	-0.185	0.002***
int_income_mean_hh	0.008	0.949	-0.012	0.927
int_employment_rate_total	0.039	0.394	0.003	0.958
int_elderly_rate	-0.238	0.171	0.324	0.069*
int_youth_rate	-0.074	0.725	0.029	0.892
Extensive Variables				
ext_built_mass_pc	0.680	<0.001***	0.049	0.453
ext_age_income_poverty_pc	0.365	<0.001***	-0.166	0.076*
ext_foreign_total	0.004	0.941	-0.275	0.002***
ext_edu_high_comp_count	-0.241	<0.001***	0.519	<0.001***

Note: $^{*}p < 0.10$, $^{**}p < 0.05$, $^{***}p < 0.01$. Standard errors and z-statistics for all coefficients are reported in Appendix D.

5.3.6. Direct and Spatially Lagged Effects: Poland

Figure 5.10 shows the same hazard-only to full model comparison as in the preceding regions, this time revealing which hazard effects hold up once susceptibility indicators are added for Poland. Elevation does not appear in this comparison, since it was excluded from the full model due to multicollinearity. NDVI's direct effect loses significance once susceptibility indicators are introduced, while HAND moves in the opposite direction, becoming significant and more negative in the full model. NDVI's spatially lagged effect, by contrast, stays significant and grows more positive. Slope's spatial lag loses significance once susceptibility is added. The remaining hazard controls show no statistical significance in either run.

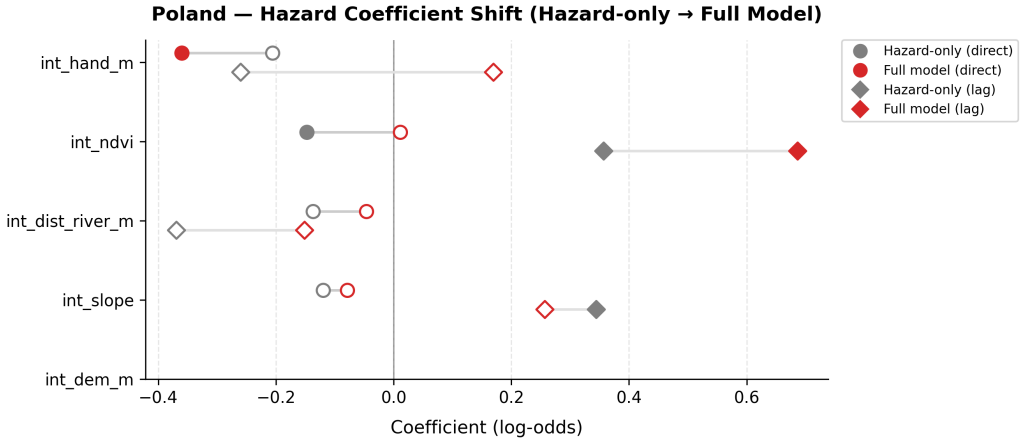


Figure 5.10: Coefficient shift for hazard variables between the hazard-only and full model for Poland (p < 0.05)

The full set of coefficients underlying this shift is reported next, in Table 5.17 and Figure 5.11.

For Poland, far fewer indicators enter the full model, since the initial reduced indicator set showed high mul-

Table 5.17: Ordinal SLX model coefficients for Poland (direct and spatially lagged effects)

	Direct		Spatial Lag (WX)	
Variable	Coef.	p	Coef.	p
Intensive Variables				
`int_ndvi`	0.015	0.855	0.719	<0.001***
`int_road_density_m_per_km2`	0.415	<0.001***	0.066	0.677
`int_dist_nearest_primary_road_m`	-4.272	0.281	4.729	0.232
`int_dist_nearest_critical_infra_m`	-2.406	<0.001***	2.508	<0.001***
`int_foreign_share`	1.272	0.356	-0.984	0.479
`int_dist_river_m`	-0.040	0.790	-0.189	0.365
`int_slope`	-0.080	0.503	0.326	0.080*
`int_hand_m`	-0.359	0.001***	0.169	0.408
`int_elderly_rate`	-0.080	0.766	0.117	0.687
Extensive Variables				
`ext_built_mass_pc`	0.309	0.001***	0.007	0.968
`ext_sociodemographic_mass_pc`	0.225	0.319	0.105	0.670
`ext_foreign_total`	0.038	0.838	-0.160	0.458

Note: $^{*}p < 0.10$, $^{**}p < 0.05$, $^{***}p < 0.01$. Standard errors and z-statistics for all coefficients are reported in Appendix D.

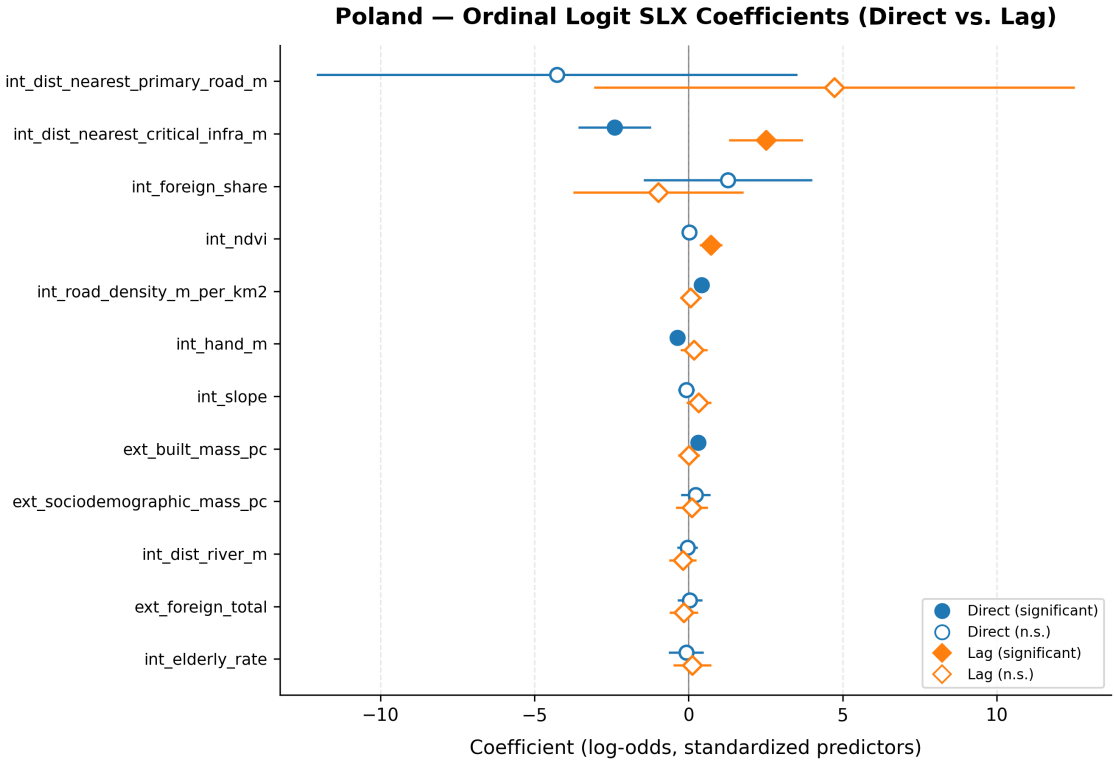


Figure 5.11: Forest plot of the direct and lag coefficients of the variables in Poland's full model (p < 0.05)

ticollinearity, as shown in Table 5.17. A noticeable variable is the distance to nearest critical infrastructure, where its direct coefficient is negative (-2.406, $p < 0.001$), while its lagged coefficient is positive (2.508, $p < 0.001$). Additional positively correlated variables include the spatial lag of NDVI (0.719, $p < 0.001$), and the direct coefficients of road density (0.415, $p < 0.001$) and built-mass PC (0.309, $p < 0.01$). The only remaining negatively correlated variable is the direct correlation of HAND (-0.359, $p < 0.01$).

5.3.7. Direct and Spatially Lagged Effects: Spain

As with the other regions, Figure 5.12 isolates the shift in hazard coefficients behind the fit improvement already established in Section 5.3.3. NDVI's direct effect loses significance in the full model, while its lag stays significant, though its negative coefficient shrinks somewhat. Both distance to river coefficients remain significant across both runs, with each growing larger in its own direction, direct effects more negative and lagged effects more positive. Slope and HAND also strengthen in the full model, both in the same direction they already had in the hazard-only run.

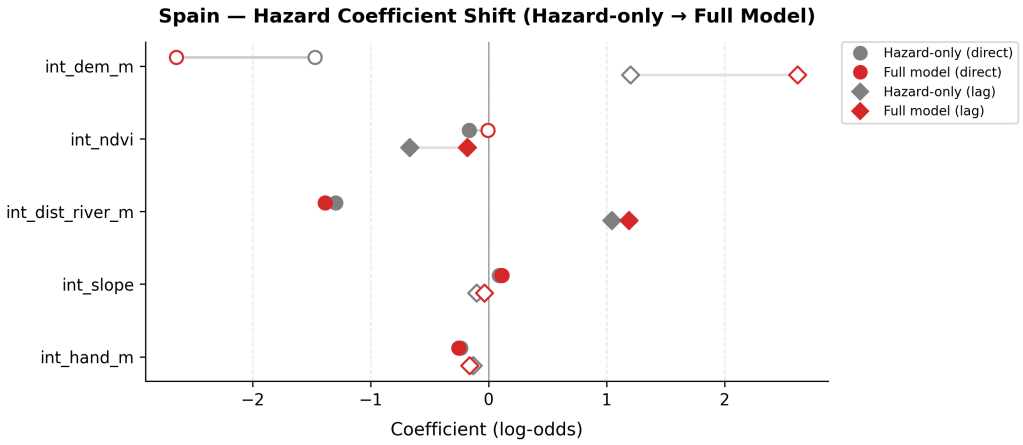


Figure 5.12: Coefficient shift for hazard variables between the hazard-only and full model for Spain ($p < 0.05$)

Table 5.18 and Figure 5.13 give the complete direct and spatially lagged effects for the full model.

Spain's model results in the largest number of statistically significant variables compared to the other regions, reported in Table 5.18. The details of those variables are as follows. The distance to the river is split, with its direct effects being negatively correlated (-1.385, $p < 0.001$) and its lagged effects positively correlated (1.190, $p < 0.001$). A similar pattern occurs for the socio-demographic mass PC on a smaller scale (-0.113 direct, 0.120 lag, both significant). The remaining two variables with statistical significance in both of their coefficients are the built-mass PC (0.175 direct, 0.427 lag) and the road density (0.415 direct, 0.120 lag), both with positive correlation across their coefficients. The remaining variables with positive coefficients are the spatial lags of average household income (0.365, $p < 0.001$), foreign share (0.295, $p < 0.001$), women per population (0.229, $p < 0.01$), and the aging and dependency PC (0.127, $p < 0.05$), as well as the direct effect of slope (0.111, $p < 0.01$). On the other hand, the remaining negatively correlated variables are the direct effects of HAND (-0.255, $p < 0.05$) and the spatial lag of NDVI (-0.183, $p < 0.001$).

Table 5.18: Ordinal SLX model coefficients for Spain (direct and spatially lagged effects)

	Direct		Spatial Lag (WX)	
Variable	Coef.	p	Coef.	p
Intensive Variables				
int_elderly_dependency_pc	0.010	0.641	0.127	0.010***
int_ndvi	-0.006	0.826	-0.183	<0.001***
int_road_density_m_per_km2	0.415	<0.001***	0.120	0.007***
int_dist_nearest_primary_road_m	-0.104	0.808	0.020	0.962
int_dist_nearest_critical_infra_m	-0.720	0.267	0.929	0.153
int_dem_m	-2.645	0.170	2.616	0.175
int_dist_river_m	-1.385	<0.001***	1.190	<0.001***
int_slope	0.111	0.008***	-0.035	0.525
int_employment_rate_total	0.027	0.667	0.052	0.458
int_women_per_pop	-0.027	0.732	0.229	0.007***
int_foreign_share	-0.042	0.572	0.295	<0.001***
int_hand_m	-0.255	0.013**	-0.161	0.134
int_persons_per_household	0.073	0.285	0.053	0.480
int_income_mean_hh	-0.116	0.060*	0.365	<0.001***
Extensive Variables				
ext_built_mass_pc	0.175	<0.001***	0.427	<0.001***
ext_sociodemographic_mass_pc	-0.113	0.004***	0.120	0.021**

Note: $^{*}p < 0.10$, $^{**}p < 0.05$, $^{***}p < 0.01$. Standard errors and z-statistics for all coefficients are reported in Appendix D.

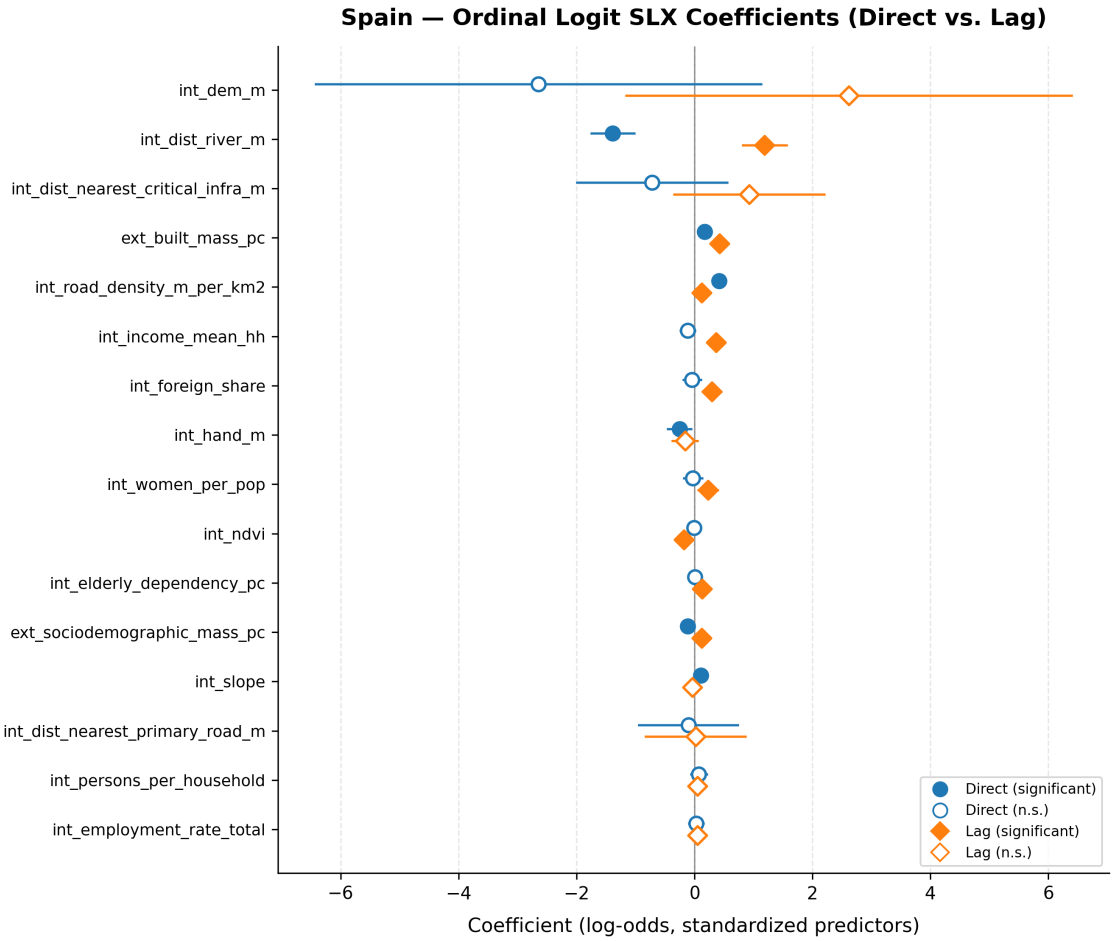


Figure 5.13: Forest plot of the direct and lag coefficients of the variables in Spain's full model (p < 0.05)

5.3.8. Ex-Post Spatial Diagnostics

Having estimated the SLX specification for each region, two ex-post diagnostics assess how well the spatial model performs. The first, a likelihood ratio test comparing the non-spatial ordinal logit against the SLX specification, tests whether the added spatial lag terms improve model fit. The second, Moran's I on the SLX model's residuals, tests whether this improvement in fit is sufficient to fully account for the spatial dependence identified in the ex-ante diagnostic.

Table 5.19 reports the likelihood ratio test for all four regions. In every region, the SLX specification significantly improves model fit over the non-spatial ordinal logit, confirming that the spatial lag terms carry genuine explanatory power.

Table 5.19: Likelihood ratio test, non-spatial vs. SLX ordinal logit, by region

Region	LR statistic	d.f.	p-value	Conclusion
Germany	119.70	14	$<$0.001	SLX improves fit
Italy	85.97	19	$<$0.001	SLX improves fit
Poland	56.48	12	$<$0.001	SLX improves fit
Spain	296.27	16	$<$0.001	SLX improves fit

Table 5.20 compares Moran's I on the ex-ante OLS residuals against Moran's I on the residuals of the fitted SLX model. In Germany and Poland, both Moran's I and its associated z_{sim} statistic are lower under SLX, consistent with the spatial lag terms absorbing some of the residual spatial dependence identified in the ex-ante diagnostic. In Italy and Spain, Moran's I is essentially unchanged, while z_{sim} is somewhat higher, though this comparison is not perfectly like-for-like, since the two diagnostics come from different model families, linear OLS and ordinal logit, with structurally different residuals. In all four regions, residual spatial autocorrelation under the final SLX specification remains statistically significant, indicating that spatial dependence in the data is not fully captured by lagging the observed covariates alone. The implications of this result are discussed further in Chapter 6.

Table 5.20: Residual spatial autocorrelation before and after the SLX specification

	OLS residuals		SLX residuals	
Region	I	z_{sim}	I	z_{sim}
Germany	0.252	14.37	0.200	12.39
Italy	0.248	50.83	0.244	54.27
Poland	0.222	15.63	0.210	14.75
Spain	0.341	68.83	0.343	72.75

5.4. Summary of Key Findings

This chapter has traced the empirical outcomes of the spatial analysis workflow for Germany, Italy, Poland, and Spain. Blockwise PCA has reduced indicator redundancy while preserving domain content, clustering has identified recurring vulnerability typologies, and spatial regression has quantified relationships between indicators and damage under spatial dependence. Together, these results indicate that certain combinations of built environment, demographic, and socio-economic conditions are consistently associated with higher flood impacts, although the exact configurations vary by region. The next chapter discusses these findings in light of existing vulnerability frameworks and implications for policy.

6

Discussion

This discussion chapter returns to the main research question and examines how the mapped indicators and empirical damage patterns relate across the four flood events. It first interprets the core findings from the clustering and spatial regression results, paying attention to where theoretical vulnerability constructs align with the observed impact zones and where they do not. It then connects these findings back to established vulnerability frameworks and literature, to assess how far the case study results support, refine, or challenge existing conceptualizations. The cross-case sections focus on regional characteristics and recurring vulnerability typologies, and ask whether similar combinations of susceptibility and hazard indicators emerge in different flood contexts. Finally, the chapter outlines policy implications, reflects on methodological choices and limitations, and identifies directions for future research that follow from the identified spatial typologies.

6.1. Cross-Case Synthesis of Vulnerability Patterns

This section brings together the main empirical results across the four flood events. It compares how indicators were structured through blockwise PCA, how they combined into spatial typologies through clustering, and how they were associated with observed infrastructure damage in the spatial regression models. The aim is to identify which vulnerability patterns recur across Germany, Italy, Poland, and Spain, and which remain dependent on local data structures, terrain, settlement patterns, and flood-event conditions.

6.1.1. Indicator Structures Across Case Studies

The PCA results reveal several recurring features in the indicator structure across Germany, Italy, Poland, and Spain. Built-mass components based on built surface and built volume emerge in every case. Broad socio-demographic mass components also appear repeatedly, although their composition differs between regions. These components absorb strongly correlated extensive variables into aggregates, whereas intensive indicators, particularly hazard variables and rates, are more often retained as singletons and enter the clustering and regression models directly.

Each retained block in all four regions is represented by a single principal component, which is sufficient to meet the 80% variance-retention threshold. All four regions form at least one PCA block from extensive indicators, whereas most intensive indicators remain as singletons. Germany and Spain each contain a component combining age dependency rate and elderly rate, while Poland has a distinct intensive component combining household income and persons per household.

Built surface and built volume consistently form a separate built-mass component in every region. Germany and Spain aggregate most remaining extensive indicators into a broad socio-demographic mass component. Poland follows a similar pattern, although foreign population count remains separate. Italy differs more clearly, with three extensive components and several extensive singleton variables. Italy is also the only case without an intensive-variable component.

6.1.2. High-Impact Spatial Typologies Across Case Studies

Across all four regions, the cluster with the highest damaged-cell share is an urban-core typology. These clusters are smaller than the dominant rural or residential clusters in each study area, but they contain a larger proportion of low- and high-damage grid cells. The cross-case comparison therefore distinguishes between absolute damage burden, which is often greatest in the largest cluster, and damage concentration, which is consistently greatest in the urban core.

Table 6.1: Damage distribution by cluster, all regions

Region	Cluster	No dmg	Low dmg	High dmg	Total grids	Any-dmg (%)	High-dmg (%)
Germany	0 = Rural Upscale Periphery	4189	0	0	4189	0.00	0.00
Germany	1 = River Valley Slopes	6982	255	172	7409	5.76	2.32
Germany	2 = Urban Core	1808	192	178	2178	16.99	8.17
Italy	0 = Rural Periphery	98097	3312	236	101645	3.49	0.23
Italy	1 = Urban Core	3878	436	74	4388	11.62	1.69
Poland	0 = Rural Periphery	21142	337	154	21633	2.27	0.71
Poland	1 = Suburban Family Belt	32151	106	13	32270	0.37	0.04
Poland	2 = Urban Core	2011	135	16	2162	6.98	0.74
Spain	0 = Rural Elderly Periphery	51744	150	110	52004	0.50	0.21
Spain	1 = Employed Residential Belt	115062	3156	816	119034	3.34	0.69
Spain	2 = Urban Core	15105	1621	612	17338	12.88	3.53

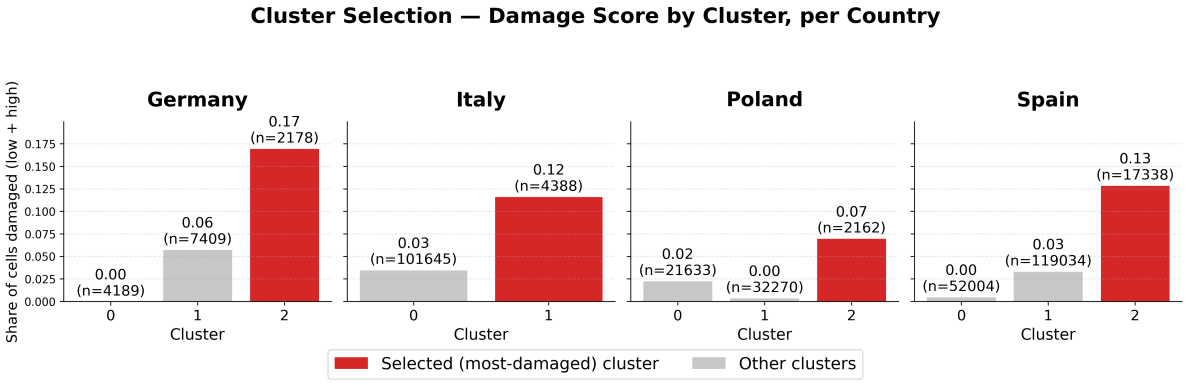


Figure 6.1: Share of damaged grids per cluster per region

Table 6.1 consolidates the per-region damage distributions reported in Chapter 5 (Tables 5.9–5.12) to allow direct cross-region comparison. Across regions, damaged grids appear to distribute across all clusters except for Germany's Rural Upscale Periphery cluster. Figure 6.1 highlights which cluster per region has the most damaged grids per total number of grids in that cluster, both high and low, with each cluster's total grids in parentheses. Based on this, the clusters with the highest share of damaged grid cells are the Urban Core clusters of all regions (Germany's Cluster 2, Italy's Cluster 1, Poland's Cluster 2, and Spain's Cluster 2). Subsequently, Figure 6.2 details the relative feature profile, or typology, of those selected clusters.

This pattern holds in every region's own results, where the largest cluster consistently contains the greatest absolute number of damaged grids while a smaller, denser cluster carries the highest concentration of damage relative to its size, confirming that the distinction is a structural feature of the data rather than a consequence of how the comparison cluster is selected.

The Cleveland dot plot lists all variables present in all selected clusters and plots the standardized cluster mean (z-score) values of each. The region representative clusters are represented with shapes along the line. The shaded color represents the absolute threshold, set at 0.8, determined visually from the per-region heatmaps that would indicate superlative positioning across the clusters in their own respective regions. The vote count plot counts the number of countries whose features go above the extreme threshold. The variable sorting is determined by two factors. The first factor points to consistency, how many clusters have a certain variable within the extreme threshold. Should there be ties, the second factor settles this by averaging the absolute mean of the z-score of the variable from the clusters.

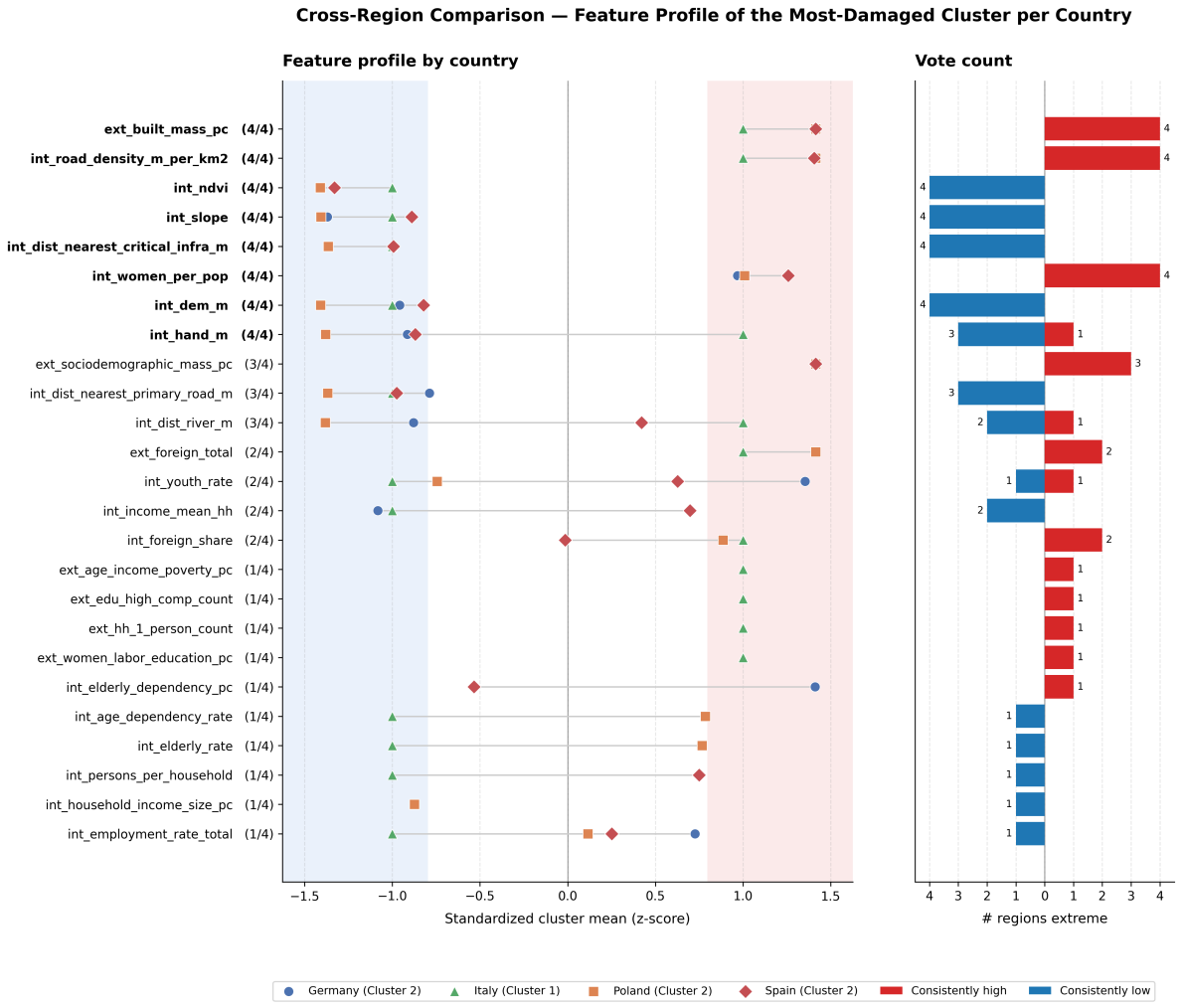


Figure 6.2: Typologies of clusters with the highest share of damaged grids per cluster per region

The selected clusters all represent the ”urban core” of their respective regions. A total of nine variables appear in all of the clusters. Among them, four are hazard variables (NDVI, slope, elevation, and HAND), and five are susceptibility variables. The susceptibility variables are further segmented into two extensive variables and three intensive variables. The extensive variables of note are the built-mass PC and the sociodemographic mass PC, but looking down the plot, built-mass components and broad socio-demographic mass components are consistently elevated in the selected urban-core clusters, although the precise indicators absorbed by these components mostly differ across regions. The intensive variables are the physical susceptibility variables road density, distance to nearest critical infrastructure, and the human susceptibility variable women per population. Among the extreme variables, the direction is consistent for most extreme variables, except for HAND, where Italy's values are extreme positive compared to the majority negative.

The clusters are compared using damage share, calculated as the number of damaged grids divided by the total number of grids in each cluster. This differs from a comparison based on raw damage count. Large rural clusters often contain many damaged grids because they cover a large area, not necessarily because damage is more concentrated within that typology. Damage share therefore provides a clearer descriptive measure of how strongly mapped damage is concentrated within each cluster.

Once clusters are compared on this basis, the clearest cross-case pattern is the urban-core typology identified in the previous chapter. In all four regions, the cluster with the highest damage share combines high built mass, dense road networks, low NDVI, and proximity to critical infrastructure. In Italy, the urban-core cluster covers a comparatively small share of the study area and contains fewer damaged grids in absolute terms than the rural periphery cluster. It nevertheless has a substantially higher proportion of damaged grids. The recurring urban-core pattern suggests that dense urban fabric is a common feature of locations with concentrated mapped flood damage across the four case studies, despite differences in terrain, event scale, and national data structures.

Beyond this shared physical signature, the socio-demographic composition of the high-impact typology varies more across cases. In all regions, the urban core cluster also carries a positive loading on the aggregated socio-demographic mass component, which combines age structure, education, employment, and household counts into a single measure of population volume. Intensive variables show more variation, where mean household income is negatively loaded in all regions but age dependency is more mixed. Germany, for instance, has a high positive loading on youth rate, while Italy and Poland both load it negatively. This suggests that while the physical exposure and built environment side of the typology travels well across the four cases, the socio-demographic profile that accompanies it is more sensitive to each country's settlement pattern and the specific composition of its census-derived indicators.

The consistency observed for the urban core typology is mirrored, in the opposite direction, by a recurring low-damage typology at the other end of each region's cluster structure, though this mirror image is not uniform across all four cases. Germany's rural upscale periphery, Italy's rural periphery, and Spain's rural elderly periphery share a common profile despite their different names, greater distance from rivers and critical infrastructure, higher elevation, and low built mass, and each records the lowest damage share of its region's clusters, close to zero in Germany's case. This suggests the same physical exposure logic driving the urban core's high damage concentration operates in reverse just as reliably, distance from hazard-relevant infrastructure and terrain is protective in a way that is as consistent across countries as proximity is damaging.

Poland is an exception to this pattern. Its rural periphery cluster follows the same distance-based profile as the other three regions but is not its lowest-damage typology, that position instead belongs to the suburban family belt cluster, an affluent, well-connected typology with high household income, high employment, and a young population, rather than a remote one. This indicates that low damage concentration can arise through two distinct mechanisms, physical remoteness from hazard pathways in most cases, or newer, better-resourced development in at least one, and that the demographic composition attached to the low-damage pole is no more uniform across countries than the composition attached to the high-damage pole already discussed above.

With these in mind, these results offer reasonably strong support for the idea of a transferable physical vulnerability profile. Built mass and infrastructure density recur across all four cases regardless of flood mechanism, event scale, or national data structure, which suggests these two dimensions could reasonably anchor a general-purpose screening typology for European flood risk. The demographic composition of that typology, however, cannot be assumed to transfer without adjustment, since its strength and specific makeup differ by

country. Any attempt to apply these typologies operationally would need to treat the physical core as the stable component and the socio-demographic layer as one requiring local calibration. The regional discussion below adds a further layer to this picture, drawing on resilience-related context, terrain and warning time in particular, that sits outside the spatial indicator system but helps account for differences in severity the regression coefficients alone do not fully explain.

Having established consistency within clustering, the same consistency check is now applied to the regression results, before the two methods are compared directly against each other.

6.1.3. Regression-Based Evidence on Damage Associations

Across the four case studies, several indicators are significantly associated with the ordered damage outcome through direct effects, spatially lagged effects, or both. Road density and built mass recur among the most important predictors across the regional models, whereas hazard, distance, and socio-demographic indicators vary more by case. Because the models use different samples and retain different predictor sets after VIF screening, the comparison focuses on the direction, significance, and relative rank of indicators within each regional model.

Table 6.2 lists the consensus ranking obtained by averaging each indicator's rank across the regions in which it was retained. Road density and the built-mass PC occupy the top two positions, with a mean rank around two to three and retention in all four regions, matching the pattern already visible in the clustering results above. Distance to nearest primary road, elevation, and employment rate sit near the bottom of the table, consistent with the earlier observation that these indicators show no statistical significance in any region. A handful of variables retained in only one or two regions, such as youth rate or the education completion counts, appear at the extremes of the table largely because they were not available for comparison elsewhere, and their position should not be read as evidence of particular importance or unimportance.

Table 6.2: Rank-averaged consensus of indicator importance across regions

Indicator	Germany	Italy	Poland	Spain	Regions	Mean rank
Road density	5	2	1	1	4	2.25
Built-mass PC	4	1	4	2	4	2.75
Age-income-poverty PC (IT only)	—	4	—	—	1	4.00
NDVI	7	3	2	5	4	4.25
High education count (IT only)	—	5	—	—	1	5.00
Sociodemographic mass PC	2	—	8	7	3	5.67
Slope	3	8	6	9	4	6.50
Distance to critical infrastructure	1	14	3	12	4	7.50
Elderly-dependency PC	6	—	—	10	2	8.00
Distance to river	10	10	10	3	4	8.25
Women per population	9	9	—	8	3	8.67
Foreign share	—	11	9	6	3	8.67
Foreign population count (extensive)	—	7	11	—	2	9.00
HAND	8	13	5	11	4	9.25
Persons per household	—	6	—	14	2	10.00
Income per household	12	19	—	4	3	11.67
Elderly rate	—	12	12	—	2	12.00
Distance to primary road	13	18	7	16	4	13.50
Elevation	14	15	—	13	3	14.00
Employment rate	11	16	—	15	3	14.00
Youth rate (IT only)	—	17	—	—	1	17.00

Note: rank 1 indicates the strongest importance within a region. Indicators tested in fewer than four regions were not available for full cross-region comparison, so their mean rank should be read with that in mind.

Only the built-mass PC and road density reach statistical significance in every region. Both are physical indicators, built structures and roads, the kind of built environment that reviews link directly to flood exposure and damage (Pulvirenti et al., 2024; Taramelli et al., 2022). Road density is the steadier of the two, with a positive and significant direct effect in all four regions and a lag effect only in Spain. Built-mass PC follows the same positive pattern in Italy, Poland, and Spain, but turns negative in Germany. Section 6.3.1 traces this reversal

to where Germany's built mass happens to sit in the valley, not to any protective effect from dense development. The sociodemographic mass PC, distance to nearest critical infrastructure, slope, and distance to river also come up often, though not in every region.

Elevation, distance to the nearest primary road, and employment rate show no statistically significant effects across the regional models. Elevation may be less informative because the regression sample is already restricted to cells inside the observed flood footprint, where broad flood-prone terrain conditions have partly been conditioned on. Section 4.4.1 restricts it to the flooded footprint, which already selects for the physical conditions that produce flooding in the first place, so within that sample elevation has little variation left to explain. Distance to nearest primary road and employment rate sit in a different susceptibility domain, describing general accessibility and economic conditions rather than the physical structures that IRL and related frameworks treat separately as physical susceptibility (Birkmann et al., 2013; Cutter et al., 2003), consistent with damage being driven more by what is actually built near a hazard than by an area's broader economic profile.

Having established consistency within each method separately, the next step is to check whether clustering and regression agree with each other on the same indicators.

6.1.4. Convergence and Divergence Between Clustering and Regression

Clustering identifies indicator profiles that characterize the highest-damage-share typology. Regression estimates whether individual indicators remain associated with damage after the remaining predictors are considered. The two methods are compared for each region through an evidence table based on two signals.

The cluster signal records whether an indicator has an extreme standardized mean above or below the absolute threshold of 0.8 in the highest-damage-share cluster. The regression signal records the direction and significance of its direct or spatially lagged coefficient, or notes where the indicator was not retained in the model. Indicators are classified as strongly consistent when the cluster and regression signals have the same direction and the regression effect is significant at $p < 0.05$. Indicators are classified as consistent but weak when the signs agree but the regression effect reaches only $p < 0.10$.

Indicators are classified as conflicting when the cluster signal is extreme and a significant regression coefficient at $p < 0.05$ has the opposite direction. Indicators are classified as scale-dependent when significant direct and spatially lagged regression coefficients have opposite signs. This category identifies differences between local and neighborhood associations with damage. It does not imply disagreement between clustering and regression. Remaining indicators are classified as partial when one method provides a meaningful signal but the other does not. Indicators are classified as irrelevant when neither method provides a meaningful signal.

These categories provide a structured descriptive comparison. They do not constitute a separate statistical test of causal importance.

Table 6.3: Evidence table classification counts by region

Classification	Germany	Italy	Poland	Spain
Strongly consistent	3	4	3	5
Consistent but weak	1	0	0	0
Conflicting	1	4	1	1
Scale-dependent	2	3	1	3
Partial	6	11	9	5
Irrelevant	2	0	4	3

Table 6.3 summarizes the classification counts by region. Partial is the largest category in Germany, Italy, and Poland. In Spain, it is tied with the strongly consistent category. This pattern reflects the different analytical roles of the two methods. Clustering identifies variables that characterize an extreme typology, while regression evaluates whether individual indicators remain associated with damage after accounting for the other retained predictors. An indicator can therefore characterize the urban-core cluster without showing an independent association in the regression model. The strongly consistent category provides the clearest evidence of convergence across the two methods.

Table 6.4: Indicators classified as strongly consistent, by region

Region	Indicator	Cluster z	Regression signal
Germany	Sociodemographic mass PC	1.414	+ (p < 0.05)
Germany	Elderly-dependency PC	1.412	+ (p < 0.05)
Germany	Road density	1.413	+ (p < 0.05)
Italy	Built-mass PC	1.000	+ (p < 0.05)
Italy	Persons per household	-1.000	− (p < 0.05)
Italy	Road density	1.000	+ (p < 0.05)
Italy	Slope	-1.000	− (p < 0.05)
Poland	Built-mass PC	1.414	+ (p < 0.05)
Poland	HAND	-1.381	− (p < 0.05)
Poland	Road density	1.414	+ (p < 0.05)
Spain	Built-mass PC	1.414	+ (p < 0.05)
Spain	HAND	-0.869	− (p < 0.05)
Spain	NDVI	-1.331	− (p < 0.05)
Spain	Road density	1.406	+ (p < 0.05)
Spain	Women per population	1.257	+ (p < 0.05)

Note: cluster z is the standardized cluster mean of the indicator in the region's highest-damage-share cluster. Full classification tables for all indicators and regions, including consistent but weak, conflicting, scale-dependent, partial, and irrelevant categories, are reported in Appendix E.

Table 6.4 lists the strongly consistent indicators by region. Road density is the only indicator classified as strongly consistent in all four cases. It is elevated in every highest-damage-share cluster and has a significant positive regression coefficient in Germany, Italy, Poland, and Spain. Road density therefore provides the strongest cross-method and cross-case evidence in this thesis. Dense road networks are associated with impervious surfaces and concentrated infrastructure, both of which may contribute to the accumulation of damage within urban areas.

The built-mass PC is strongly consistent in Italy, Poland, and Spain, but classified as conflicting in Germany, with a negative regression association despite its high value in the urban-core cluster. Section 6.3.1 examines this pattern in relation to the Ahr Valley's flood geometry and the location of built-up areas within the valley. The German result shows why cross-case patterns require country-specific interpretation.

Several indicators are strongly consistent in one region only. These include NDVI and women per population in Spain, persons per household and slope in Italy, and the elderly-dependency and sociodemographic mass components in Germany. These indicators describe case-specific features of the broader vulnerability pattern. Their limited recurrence across regions prevents them from being treated as transferable signals.

Table 6.5: Indicators classified as conflicting, by region

Region	Indicator	Cluster z	Regression signal
Germany	Built-mass PC	1.414 (high)	− (p < 0.05)
Italy	Foreign population count	1.000 (high)	− (p < 0.05)
Italy	Foreign share	1.000 (high)	− (p < 0.05)
Italy	NDVI	-1.000 (low)	+ (p < 0.05)
Italy	Women per population	1.000 (high)	− (p < 0.05)
Poland	NDVI	-1.411 (low)	+ (p < 0.05)
Spain	Slope	-0.889 (low)	+ (p < 0.05)

Note: cluster z and regression signal are defined as in Table 6.4. The full classification for every indicator, including partial and irrelevant categories, is reported in Appendix E.

Table 6.5 lists the conflicting indicators by region. Germany's built-mass PC is high in the urban-core cluster but negatively associated with damage in the regression model. The country-specific discussion links this pattern to the geometry of the Ahr Valley and the location of built-up areas relative to the most confined flood reaches. The result does not imply that dense development reduces flood damage.

Italy and Poland also show opposing NDVI signals. Low vegetation cover characterizes the urban-core typol-

ogy, while NDVI has a positive association with damage within the flooded footprint. One possible interpretation is that vegetated floodplain land uses contribute to the positive regression association. This remains tentative because the analysis does not directly model agricultural land use, flood intensity, asset value, or the spatial distribution of farm infrastructure.

Italy's foreign population count, foreign share, and women-per-population indicators are elevated in the urban-core cluster but negatively associated with damage after the regression controls for built mass, road density, and other predictors. These indicators may capture demographic characteristics that are spatially concentrated in urban areas without independently increasing mapped infrastructure damage. The available data do not allow this mechanism to be tested directly.

Spain shows a separate unresolved pattern. Slope is low in the highest-damage-share cluster but has a positive regression association with damage. The present analysis does not identify a clear explanation, and this relationship should be examined through a more detailed country-level study.

Nine indicators are classified as scale-dependent because their direct and spatially lagged regression coefficients have opposite signs. Italy and Spain each contain three of these indicators, Germany contains two, and Poland contains one. These patterns may reflect a difference between local and neighborhood associations with damage. They may also reflect model sensitivity to spatial structure, sample size, or the specific configuration of predictors retained in each regional model. The present analysis cannot distinguish between these explanations. The full list of scale-dependent indicators is reported in Appendix E.

The cross-method comparison supports the same conclusion as the clustering results. The recurring high-impact typology is an urban core with dense roads and high built mass. Road density is supported by both clustering and regression in every region. Built mass is supported in three regions and requires a terrain-based interpretation in Germany. Socio-demographic indicators contribute to urban-core profiles, although their composition and regression effects vary across cases. The physical built-environment pattern provides a useful starting point for cross-case screening, while social and demographic indicators require local calibration.

6.2. Interpreting the Findings Through Vulnerability Theory

This section situates the empirical results within the vulnerability concepts and frameworks outlined in Chapter 2. The analysis began with a literature-based indicator set grounded in IRL and related frameworks. Hazard indicators describe the physical setting of the flood, while susceptibility indicators describe the physical, social, and human characteristics of exposed elements. Resilience remains primarily an interpretive dimension because it could not be represented consistently in the spatial indicator system.

The spatial results provide partial support for this distinction. Topographic and physiographic indicators, including slope, elevation, HAND, and distance to river, describe the physical setting within the observed flood footprint. Within this already exposed sample, susceptibility indicators help distinguish locations associated with higher recorded infrastructure damage.

6.2.1. Built Environment, Land Cover, and Hazard Amplification

Built environment indicators that IRL and other frameworks (Birkmann et al., 2013; Cutter et al., 2003; McCarthy, 2001) group under physical susceptibility, such as road density and built-mass PCs derived from built surface and built volume, consistently show distinct clustering profiles and significant spatial regression coefficients. They form components that represent compactness and intensity of development, in line with reviews that link imperviousness and dense urban form to flood exposure and damage (Pulvirenti et al., 2024; Taramelli et al., 2022).

Hazard indicators also behave in line with IRL's dual path. Where detailed hydrodynamic data are not available, proxies such as NDVI, slope, HAND, and distance to river capture the broad hazard context, but their direct effects on damage often weaken once susceptibility indicators are included, while spatial lag terms remain important, particularly for distance-based variables such as distance to river or distance to critical infrastructure, which often enter with negative direct effects and positive spatial lags, indicating both local and neighborhood roles. This supports the notion that hazard shapes neighborhood-scale patterns, with susceptibility differentiating damage within those patterns (Rincón et al., 2018; Taromideh et al., 2022).

6.2.2. Socio-Demographic Vulnerability and Exposure

Social and human susceptibility indicators, including age structure, income, and household composition, form broad socio-demographic and aging components in several cases. These components are prominent in selected cluster profiles and regression models, although their relationships with damage vary across regions. The results support the inclusion of demographic and socio-economic conditions in vulnerability frameworks such as PAR, MOVE, and IRL, while also showing that their empirical expression depends on local context.

At the same time, the results refine some expectations from the literature. The PCA shows that extensive socio-demographic indicators rarely form separate axes of poverty, income, age, or education, but rather coagulate into single components representing overall human and socio-economic volume. This pattern suggests that, at the grid scale used here, vulnerability related to social conditions is expressed through combined presence of people, labor, and resources, in place of sharply separated sub-dimensions.

6.2.3. Place-Based and Context-Dependent Vulnerability

Although this chapter primarily addresses SQ 3, the findings also provide a retrospective assessment of SQ 1. The literature-derived indicators capture several empirically relevant domains, especially built environment intensity, flood-pathway proximity, and concentrated socio-demographic conditions. Their importance varies across cases, which supports the use of a shared conceptual framework alongside local adaptation of the indicator set.

Some conceptual dimensions, particularly resilience-related criteria, could not be operationalized due to data limitations, and therefore remain part of the interpretive context used in the following section rather than the spatial indicator system itself. This points to a broader feature of the results. While the physical and demographic domains discussed above hold reasonably consistently across the four case studies, the way vulnerability actually translates into damage is also shaped by context-specific factors, terrain, governance, and event characteristics, that these frameworks position as resilience or response capacity instead of susceptibility. Section 6.3 examines these context-dependent factors directly for each case. Within the constraints of what could be mapped spatially, the results reinforce the relevance of the chosen indicators and show that the literature-based selection provides a workable backbone for explaining how mapped vulnerability constructs align with observed flood impacts.

6.3. Explaining Cross-Case Differences

This section explains country-specific deviations from the cross-case patterns identified above. Each case is discussed through its PCA structure, regression results, and relevant resilience-related context drawn from event documentation.

Two analytical patterns require attention before discussing the individual cases. First, extensive variables are often strongly correlated across all four regions. Several of these variables were redistributed to the grid using the same WorldPop ancillary layer, which may give count variables similar spatial distributions. A sensitivity check using a lower correlation threshold of 0.8 grouped more extensive variables into the same blocks. Some variables still remained separate, indicating that their spatial distributions retain information beyond the shared disaggregation procedure.

Second, several distance-based variables show negative direct effects and positive spatially lagged effects. A negative direct coefficient indicates lower damage at cells located farther from a river or critical infrastructure. A positive spatial lag indicates that cells may be close to the feature when surrounding cells are farther away. This spatial arrangement can produce opposite local and neighboring effects. Italy's distance-to-river result and Germany's distance-to-critical-infrastructure result illustrate this pattern (Koks et al., 2022).

Event documentation also points to warning and coordination failures in Germany and Spain. These institutional conditions lie outside the spatial indicator system, but they may help explain how similar physical vulnerability patterns translated into different levels of damage.

6.3.1. Germany

The blockwise PCA results surface a component combining age dependency rate and elderly rate, a pattern that recurs in Spain. Since the dependency rate includes both elderly and youth populations, this component indicates that variation in dependency is closely aligned with variation in the elderly population within the German and Spanish study areas. This aligns with Fekete (2010), who identify residents aged 65 and older as a

particularly high-loading vulnerability indicator in Germany, supporting the decision to incorporate country-specific literature into the indicator selection process. Built surface and built volume also form a shared component in Germany, consistent with the pattern found across all four regions. Their common source and related construction are discussed further in the limitations section.

Germany is also the only region where this built-mass component is negatively associated with damage, in both its direct and, more strongly, its spatially lagged form. One plausible interpretation is that buildings are concentrated on flatter terrain, since steep valley sides are rarely built on. The same logic appears in the slope coefficients. Slope's direct effect is negative, meaning steeper grid cells see less damage, likely because fewer buildings sit there to be damaged, while its spatial lag is positive, meaning grids near steep terrain, consistent with valley floors, see more damage. This is consistent with the clustering map, where the lowest-elevation, lowest-slope cluster is surrounded by the highest-slope cluster, indicating that grids downstream of steep terrain experienced disproportionately higher damage.

This terrain pattern plausibly compounds a resilience-related factor the regression cannot directly test. The Ahr Valley's steep, confined topography channeled the 2021 floodwaters into a fast, high-velocity flow, identified elsewhere as a major contributor to the event's 134 fatalities (Tradowsky et al., 2023), and the same confinement that concentrates damage downstream also compresses the time available for warning and evacuation. This is consistent with documented shortcomings in the region's early warning system, which involved a sequence of separate actors, each responsible for a different stage of the warning process, without a single point of coordination ensuring the information moved fast enough end to end:

1. **National forecasting.** The German national weather service (DWD) issued flood warnings roughly three days in advance, but its river-level forecast substantially underestimated the eventual peak, predicting a water depth of approximately 5.7 m at the Altenahr gauge against an observed peak of roughly 10.2 m (Thieken et al., 2023).
2. **District-level warning.** The Landkreis Ahrweiler district authority issued its own flood warning only in the early afternoon of 14 July, the day of the flood itself, several days after the initial national forecast (Mohr et al., 2022).
3. **Municipal evacuation.** The municipality of Altenahr did not declare a state of emergency or order evacuation until 23:09 that night, by which point floodwater levels in the valley were already extreme (Nick et al., 2023).

Fragmented institutional responsibility for passing information between these three levels, as opposed to a lack of forecasting capability at the national level, is identified as a central factor in the event's high fatality count (Mohr et al., 2022; Nick et al., 2023; Thieken et al., 2023). Germany's urban-core typology should therefore be interpreted alongside a terrain-driven constraint on response time and documented coordination failures. These factors were not included in the spatial model, but they may have influenced how physical exposure and susceptibility translated into realized damage and loss.

6.3.2. Italy

Italy's PCA components all occur among the extensive variables. Beyond the built-mass and socio-demographic PCs, a third component clusters number of women, population with low educational completion, and number of employed persons. Both extensive PCs are positively associated with the urban core cluster, indicating that it carries a broader socio-demographic mass beyond built environment alone. Whether this reflects a single undifferentiated population-density effect or two more specific but co-located patterns, household-anchored dependency and income on one hand, working-age labor force presence on the other, cannot be distinguished at the two-cluster resolution used for Italy, and would require either a finer k or grid-level correlation analysis to confirm.

Distance to river is among the most important predictors in Italy's spatial regression model. Its negative direct effect and positive spatially lagged effect follow the local and neighborhood pattern described above. NDVI is also significant in Italy and has a positive regression association, even though the urban-core cluster has lower NDVI than the rural periphery. This difference reflects the distinction between typological and conditional analysis. At the typology scale, the urban core is densely built and has limited vegetation cover. Within the observed flood footprint used for regression, higher NDVI may identify vegetated floodplain land uses that were also exposed to damage. The model does not include agricultural land use, asset value, or flood intensity directly, so this interpretation remains tentative.

Italy provides a partial contrast to Germany on the resilience dimension. The Emilia-Romagna floods developed across a flat, low-relief plain and involved successive rainfall events instead of a rapid valley surge. These conditions may have allowed more time for warning and evacuation before peak water levels. This could help explain why extensive flooding did not produce the same concentration of severe damage observed in the Ahr Valley. Warning time and response capacity were not included in the spatial models, so this remains an interpretation based on event context.

6.3.3. Poland

Poland contains a distinct principal component combining mean household income and persons per household, which does not appear in the other three regions. This component is strongly positive in the suburban family-belt cluster, the region's lowest-damage typology, together with a relatively high youth rate. The combination is consistent with comparatively well-resourced family-oriented suburban areas. The analysis cannot determine whether this reflects household composition, housing form, settlement history, or another unmeasured local condition.

Poland shares some physical characteristics with Germany, including a fluvial flood setting and the recurring importance of built-environment indicators. Its typology and regression structure remain distinct. The income and household-size component, the suburban family-belt low-damage cluster, and the different slope and youth-rate patterns show that Poland should not be treated as a direct counterpart to the German case. Slope is negatively associated with direct damage in Germany but positively associated in Poland. One possible explanation is that Poland's less confined terrain allows infrastructure to be built on sloping land that remains exposed to flooding. This is a contextual interpretation and not a direct test of flood mechanics.

No comparable large-scale warning or institutional failure was identified in the material reviewed for the Polish event. The discussion therefore focuses on terrain, settlement structure, and typology differences, while recognizing that unmeasured response conditions may also have influenced observed impacts.

6.3.4. Spain

Spain's typology is distinguished by road density, which is significant in both its direct and spatially lagged effects. Higher local road density is associated with a greater probability of belonging to a higher damage category. The positive spatial lag indicates that the surrounding road-density context is also associated with damage. The Valencia event illustrates how transport corridors can channel, concentrate, and themselves sustain flood impacts (Fekete et al., 2025). Taken together, these findings are consistent with a broader infrastructure-intensive pattern of damage across connected urban areas.

Spain's socio-demographic indicators also show a distinct local and neighborhood pattern. At the grid-cell level, the composite socio-demographic component is negatively associated with damage. Its spatial lag, together with lags of education, income, women's share, and foreign share, is positively associated with damage. This pattern suggests that socio-demographic conditions are spatially structured. Central cells with high socio-demographic intensity may have limited mapped damage, while surrounding metropolitan areas combine different settlement, infrastructure, and exposure conditions. The protection associated with the Turia diversion provides relevant context, but it was not represented in the spatial model and cannot be treated as a tested explanation.

Response time adds a further dimension to Spain's resilience profile. Analyses of the October 2024 Valencia event describe delayed emergency alerts, late mobilization of resources, and institutional disputes over responsibility during the crisis (Fekete et al., 2025; Hedgecoe, 2024). These governance conditions lie outside the spatial indicator system, yet they may have shaped how exposure and susceptibility translated into damage and loss. In an area with high asset concentration along roads and urban belts, slow warning and weak coordination can intensify the consequences of severe flooding. Spain's typologies should therefore be interpreted in relation to physical exposure, socio-demographic structure, and crisis-management capacity.

6.4. Implications and Contributions

6.4.1. Policy Implications

The cross-case findings support a place-based flood policy focus on dense urban infrastructure, coordination across neighboring jurisdictions, and locally adapted warning and response systems. These implications draw on recurring physical patterns while recognizing that terrain, flood dynamics, and governance condi-

tions differ across regions. This focus on vulnerability, not hazard alone, is consistent with broader evidence that global declines in flood-related fatalities since the mid-1990s, despite continued population growth in flood-prone areas, are primarily attributable to vulnerability reduction measures such as improved risk awareness and structural defenses, rather than to any reduction in flood hazard itself (Merz et al., 2021).

Across all four regions, the clusters with the highest damage share have high built mass, dense road networks, and proximity to population centers. These urban-core typologies can support risk-based land-use planning. Areas with concentrated roads, buildings, and critical infrastructure can be prioritized for structural protection, retrofit measures, and flood-compatible development controls (Dharmavaram et al., 2017). The regression results support this focus because road density and built mass are among the most consistently significant indicators across the four cases.

Risk reduction measures should also reduce dependence on single facilities. Shelters, health services, and emergency resources can be distributed across several accessible locations, since a centrally located facility may be damaged or isolated during the same event it is intended to address. Measures such as soil-cover maintenance, flood storage, and space for rivers can complement building-level resilience measures in dense urban areas (Dharmavaram et al., 2017).

The spatially lagged coefficients found throughout the regression results complicate a purely local reading of risk, and here too there is a useful parallel in existing planning practice. Several indicators, including distance to critical infrastructure and, in Germany and Spain, the aging and socio-demographic mass components, carry significant effects through their spatial lag rather than, or in addition to, their direct value, meaning a grid cell's damage outcome depends partly on the conditions of its neighbors. This mirrors a documented weakness in conventional flood mapping, where sharply delineated flood zone boundaries understate the real uncertainty at their edges, so that a facility located just outside a mapped flood line can face a similar risk to one inside it (Dharmavaram et al., 2017). Norfolk, Virginia's response to this problem, using deliberately fuzzy boundaries between risk zones in its long-term planning framework instead of sharp lines, offers one way to build this uncertainty into land use decisions (Dharmavaram et al., 2017). For flood risk planning generally, this argues against drawing intervention boundaries strictly along administrative lines, since neighboring municipalities or districts with elevated vulnerability can influence outcomes beyond their own borders. Coordination across municipal boundaries would better match the spatial structure the regression results reveal.

The cross-regional comparison also shows that similar indicator combinations do not necessarily carry the same policy implications everywhere. As discussed in the regional characteristics above, Germany's terrain-driven constraints on warning lead time and Spain's political fragmentation during the 2024 event both suggest that governance and response capacity interact with the physical vulnerability typology. Italy stands apart from the other three cases in a different way, where the flat, slow-onset character of the Emilia-Romagna floods appears to have moderated damage severity even without a comparable governance story. This divergence indicates that while physical susceptibility indicators travel reasonably well across contexts, their translation into intervention priorities depends on the local governance and planning legacy and the terrain-driven pace of a flood event itself, and typologies derived from one country should not be applied uncritically to another without accounting for these differences (Fekete et al., 2025).

Germany and Spain also show the importance of warning and response systems. Structural protection cannot remove all flood risk, and defenses can create downstream risk or encourage over-reliance if they are treated as complete protection (Dharmavaram et al., 2017). Warning systems should therefore remain part of flood-risk planning. They also require redundancy, since floods can damage the communication infrastructure used to issue alerts. Manual systems such as sirens or horns can provide a backup when digital networks fail (Thieken et al., 2023).

6.4.2. Academic Contribution

Section 1.5 introduced disaster and emergency management as a Grand Challenge (Miller et al., 2025), a framing this thesis returns to here in light of its empirical findings. Rising flood frequency and severity are increasingly outpacing the capacity of purely structural defenses, making evidence-based, vulnerability-focused approaches such as the one developed here an increasingly necessary complement to hazard-centered planning (Birkmann et al., 2013; UNISDR, 2015). Beyond the specific findings discussed above, this thesis contributes to that broader effort in three respects.

First, prior vulnerability typology research has repeatedly identified a lack of empirical validation against observed impacts as a persistent gap, since most typologies are constructed and interpreted without formally testing whether they hold across more than one case (Moreira et al., 2021). By comparing the profiles and damage associations of independently derived typologies across four countries, this thesis responds to the need for empirical validation beyond single-case studies. The comparison identifies a recurring physical vulnerability profile across the cases, while the social and institutional features vary by region.

Second, the thesis develops a structured approach for comparing independently estimated clusters and regional regression models. The comparison uses damage shares, standardized cluster profiles, regression significance, and a cross-method evidence table. This approach avoids direct comparison of raw coefficients or cluster means across models with different samples and predictor sets. It provides a transparent basis for identifying recurring indicators while preserving country-specific interpretation.

Third, the regional analysis identifies institutional coordination and warning systems as an important interpretive layer beyond the spatial indicators modeled in this thesis. Evidence from Germany and Spain suggests that forecasting, warning issuance, and evacuation decisions shaped how physical exposure and susceptibility translated into observed impacts. These mechanisms were not tested in the spatial models, but they provide a relevant extension for future vulnerability research. This multi-actor dimension of flood risk, distinct from and additional to the spatial indicators modeled here, is consistent with calls in the disaster literature for flood risk to be understood as jointly produced by physical exposure and the institutional systems responsible for managing it (Merz et al., 2021), and represents a natural extension of the spatial vulnerability perspective developed in this thesis toward the multi-actor systems that determine whether that vulnerability is realized as damage.

6.5. Methodological Reflections and Limitations

The analytical workflow adopted in this thesis involved a series of choices regarding spatial resolution, clustering, and regression specification, each of which carries implications for how the results should be interpreted. This section reflects on these choices, on the limitations of the underlying data, and on how both may have shaped the typologies identified and the estimated relationships with flood damage.

Working at a 100 m grid across multiple municipalities and four countries required a resolution fine enough to capture within-city variation while remaining computationally manageable across large study areas. This choice smooths some local variation that a finer grid, or parcel-level data, would preserve, particularly for compact urban features such as individual buildings. Administrative boundaries also vary in size and shape between countries and sit awkwardly against a uniform grid, so the same physical distance can represent different fractions of a municipality depending on the case study region. The consistency gained by applying one resolution across all four countries came at the cost of resolution appropriate to each individual context.

Clustering involved a similar trade-off between rigor and computational feasibility. The optimal number of clusters was determined using a single random state due to computational constraints. The selected values range from $k = 2$ in Italy to $k = 3$ in Germany, Poland, and Spain. These choices should be treated as indicative, and repeated runs across multiple random states would provide a stronger assessment of cluster stability. Hierarchical clustering was considered, and given that the typology literature this thesis draws on (Rufat, 2012; Tate et al., 2025) generally favors hierarchical methods for their reproducibility and lack of dependence on a predefined k, it may be the more defensible choice going forward, provided sufficient computational capacity is available to run it at this scale.

The regression stage went through a comparable process of trial and correction before settling on its final specification. Reintroducing indicators pruned during blockwise PCA back into the regression input table, in an attempt to broaden the distribution of predictors, proved counterproductive, as the pruned variables carried missing values that effectively told the optimizer every observation had a strictly positive outcome. A staged VIF procedure was applied instead, screening all candidate predictors in an OLS framework and removing any exceeding a threshold of 5 before repeating the check on the reduced matrix. Poisson and negative binomial models were also tested; dispersion values were low enough across all regions for Poisson to be preferred. For Germany specifically, reattaching raw census indicators reduced the usable sample from 802 to 295 cells, since those variables covered only around a third of the flood event footprint, and within that smaller sample fewer than 2 percent of observations were zero, making the model unusable. Excluding the raw census indicators restored the full sample and a more balanced zero rate, after which the model converged. Given that

the damage variable is a composite score rather than a genuine count, and that a two-part hurdle structure implies a zero-generating mechanism distinct from the damage process itself, an ordinal logit specification was ultimately adopted as the primary approach, with the count-based models retained as a record of the specification search.

Although the likelihood ratio test confirms that including spatially lagged covariates significantly improves model fit in every region, this test only establishes that the added lag terms are jointly different from zero, a comparatively low bar, particularly given the large sample sizes in Italy and Spain ($n > 10{,}000$), where even modest improvements in fit are readily detected as statistically significant. The residual Moran's I test asks a stronger question, whether spatial dependence in the model's errors has been fully absorbed, and the two results can diverge. Spatially lagged covariates can carry genuine, statistically significant explanatory power without fully resolving the spatial structure present in the residuals. This is consistent with the pattern as shown in Table 5.20 in Chapter 5. Italy and Spain pass the likelihood ratio test but show little to no reduction in residual spatial autocorrelation, suggesting that whatever spatial dependence remains is not well captured by lagging the observed covariates alone.

Beyond these specification choices, several limitations in the underlying data affect how the indicators themselves should be interpreted. Income variables are not defined consistently across the four countries, varying in whether they refer to taxable or net income and whether they are measured per household or per tax unit, which limits strict cross-country comparability even where the variable name is shared. Documentation and metadata for most indicators were only available in the national language of the corresponding case study, and translation, assisted where necessary by AI tools, may not have captured every definitional nuance precisely. Several socio-economic and demographic datasets are also subject to statistical disclosure control, including statistical suppression (Statistisches Bundesamt (Destatis), 2024) and the newer cell-key methods (Enderle & Kleber, 2024) applied to preserve confidentiality at fine spatial scales. In some cases indicators had to be represented through proxies where a more direct measure existed elsewhere but was unavailable for a given country. These forms of measurement inconsistency are difficult to correct for after the fact and likely contribute some of the noise observed in the weaker regression relationships.

Indicator construction required several country-specific validation steps. These included correcting spatial joins for count variables, interpreting disclosure-control codes, harmonizing percentage and fractional scales, and verifying that source variables matched their intended concepts. These checks improved consistency across the four case studies, but they also show the difficulty of combining independently structured national datasets. Detailed examples are provided in Appendix F.

Source-level validation also identified inconsistencies in derived indicators. Italy's mean household income indicator initially combined a population-weighted income allocation with a separate household-count denominator. This produced extreme outliers in sparsely populated census sections because the numerator and denominator followed different spatial distributions. The final procedure used household counts as the allocation weight for the income total. This ensured that the numerator and denominator were based on the same source structure.

The indicator selection process itself carries forward limitations from the literature review stage. Relying on existing systematic reviews and purposive literature searches as starting points means some relevant frameworks or indicators may not have been captured. Country-specific studies employing PCA or factor analysis, used to refine the indicator set for local relevance, were also unevenly available across the four regions, meaning some countries' indicator selection benefited from more targeted local evidence than others. Finally, dimensions of vulnerability identified as conceptually important but consistently under-represented in the literature, such as health status, preparedness, and social cohesion, could not be operationalized as spatial indicators due to data availability constraints, and remain part of the interpretive context discussed in this chapter's regional analyses rather than the spatial indicator system itself.

A further limitation concerns the information captured by the hazard indicators. Slope, elevation, NDVI, distance to river, and HAND describe a grid cell's position within flood-prone terrain. They do not measure the depth, velocity, duration, or timing of the floodwater that reached each location. Damage reflects both vulnerability and flood intensity. Two grid cells with similar vulnerability profiles may experience very different impacts if one is exposed to deeper or faster water. Each regional model focuses on a single flood event, which avoids pooling fundamentally different events within the same regression. Substantial variation in flood depth, velocity, duration, and timing remains within each event. The models cannot fully separate haz-

ard intensity from vulnerability-related associations.

Two further limitations concern how consistently the indicators represent conditions in space and time. The Copernicus elevation product used in this thesis is a digital surface model instead of a bare-earth digital terrain model. Buildings and tree canopy can therefore inflate elevation values, especially in urban and forested cells. A bias-corrected version of the DEM (Hawker et al., 2022) was identified only near the end of the analysis and was not incorporated, though it would be a natural substitution for future iterations. Temporal alignment is a separate concern, since the analysis is essentially a single cross-section for each country and the underlying datasets are not perfectly aligned in time with the flood events themselves. Census data in particular predates some of the events by several years, and for Germany the 2022 census was used to characterize conditions during a 2021 flood, meaning population and socio-economic indicators may not fully reflect conditions at the time of the event.

Dasymetric mapping introduces a related limitation. WorldPop population was used as the ancillary surface for several extensive variables. WorldPop is itself a modeled population surface informed by settlement and built-environment covariates. Variables redistributed through the same weighting surface can therefore inherit a shared spatial pattern. This may contribute to the strong correlations among count variables and to the broad socio-demographic mass components identified through blockwise PCA. The procedure was necessary to achieve a common grid resolution, but components based mainly on extensive variables should be interpreted partly as measures of spatial concentration alongside their substantive social meaning.

The impact variable carries its own limitations, and these matter more than any single indicator limitation, since they affect what the regression is estimating in the first place. Grid cells without a Copernicus damage grading were treated as zero damage. This assumes that missing grades indicate no observed damage and do not reflect incomplete mapping coverage. The underlying grades come from remote sensing interpretation of satellite imagery, and although the Copernicus Emergency Management Service applies collective quality control across releases, some grading bias is plausible, particularly for the possibly damaged category, which is better understood as a confidence flag than as a genuine midpoint between no damage and confirmed damage. Infrastructure damage is also, by necessity, used as a proxy for flood impact more broadly, which likely explains why the indicators most strongly associated with damage in this thesis tend to relate to physical susceptibility more than social or human susceptibility, since the dependent variable itself is a physical measure. Other dimensions of impact, such as loss of life, displacement, or broader economic disruption, are not captured here and would typically require survey data (Fekete et al., 2025), emergency service records (Moreira et al., 2021), or social media based measures (Kruspe et al., 2021), all considerably harder to obtain consistently across four European countries.

Relative to the gaps identified by Moreira et al. (2021) in prior vulnerability typology work, this thesis addresses dimensionality reduction directly, is explicit about the disaggregation choices made at each stage, and applies some sensitivity testing to the correlation threshold used in blockwise PCA, settling on 0.9 after comparing several alternatives, and to the determination of k through multiple clustering methods. A fuller sensitivity analysis, covering the correlation threshold, the minimum non-null share used to admit indicators, and the stability of k across random states, remains a limitation shared with much of the reviewed literature (Hamidi et al., 2025; Moreira et al., 2021), and would strengthen confidence in the typologies reported here.

A further limitation concerns how far these findings can be generalized. Four flood events across four countries were deliberately chosen for their scale and for their diversity in flood mechanism, terrain, and institutional context. This supports some transferability in kind, since the recurring importance of built mass and road density across all four regions is a pattern worth taking seriously. It does not establish how common this pattern is across the wider range of European flood types, since coastal and pluvial flooding are not represented in this sample. The country-specific divergences documented in this chapter, such as Germany's built-mass reversal, are also limited to the small number of cases available and should not be read as a full account of when and why such reversals occur. A larger and more varied set of cases would be needed before these patterns can be treated as general findings instead of illustrative ones.

Several refinements follow directly from the limitations discussed above. Repeating the clustering procedure across multiple random states, and applying hierarchical clustering at full scale, would test the stability of the reported typologies. Replacing built surface and built volume with built surface and built height would introduce genuinely independent variation into the built environment indicators, instead of two measures derived from the same underlying source. Incorporating the bias-corrected DEM and more temporally consis-

tent socio-economic data would address the spatial and temporal misalignments noted above. Finally, the nearest-neighbor imputation used for HAND values in Italy, where flat terrain caused the underlying hydrological computation to fail, is defensible given that the median value is close to zero, but a raster-based recomputation with a corrected DEM would be more rigorous for the small number of non-zero pockets associated with levees and embankments.

6.6. Future Research

Several directions for future research follow from the findings and methodological reflections presented in this chapter. The clustering and regression stages in this thesis were run in parallel on the same indicator set. A sequential design could first identify typological groups through clustering and then estimate separate regressions within each group. This approach could identify indicator-damage relationships that differ between urban-core, rural-periphery, and suburban typologies (Lazarevic et al., 1999).

A second extension would apply Local Indicators of Spatial Association (LISA) directly to vulnerability indicators or damage outcomes. LISA could identify statistically significant hot and cold spots and provide a more direct measure of local spatial concentration than the current overlay of damage on cluster typologies.

Residual Moran's I remains statistically significant in all four regions even after fitting the SLX specification, indicating that spatially lagged covariates alone do not fully absorb the spatial dependence present in the data. This could reflect spatially patterned determinants of damage not captured by the indicator set used here, such as local emergency response capacity or infrastructure condition, or it could reflect genuine spatial diffusion in damage itself, for instance where damage to one building's utility connections propagates to physically connected neighboring structures. Distinguishing between these explanations is not possible from the residual diagnostic alone. A spatial error model, which explicitly models spatial dependence in the error term, or a spatial autoregressive specification that lags the damage outcome itself, would be a natural next step for isolating which mechanism is driving this remaining structure, and is left for future work.

Beyond the analytical structure, several data-related extensions would strengthen future applications of this approach. Incorporating more temporally dynamic socio-economic indicators would help address the temporal misalignment between data collection and flood events discussed in the methodological reflections, and would allow the typologies to better reflect conditions closer to the time of impact. Extending the analysis to additional hazard types, such as coastal or pluvial flooding, or to further regions beyond the four cases studied here, would test whether the recurring built-mass and infrastructure-density signal holds more broadly or is specific to the fluvial and flash-flood contexts examined in this thesis. Finally, translating the typologies into an operational tool, such as a dashboard that flags high-risk combinations of indicators for planners, would help bridge the gap between the academic contribution of this thesis and its practical use, though this would first require the sensitivity and robustness testing outlined earlier in this chapter to ensure the underlying typologies are stable enough to support real decisions. Together, these directions connect the spatial patterns identified in this thesis to the broader challenge of integrating vulnerability evidence into flood risk management and climate adaptation practice across Europe (Birkmann et al., 2013; UNISDR, 2015).

7

Conclusion

This chapter returns to the main research question and summarizes the answers to the three sub-research questions. It then presents the central empirical contribution of the thesis.

To what extent do theoretical flood vulnerability indicators align with actual post-disaster impact zones to define spatial typologies across recent European flood events?

The main research question is answered below through the three sub-research questions.

SQ 1: Which indicators are identified in academic literature as the critical drivers of flood vulnerability?

Desk research grounded in recent systematic reviews of flood vulnerability frameworks (Hamidi et al., 2025; Moreira et al., 2021; Shehzad et al., 2026; Tabasi et al., 2025) produced a structured indicator set organized around the Integrated Risk Linkages framework, separating hazard from susceptibility and further dividing susceptibility into physical, social, and human dimensions. A hybrid deductive-inductive approach was used. The literature-derived framework provided a common conceptual backbone, while country-specific vulnerability studies informed the selection and interpretation of locally relevant indicators. This process supported the inclusion of indicators such as elderly population structure in Germany, where prior research identifies older residents as an important vulnerability group (Fekete, 2010).

The resulting list covers five hazard indicators, NDVI, distance to nearest river, HAND, elevation, and slope, alongside physical susceptibility indicators (road density, distance to critical infrastructure) and a set of social and human susceptibility indicators spanning income, poverty, unemployment, population density, household composition, and age structure. SQ 1 is answered through a literature-grounded indicator framework that guided the spatial operationalization in the subsequent chapters. Data availability and cross-country harmonization limited the inclusion of several resilience-related and detailed social vulnerability dimensions. These factors therefore remained part of the interpretive context in the Discussion.

SQ 2: Using spatial statistics, to what extent do the mapped vulnerability indicators cluster and correlate with the actual flood impact zones?

The spatial analysis shows that the mapped indicators cluster and correlate with observed flood impact zones to a meaningful extent, though the strength and form of this relationship differs by indicator domain. Blockwise PCA reduced the indicator set while preserving domain content, and in every region extensive variables coalesced into a small number of components representing built mass and broad socio-demographic volume, while hazard variables and most intensive indicators remained interpretable as singletons. This structure carried through to clustering and regression. Each region contained an urban-core cluster that was distinct from rural, peripheral, or suburban profiles. The urban-core clusters had the highest share of damaged grid cells in all four cases. They were consistently characterized by high road density and high built mass, while socio-demographic components varied in composition across regions. Spatial regression added a grid-level perspective. Road density had a positive and statistically significant direct association with damage in all four regions. Built-mass components also appeared among the most important predictors, although Germany

showed a negative association linked to local valley conditions. Socio-demographic components were significant in selected cases, but their direction and composition differed across regions.

The analysis also refines the theoretical treatment of social vulnerability indicators. Poverty, income, education, age, employment, and household measures frequently formed broad components of socio-demographic volume instead of separate dimensions. At the 100 m grid scale, these indicators often reflected the spatial concentration of people, services, and resources within the same areas.

SQ 2 is therefore answered by showing that mapped indicators align with observed impact zones to a meaningful extent. The strongest and most consistent relationships concern the built environment, especially road density and built mass. Socio-demographic conditions contribute to the high-impact typologies, though their composition and regression effects differ across countries.

SQ 3: Based on these spatial correlations, what high-impact vulnerability typologies consistently emerge across case studies?

Comparing the four case studies on the basis of damage share in lieu of raw damaged grid counts reveals a consistent urban core typology across flood events in Germany, Italy, Poland, and Spain that combines high built mass, dense road networks, low vegetation cover, and proximity to critical infrastructure. This typology held even in Italy, where the wider rural periphery cluster dominates the study area, since the smaller urban core cluster nonetheless carries a substantially higher share of damaged grids. Road density provides the strongest shared signal across methods and countries. It is elevated in every highest-damage-share urban-core cluster and has a positive, statistically significant regression association with damage in all four regions. Built mass also recurs in the urban-core typology and is important in three regional models, while Germany shows a negative association linked to the location of urban development within the Ahr Valley.

The socio-demographic composition attached to this physical core is less consistent, varying with each country's settlement pattern and the specific structure of its census indicators. Case-specific factors outside the spatial indicator system, such as the terrain-driven compression of warning lead time in Germany's Ahr Valley, the flat, slow-onset character of the Emilia-Romagna floods, and institutional fragmentation during the 2024 Valencia floods, help explain differences in damage severity that the regression coefficients alone cannot fully account for. SQ 3 is answered through a two-part typology. The transferable physical core consists of dense roads, high built mass, and concentrated infrastructure within urban areas. The socio-demographic and governance dimensions require local interpretation because their composition and relationship with damage vary across countries.

The main research question is answered as follows. Theoretical flood vulnerability indicators align with observed post-disaster impact zones to a meaningful extent. The strongest alignment concerns built environment indicators, especially road density and built mass. The resulting spatial typologies show a recurring urban-core profile with a high concentration of damaged grid cells across all four flood events.

Socio-demographic indicators also contribute to vulnerability patterns, but their structure and association with damage vary across countries. Mapped indicators can therefore support the identification of areas where flood damage is likely to concentrate. Their use in policy requires local knowledge of settlement patterns, terrain, planning history, warning systems, and emergency response capacity.

This thesis contributes a cross-case perspective to flood vulnerability research by applying a literature-derived indicator framework to empirical damage data from four European flood events. The analysis compares independently derived typologies and regression results across cases, responding to the limited validation against observed impacts identified in previous vulnerability research (Moreira et al., 2021).

The methodological reflections, policy implications, and future research directions identify several ways to strengthen this approach. The central empirical contribution is the identification of a recurring urban-core vulnerability pattern across diverse European flood events. Its physical built-environment features recur across cases, while its socio-demographic and institutional context remains locally specific.

References

Adger, W. N. (2006). Vulnerability. *Global Environmental Change*, *16*(3), 268–281. https://doi.org/10.1016/j.gloenvcha.2006.02.006

Alabbad, Y., & Demir, I. (2022). Comprehensive flood vulnerability analysis in urban communities: Iowa case study. *International Journal of Disaster Risk Reduction*, *74*, 102955. https://doi.org/10.1016/j.ijdrr.2022.102955

Amadio, M., Mysiak, J., & Marzi, S. (2018). Mapping socioeconomic exposure for flood risk assessment in italy. *Risk Analysis*, *39*(4), 829–845. https://doi.org/10.1111/risa.13212

Bekić, D. (2026). Loss of life in river and flash floods in europe: Evaluation of deterministic approaches and implications for risk assessment. *Water*, *18*(9), 1011. https://doi.org/10.3390/w18091011

Birkmann, J., Cardona, O. D., Carreño, M. L., Barbat, A. H., Pelling, M., Schneiderbauer, S., Kienberger, S., Keiler, M., Alexander, D., Zeil, P., & Welle, T. (2013). Framing vulnerability, risk and societal responses: The move framework. *Natural Hazards*, *67*(2), 193–211. https://doi.org/10.1007/s11069-013-0558-5

Biswas, A. K., & Tortajada, C. (2020). China can water down impact of floods - Third World Centre for Water Management — thirdworldcentre.org [[Accessed 12-03-2026]].

Blaikie, P., Cannon, T., Davis, I., & Wisner, B. (1994). *At risk: Natural hazards, people's vulnerability, and disasters*. Routledge.

Blöschl, G., Kiss, A., Viglione, A., Barriendos, M., Böhm, O., Brázdil, R., Coeur, D., Demarée, G., Llasat, M. C., Macdonald, N., Retsö, D., Roald, L., Schmocker-Fackel, P., Amorim, I., Bělínová, M., Benito, G., Bertolin, C., Camuffo, D., Cornel, D., … Wetter, O. (2020). Current european flood-rich period exceptional compared with past 500 years. *Nature*, *583*(7817), 560–566. https://doi.org/10.1038/s41586-020-2478-3

Bonnevie, I. M., Hansen, H. S., & Schrøder, L. (2024). Dasymetric algorithms using land cover to estimate human population at smaller spatial scales. *ISPRS International Journal of Geo-Information*, *13*(12), 427. https://doi.org/10.3390/ijgi13120427

Buijs, J., Cosoveanu, F., Bakker, M., & Terpstra, T. (2020). Transition towards integrated flood risk management strategies. *Water Governance*, *3*, 67–75.

Caliński, T., & Harabasz, J. (1974). A dendrite method for cluster analysis. *Communications in Statistics*, *3*(1), 1–27. https://doi.org/10.1080/03610927408827101

Castro-Melgar, I., Falaras, T., Basiou, E., & Parcharidis, I. (2025). Assessment of the october 2024 cut-off low event floods impact in valencia (spain) with satellite and geospatial data. *Remote Sensing*, *17*(13), 2145. https://doi.org/10.3390/rs17132145

Charrad, M., Ghazzali, N., Boiteau, V., & Niknafs, A. (2014). NbClust: An R package for determining the relevant number of clusters in a data set. *Journal of Statistical Software*, *61*(6), 1–36. https://doi.org/10.18637/jss.v061.i06

Copernicus. (2024). Definition and digitisation of area of interest | copernicus ems on demand mapping [[Online; accessed 2026-06-06]]. https://mapping.emergency.copernicus.eu/about/rapid-mapping-manual/related-documents/definition-and-digitisation-of-area-of-interest/

Copernicus Land Monitoring Service. (2021). Normalised difference vegetation index 2020-present (raster 300 m), global, 10-daily - version 2. https://doi.org/10.2909/AE760A70-708E-459A-8EEC-6852462A5FAF

Crichton, D. (2001). *The implications of climate change for the insurance industry: An update and outlook to 2020*. BRE.

Cutter, S. L., Boruff, B. J., & Shirley, W. L. (2003). Social vulnerability to environmental hazards[*]. *Social Science Quarterly*, *84*(2), 242–261. https://doi.org/10.1111/1540-6237.8402002

Cutter, S. L., & Finch, C. (2008). Temporal and spatial changes in social vulnerability to natural hazards. *Proceedings of the National Academy of Sciences*, *105*(7), 2301–2306. https://doi.org/10.1073/pnas.0710375105

D'Angelo, A., & Toth, F. (2026). The essence of crisis decision-making: Saving ravenna during the 2023 floods. *Risk, Hazards & Crisis in Public Policy*, *17*(2). https://doi.org/10.1002/rhc3.70057

Davies, D. L., & Bouldin, D. W. (1979). A cluster separation measure. *IEEE Transactions on Pattern Analysis and Machine Intelligence*, *PAMI-1*(2), 224–227. https://doi.org/10.1109/TPAMI.1979.4766909

Dawson, R. J., Ball, T., Werritty, J., Werritty, A., Hall, J. W., & Roche, N. (2011). Assessing the effectiveness of non-structural flood management measures in the thames estuary under conditions of socio-economic and environmental change. *Global Environmental Change*, *21*(2), 628–646. https://doi.org/10.1016/j.gloenvcha.2011.01.013

Dharmavaram, S., Stanton-Geddes, Z., & Chia, B. (2017, April). *Land use planning for urban flood risk management* (tech. rep.). World Bank Group, Urban Floods Community of Practice (UFCOP). Washington, DC.

Diakakis, M., Deligiannakis, G., Antoniadis, Z., Melaki, M., Katsetsiadou, K.-N., Andreadakis, E., Spyrou, N. I., & Gogou, M. (2020). Proposal of a flash flood impact severity scale for the classification and mapping of flash flood impacts. *Journal of Hydrology*, *590*, 125452. https://doi.org/10.1016/j.jhydrol.2020.125452

Dong, S., Esmalian, A., Farahmand, H., & Mostafavi, A. (2020). An integrated physical-social analysis of disrupted access to critical facilities and community service-loss tolerance in urban flooding. *Computers, Environment and Urban Systems*, *80*, 101443. https://doi.org/10.1016/j.compenvurbsys.2019.101443

Doocy, S., Daniels, A., Murray, S., & Kirsch, T. D. (2013). The human impact of floods: A historical review of events 1980-2009 and systematic literature review. *PLoS Currents*, *5*, ecurrents.dis.f4deb457904936b07c09daa98ee8171 https://doi.org/10.1371/currents.dis.f4deb457904936b07c09daa98ee8171a

Enderle, T., & Kleber, B. (2024). Geheimhaltung mit der cell-key-methode im zensus 2022. *WISTA-Wirtschaft und Statistik*, *76*(6), 82–91.

European Commission, Joint Research Centre. (2020). *Manual for cems-rapid mapping products: Valid for the portfolio since april 2019, status 31 august 2020.* Publications Office. https://doi.org/10.2760/29876

European Commission, Joint Research Centre. (2023). *Towards a european wide vulnerability framework: A flexible approach for vulnerability assessment using composite indicators.* Publications Office. https://doi.org/10.2760/353889

European Environment Agency (EEA). (2019). Eu-hydro river network database 2006-2012 (vector), europe - version 1.3, nov. 2020. https://doi.org/10.2909/393359A7-7EBD-4A52-80AC-1A18D5F3DB9C

European Environment Agency (EEA). (2025). Climate Preparedness 2025 — discomap.eea.europa.eu [[Accessed 12-03-2026]].

European Space Agency. (2022). Copernicus dem. https://doi.org/10.5270/esa-c5d3d65

Eurostat. (2024). *Regions in the european union: Nomenclature of territorial units for statistics (nuts) : 2024 edition.* Publications Office. https://doi.org/10.2785/714519

Fang, B., Bevacqua, E., Rakovec, O., & Zscheischler, J. (2024). An increase in the spatial extent of european floods over the last 70 years. *Hydrology and Earth System Sciences*, *28*(16), 3755–3775. https://doi.org/10.5194/hess-28-3755-2024

Fang, B., Rakovec, O., Bevacqua, E., Kumar, R., & Zscheischler, J. (2025). Diverging trends in large floods across europe in a warming climate. *Communications Earth & Environment*, *6*(1). https://doi.org/10.1038/s43247-025-02734-y

Fekete, A. (2010). *Assessment of social vulnerability for river-floods in germany* [Doctoral dissertation, Universitäts- und Landesbibliothek Bonn].

Fekete, A., Estrany, J., & Ramírez, M. Á. A. (2025). Cascading impact chains and recovery challenges of the 2024 valencia catastrophic floods. *Discover Sustainability*, *6*(1). https://doi.org/10.1007/s43621-025-01483-4

Fekete, A., & Sandholz, S. (2021). Here comes the flood, but not failure? lessons to learn after the heavy rain and pluvial floods in germany 2021. *Water*, *13*(21), 3016. https://doi.org/10.3390/w13213016

García Guzmán, P. (2026). *Ineatlas: Access to spanish household income distribution atlas data* [R package version 0.2.0]. https://github.com/pablogguz/ineatlas

Hamidi, A. R., Novo, P., Paavola, J., & Ford, J. D. (2025). Identifying gaps in research on social vulnerability to floods: A systematic review of indicators, indexes, and methodological approaches. *Environmental Research Letters*, *20*(11), 113006. https://doi.org/10.1088/1748-9326/ae1496

Hawker, L., Uhe, P., Paulo, L., Sosa, J., Savage, J., Sampson, C., & Neal, J. (2022). A 30 m global map of elevation with forests and buildings removed. *Environmental Research Letters*, *17*(2), 024016. https://doi.org/10.1088/1748-9326/ac4d4f

Hedgecoe, G. (2024, November). Spain floods: Accusations fly over who is to blame for disaster [[Online; accessed 2026-06-13]]. https://www.bbc.com/news/articles/cp8xy03zk44o

Hendry, A., Haigh, I. D., Nicholls, R. J., Winter, H., Neal, R., Wahl, T., Joly-Laugel, A., & Darby, S. E. (2019). Assessing the characteristics and drivers of compound flooding events around the uk coast. *Hydrology and Earth System Sciences*, *23*(7), 3117–3139. https://doi.org/10.5194/hess-23-3117-2019

Hidayah, E., Wiyono, R. U. A., & Wicaksono, A. D. (2021). Development of the flood vulnerability index using a multi-element approach. *Journal of Water and Land Development*, 255–264. https://doi.org/10.24425/jwld.2021.138181

Houston, D., Werritty, A., Ball, T., & Black, A. (2020). Environmental vulnerability and resilience: Social differentiation in short- and long-term flood impacts. *Transactions of the Institute of British Geographers*, *46*(1), 102–119. https://doi.org/10.1111/tran.12408

Huang, X., Wang, C., Li, Z., & Ning, H. (2020). A 100 m population grid in the conus by disaggregating census data with open-source microsoft building footprints. *Big Earth Data*, *5*(1), 112–133. https://doi.org/10.1080/20964471.2020.1776200

International Federation of Red Cross and Red Crescent Societies. (2023, June). Italy flood 2023, dref operation mdrit004 - italy | reliefweb [[Online; accessed 2026-06-13]]. https://reliefweb.int/report/italy/italy-flood-2023-dref-operation-mdrit004

Istat. (2026). Italian National Institute of Statistics [Accessed: 2026-05-14]. https://www.istat.it/en/

Jolliffe, I. T., & Cadima, J. (2016). *Principal component analysis: A review and recent developments* (Vol. 374). https://doi.org/10.1098/rsta.2015.0202

Kałmykow-Piwińska, A., & Witkowska, K. (2026). Impact of the 2024 flood event on trace elements contamination in floodplain sediments at the mouth of the nysa kłodzka river into the odra valley. *Environmental Geochemistry and Health*, *48*(9). https://doi.org/10.1007/s10653-026-03284-8

Kaufman, L., & Rousseeuw, P. J. (1990). *Finding groups in data: An introduction to cluster analysis*. John Wiley & Sons. https://doi.org/10.1002/9780470316801

Koks, E. E., Rozenberg, J., Zorn, C., Tariverdi, M., Vousdoukas, M., Fraser, S. A., Hall, J. W., & Hallegatte, S. (2019). A global multi-hazard risk analysis of road and railway infrastructure assets. *Nature Communications*, *10*(1). https://doi.org/10.1038/s41467-019-10442-3

Koks, E. E., van Ginkel, K. C. H., van Marle, M. J. E., & Lemnitzer, A. (2022). Brief communication: Critical infrastructure impacts of the 2021 mid-july western european flood event. *Natural Hazards and Earth System Sciences*, *22*(12), 3831–3838. https://doi.org/10.5194/nhess-22-3831-2022

Kruspe, A., Kersten, J., & Klan, F. (2021). Review article: Detection of actionable tweets in crisis events. *Natural Hazards and Earth System Sciences*, *21*(6), 1825–1845. https://doi.org/10.5194/nhess-21-1825-2021

Lazarevic, A., Xu, X., Fiez, T., & Obradovic, Z. (1999). Clustering-regression-ordering steps for knowledge discovery in spatial databases. *IJCNN'99. International Joint Conference on Neural Networks. Proceedings (Cat. No. 99CH36339)*, *4*, 2530–2534.

Li, C., Cheng, X., Li, N., Du, X., Yu, Q., & Kan, G. (2016). A framework for flood risk analysis and benefit assessment of flood control measures in urban areas. *International Journal of Environmental Research and Public Health*, *13*(8), 787. https://doi.org/10.3390/ijerph13080787

Li, Z., Tan, J., Yang, L., Xie, Z., Qin, Y., & Li, Y. (2026). Revealing the dynamics and multidimensional resilience of rainstorm-flood cascade disasters in mountain valley cities: An interpretable machine learning case study from southwestern china. *Reliability Engineering & System Safety*, *274*, 112418. https://doi.org/10.1016/j.ress.2026.112418

Liang, Y., Qi, M., Yang, Z., Zhang, X., & Duan, X. (2026). Robustness of spatial interdependent networks under extreme geographically localized attacks. *Reliability Engineering & System Safety*, *274*, 112406. https://doi.org/10.1016/j.ress.2026.112406

Lieth, J. (2026). *z22: Official Gridded Data from the German Census 2022*. Version 1.1.4. https://github.com/jslth/z22/

Lloyd, S. P. (1982). Least squares quantization in PCM. *IEEE Transactions on Information Theory*, *28*(2), 129–137. https://doi.org/10.1109/TIT.1982.1056489

Loli, M., Kefalas, G., Dafis, S., Mitoulis, S. A., & Schmidt, F. (2022). Bridge-specific flood risk assessment of transport networks using gis and remotely sensed data. *Science of The Total Environment*, *850*, 157976. https://doi.org/10.1016/j.scitotenv.2022.157976

Marchi, M., Bertolini, I., Tumedei, E., Tonni, L., Gottardi, G., et al. (2025). The response of the river embankment systems of the emilia-romagna basins to may 2023 extensive floods. *Proceedings of the 31st EWG-IE meeting (European Club Working Group on Internal Erosion in Embankment Dams, Dikes and Levees and their Foundation) and the 6th EWG-OOE meeting (European Club Working Group on Overflow and Overtopping Erosion)*, 1–6.

McCarthy, J. J. e. a. (Ed.). (2001). *Climate change 2001: Impacts, adaptation, and vulnerability*. Cambridge University Press.

McCullagh, P. (1980). Regression models for ordinal data. *Journal of the Royal Statistical Society: Series B (Methodological)*, *42*(2), 109–127. https://doi.org/10.1111/j.2517-6161.1980.tb01109.x

Merz, B., Blöschl, G., Vorogushyn, S., Dottori, F., Aerts, J. C. J. H., Bates, P., Bertola, M., Kemter, M., Kreibich, H., Lall, U., & Macdonald, E. (2021). Causes, impacts and patterns of disastrous river floods. *Nature Reviews Earth & Environment*, *2*(9), 592–609. https://doi.org/10.1038/s43017-021-00195-3

Miller, T., Dé, L. L., & Hore, K. (2025). The adaptive shift: Embracing complexity in disaster and emergency management. *International Journal of Disaster Risk Reduction*, *119*, 105323. https://doi.org/10.1016/j.ijdrr.2025.105323

Mohr, S., Ehret, U., Kunz, M., Ludwig, P., Caldas-Alvarez, A., Daniell, J. E., Ehmele, F., Feldmann, H., Franca, M. J., Gattke, C., Hundhausen, M., Knippertz, P., Küpfer, K., Mühr, B., Pinto, J. G., Quinting, J., Schäfer, A. M., Scheibel, M., Seidel, F., & Wisotzky, C. (2022). A multi-disciplinary analysis of the exceptional flood event of july 2021 in central europe. part 1: Event description and analysis. https://doi.org/10.5194/nhess-2022-137

Moos, N., Juergens, C., & Redecker, A. P. (2021). Geo-spatial analysis of population density and annual income to identify large-scale socio-demographic disparities. *ISPRS International Journal of Geo-Information*, *10*(7), 432. https://doi.org/10.3390/ijgi10070432

Moragues, A., Estrany, J., & Ruiz-Pérez, M. (2025). Assessment of social vulnerability to floods based on fuzzy logic in a mediterranean dense urban area: Palma, mallorca, spain. *International Journal of Disaster Risk Reduction*, *125*, 105594. https://doi.org/10.1016/j.ijdrr.2025.105594

Moran, P. A. P. (1950). Notes on continuous stochastic phenomena. *Biometrika*, *37*(1/2), 17–23. https://doi.org/10.2307/2332142

Moreira, L. L., de Brito, M. M., & Kobiyama, M. (2021). Review article: A systematic review and future prospects of flood vulnerability indices. *Natural Hazards and Earth System Sciences*, *21*(5), 1513–1530. https://doi.org/10.5194/nhess-21-1513-2021

Murtagh, F., & Legendre, P. (2014). Ward's hierarchical agglomerative clustering method: Which algorithms implement ward's criterion? *Journal of Classification*, *31*(3), 274–295. https://doi.org/10.1007/s00357-014-9161-z

Neil Adger, W. (1999). Social vulnerability to climate change and extremes in coastal vietnam. *World Development*, *27*(2), 249–269. https://doi.org/10.1016/s0305-750x(98)00136-3

Nick, F. C., Sänger, N., van der Heijden, S., & Sandholz, S. (2023). Collaboration is key: Exploring the 2021 flood response for critical infrastructures in germany. *International Journal of Disaster Risk Reduction*, *91*, 103710. https://doi.org/10.1016/j.ijdrr.2023.103710

Nishino, K., Nayar, S., & Jebara, T. (2005). Clustered blockwise pca for representing visual data. *IEEE Transactions on Pattern Analysis and Machine Intelligence*, *27*(10), 1675–1679. https://doi.org/10.1109/tpami.2005.193

O'Brien, R. M. (2007). A caution regarding rules of thumb for variance inflation factors. *Quality & Quantity*, *41*(5), 673–690. https://doi.org/10.1007/s11135-006-9018-6

OpenStreetMap contributors. (2017). Planet dump retrieved from https://planet.osm.org.

Pallathadka, A., Sauer, J., Chang, H., & Grimm, N. B. (2022). Urban flood risk and green infrastructure: Who is exposed to risk and who benefits from investment? a case study of three u.s. cities. *Landscape and Urban Planning*, *223*, 104417. https://doi.org/10.1016/j.landurbplan.2022.104417

Park, M., Kim, D., Moon, K., & Park, T. (2020). Integrative analysis of multi-omics data based on blockwise sparse principal components. *International Journal of Molecular Sciences*, *21*(21), 8202. https://doi.org/10.3390/ijms21218202

Pesaresi, M., Schiavina, M., Politis, P., Freire, S., Krasnodębska, K., Uhl, J. H., Carioli, A., Corbane, C., Dijkstra, L., Florio, P., Friedrich, H. K., Gao, J., Leyk, S., Lu, L., Maffenini, L., Mari-Rivero, I., Melchiorri, M., Syrris, V., Van Den Hoek, J., & Kemper, T. (2024). Advances on the global human settlement layer by joint assessment of earth observation and population survey data. *International Journal of Digital Earth*, *17*(1). https://doi.org/10.1080/17538947.2024.2390454

Pitarch, S. (2024, October). Cronología de una alerta que llegó tarde: "cuando utiel y requena se inundan, se sabe lo que va a pasar después río abajo" [[Online; accessed 2026-06-10]]. https://www.eldiario.es/comunitat-valenciana/cronologia-alerta-llego-tarde-utiel-requena-inundan-pasar-despues-rio-abajo_1_11779079.html

Poussin, J. K., Bubeck, P., Aerts, J. C. J. H., & Ward, P. J. (2012). Potential of semi-structural and non-structural adaptation strategies to reduce future flood risk: Case study for the meuse. *Natural Hazards and Earth System Sciences*, *12*(11), 3455–3471. https://doi.org/10.5194/nhess-12-3455-2012

Pulvirenti, L., Squicciarino, G., Cenci, L., Virelli, M., Candela, L., & Puca, S. (2024). Daily monitoring of the may 2023 emilia-romagna flood using cosmo-skymed data. *IGARSS 2024 - 2024 IEEE International Geoscience and Remote Sensing Symposium*, 1358–1361. https://doi.org/10.1109/igarss53475.2024.10641960

Purwanto, A., Andrasmoro, D., & Eviliyanto, E. (2025). Comparative analysis of hand with twi flood-prone mapping models in data-scarce areas. *Indonesian Journal of Geography*, *57*(2). https://doi.org/10.22146/ijg.99160

Rey, S. J., & Anselin, L. (2009). Pysal: A python library of spatial analytical methods. In *Handbook of applied spatial analysis: Software tools, methods and applications* (pp. 175–193). Springer.

Reynolds, D. A. (2009). Gaussian mixture models. *Encyclopedia of Biometrics*, 659–663. https://doi.org/10.1007/978-0-387-73003-5_196

Rhein, B., & Kreibich, H. (2025). Causes of the exceptionally high number of fatalities in the ahr valley, germany, during the 2021 flood. *Natural Hazards and Earth System Sciences*, *25*(2), 581–589. https://doi.org/10.5194/nhess-25-581-2025

Rincón, D., Khan, U. T., & Armenakis, C. (2018). Flood risk mapping using gis and multi-criteria analysis: A greater toronto area case study. *Geosciences*, *8*(8), 275. https://doi.org/10.3390/geosciences8080275

Rousseeuw, P. J. (1987). Silhouettes: A graphical aid to the interpretation and validation of cluster analysis. *Journal of Computational and Applied Mathematics*, *20*, 53–65. https://doi.org/10.1016/0377-0427(87)90125-7

Roy, S., Bose, A., & Chowdhury, I. R. (2021). Flood risk assessment using geospatial data and multi-criteria decision approach: A study from historically active flood-prone region of himalayan foothill, india. *Arabian Journal of Geosciences*, *14*(11). https://doi.org/10.1007/s12517-021-07324-8

Rufat, S. (2012). Spectroscopy of urban vulnerability. *Annals of the Association of American Geographers*, *103*(3), 505–525. https://doi.org/10.1080/00045608.2012.702485

Rüttenauer, T. (2019). Spatial regression models: A systematic comparison of different model specifications using monte carlo experiments. *Sociological Methods & Research*, *51*(2), 728–759. https://doi.org/10.1177/0049124119882467

Saxena, A., Prasad, M., Gupta, A., Bharill, N., Patel, O. P., Tiwari, A., Er, M. J., Ding, W., & Lin, C.-T. (2017). A review of clustering techniques and developments. *Neurocomputing*, *267*, 664–681. https://doi.org/10.1016/j.neucom.2017.06.053

Scheider, S., & Huisjes, M. D. (2018). Distinguishing extensive and intensive properties for meaningful geocomputation and mapping. *International Journal of Geographical Information Science*, *33*(1), 28–54. https://doi.org/10.1080/13658816.2018.1514120

Shehzad, M. F., Lyeo, J. S., Bleibel, N., Haines, S. R., Spence, N. D., & Stopps, H. (2026). A scoping review of climate vulnerability indicators: Implications for neighborhood-level vulnerability. *Climatic Change*, *179*(3). https://doi.org/10.1007/s10584-026-04122-7

Statistics Poland. (2026). *Local data bank* [Accessed: 2026-05-13]. Główny Urząd Statystyczny. https://bdl.stat.gov.pl/bdl/start

Statistisches Bundesamt (Destatis). (2024, November). *Qualitätsbericht – zensus – 2022* (tech. rep. No. 05/2022) (See §1.3 (grid-cell-level evaluations, 100 m resolution) and §1.7.2 (Cell-Key-Methode; suppression of sparsely populated table cells)). Statistisches Bundesamt. Wiesbaden, Germany. Retrieved June 12, 2026, from https://www.destatis.de/DE/Methoden/Qualitaet/Qualitaetsberichte/Bevoelkerung/zensus-2022.pdf?__blob=publicationFile

Tabasi, N., Fereshtehpour, M., & Roghani, B. (2025). A review of flood risk assessment frameworks and the development of hierarchical structures for risk components. *Discover Water*, *5*(1). https://doi.org/10.1007/s43832-025-00193-2

Tanni, S. E., Patino, C. M., & Ferreira, J. C. (2020). Correlation vs. regression in association studies. *Jornal Brasileiro de Pneumologia*, *46*(1). https://doi.org/10.1590/1806-3713/e20200030

Taramelli, A., Righini, M., Valentini, E., Alfieri, L., Gatti, I., & Gabellani, S. (2022). Building-scale flood loss estimation through vulnerability pattern characterization: Application to an urban flood in milan, italy. *Natural Hazards and Earth System Sciences*, *22*(11), 3543–3569. https://doi.org/10.5194/nhess-22-3543-2022

Taromideh, F., Fazloula, R., Choubin, B., Emadi, A., & Berndtsson, R. (2022). Urban flood-risk assessment: Integration of decision-making and machine learning. *Sustainability*, *14*(8), 4483. https://doi.org/10.3390/su14084483

Tate, E., Rahman, M. A., Emrich, C. T., & Sampson, C. C. (2021). Flood exposure and social vulnerability in the united states. *Natural Hazards*, *106*(1), 435–457. https://doi.org/10.1007/s11069-020-04470-2

Tate, E., Rufat, S., Rahman, M. A., & Hoover, S. (2025). Profiles of social vulnerability for flood risk reduction. *International Journal of Disaster Risk Reduction*, *118*, 105250. https://doi.org/10.1016/j.ijdrr.2025.105250

Thieken, A. H., Bubeck, P., Heidenreich, A., von Keyserlingk, J., Dillenardt, L., & Otto, A. (2023). Performance of the flood warning system in germany in july 2021 – insights from affected residents. *Natural Hazards and Earth System Sciences*, *23*(2), 973–990. https://doi.org/10.5194/nhess-23-973-2023

Tobler, W. R. (1970). A computer movie simulating urban growth in the detroit region. *Economic Geography*, *46*, 234. https://doi.org/10.2307/143141

Tradowsky, J. S., Philip, S. Y., Kreienkamp, F., Kew, S. F., Lorenz, P., Arrighi, J., Bettmann, T., Caluwaerts, S., Chan, S. C., De Cruz, L., de Vries, H., Demuth, N., Ferrone, A., Fischer, E. M., Fowler, H. J., Goergen, K., Heinrich, D., Henrichs, Y., Kaspar, F., … Wanders, N. (2023). Attribution of the heavy rainfall events leading to severe flooding in western europe during july 2021. *Climatic Change*, *176*(7). https://doi.org/10.1007/s10584-023-03502-7

Turner, B. L., Kasperson, R. E., Matson, P. A., McCarthy, J. J., Corell, R. W., Christensen, L., Eckley, N., Kasperson, J. X., Luers, A., Martello, M. L., Polsky, C., Pulsipher, A., & Schiller, A. (2003). A framework for vulnerability analysis in sustainability science. *Proceedings of the National Academy of Sciences*, *100*(14), 8074–8079. https://doi.org/10.1073/pnas.1231335100

Uddin, M. N., Saiful Islam, A., Bala, S. K., Islam, G. T., Adhikary, S., Saha, D., Haque, S., Fahad, M. G. R., & Akter, R. (2019). Mapping of climate vulnerability of the coastal region of bangladesh using principal component analysis. *Applied Geography*, *102*, 47–57. https://doi.org/10.1016/j.apgeog.2018.12.011

UNISDR. (2015). Sendai framework for disaster risk reduction 2015–2030 [Adopted at the Third UN World Conference on Disaster Risk Reduction, Sendai, Japan, 18 March 2015].

Valente, M., Del Prete, C., Facci, G., Martino, A., Grilli, G. R., Bravi, F., Reno, C., & Ragazzoni, L. (2025). The 2023 floods in the emilia-romagna region, italy: A retrospective qualitative investigation into response strategies and criticalities. *International Journal of Disaster Risk Reduction*, *116*, 105089. https://doi.org/10.1016/j.ijdrr.2024.105089

Xu, J., Takahashi, M., & Li, W. (2024). Identifying vulnerable populations in urban society: A case study in a flood-prone district of wuhan, china. *Natural Hazards and Earth System Sciences*, *24*(1), 179–197. https://doi.org/10.5194/nhess-24-179-2024

Yin, H., Aryani, A., Petrie, S., Nambissan, A., Astudillo, A., & Cao, S. (2026). A rapid review of clustering algorithms. *Array*, *30*, 100904. https://doi.org/10.1016/j.array.2026.100904

Yu, J., Zou, L., Xia, J., Chen, X., Wang, F., & Zuo, L. (2023). A multi-dimensional framework for improving flood risk assessment: Application in the han river basin, china. *Journal of Hydrology: Regional Studies*, *47*, 101434. https://doi.org/10.1016/j.ejrh.2023.101434

Yu, Q., Wang, Y., & Li, N. (2022). Extreme flood disasters: Comprehensive impact and assessment. *Water*, *14*(8), 1211. https://doi.org/10.3390/w14081211

A

IRL Framework Component Figures

The following are the ready-to-use list of indicators from the Integrated Risk Linkages framework by Tabasi et al. (2025).

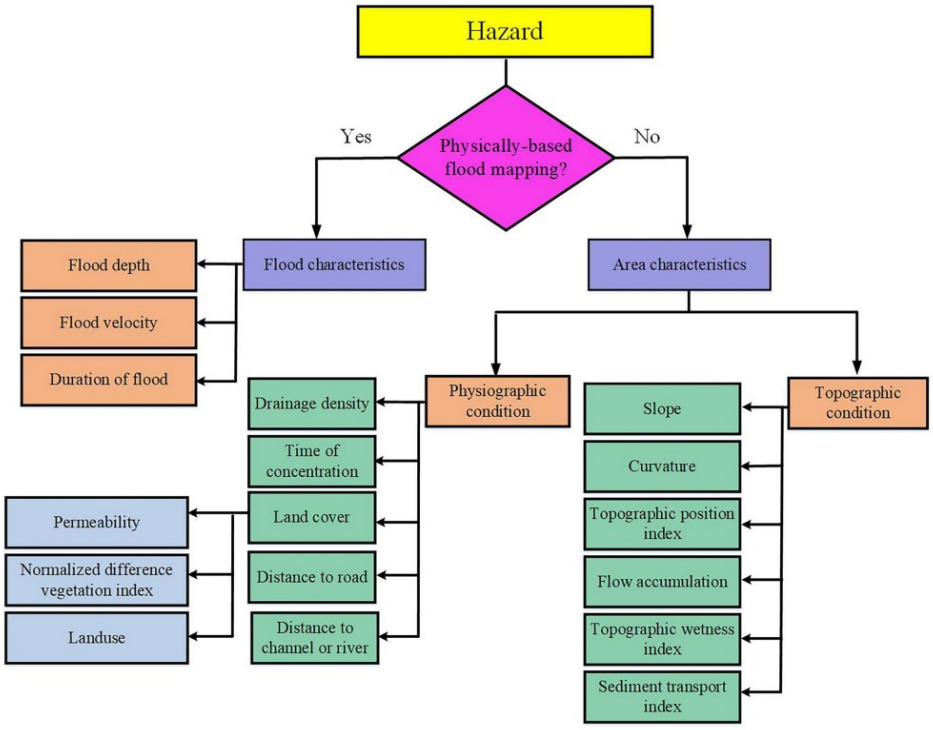


Figure A.1: Hazard hierarchy (Tabasi et al., 2025)

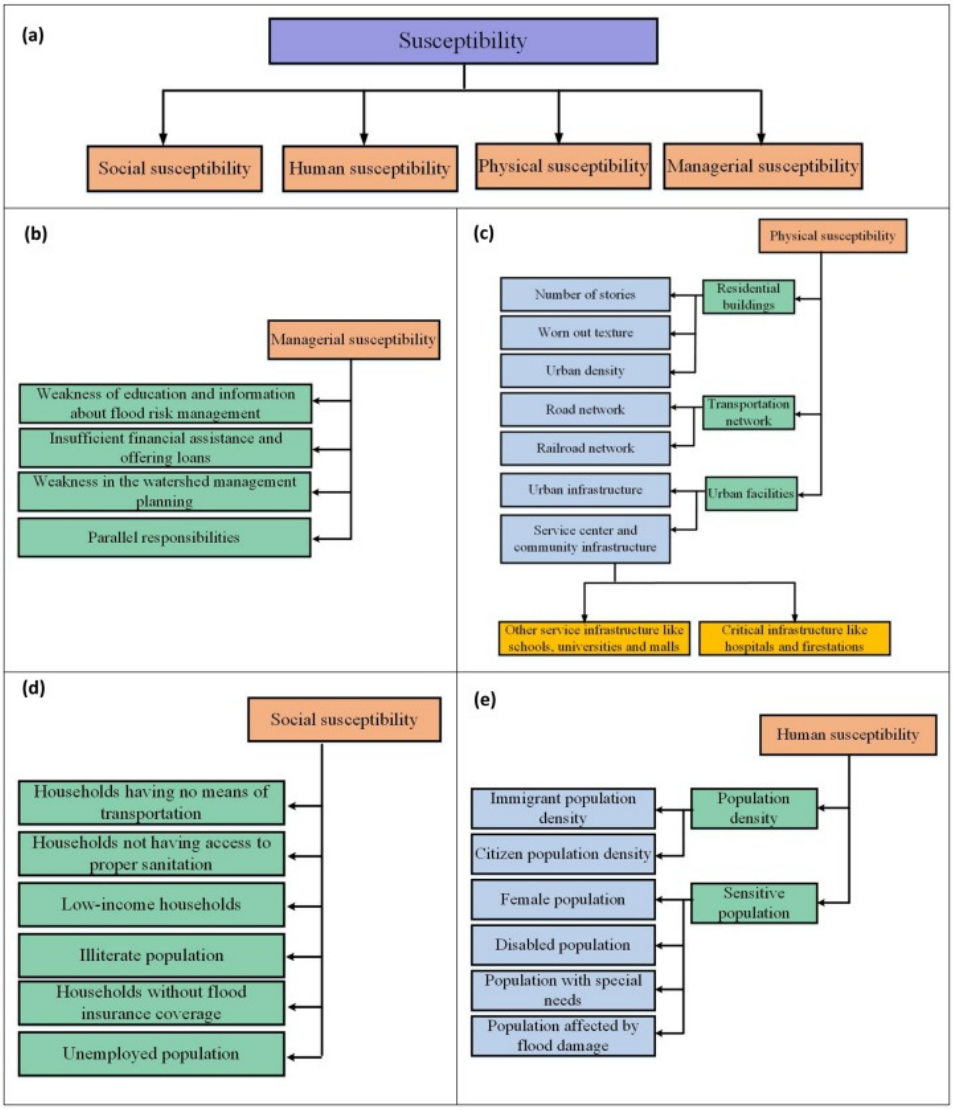


Figure A.2: Susceptibility hierarchy (Tabasi et al., 2025) a. Overall hierarchy; b. Managerial; c. Physical; d. Social; e. Human

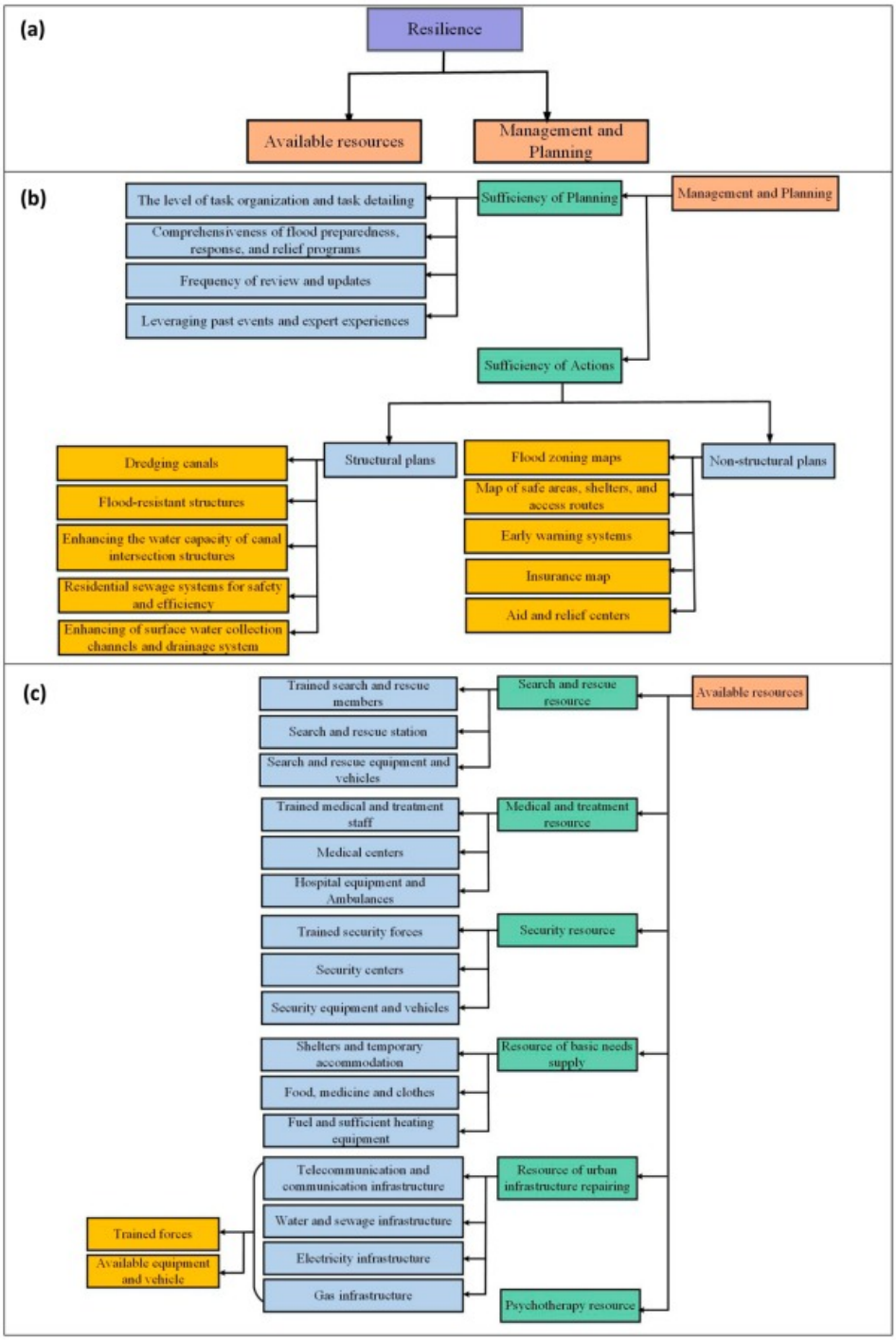


Figure A.3: Resilience hierarchy (Tabasi et al., 2025) a. Overall hierarchy; b. Management and planning; c. Available resources in flood resilience

B

Choropleths

This appendix shows the different choropleths of each region and segmented based on components based on the IRL framework.

B.1. Germany

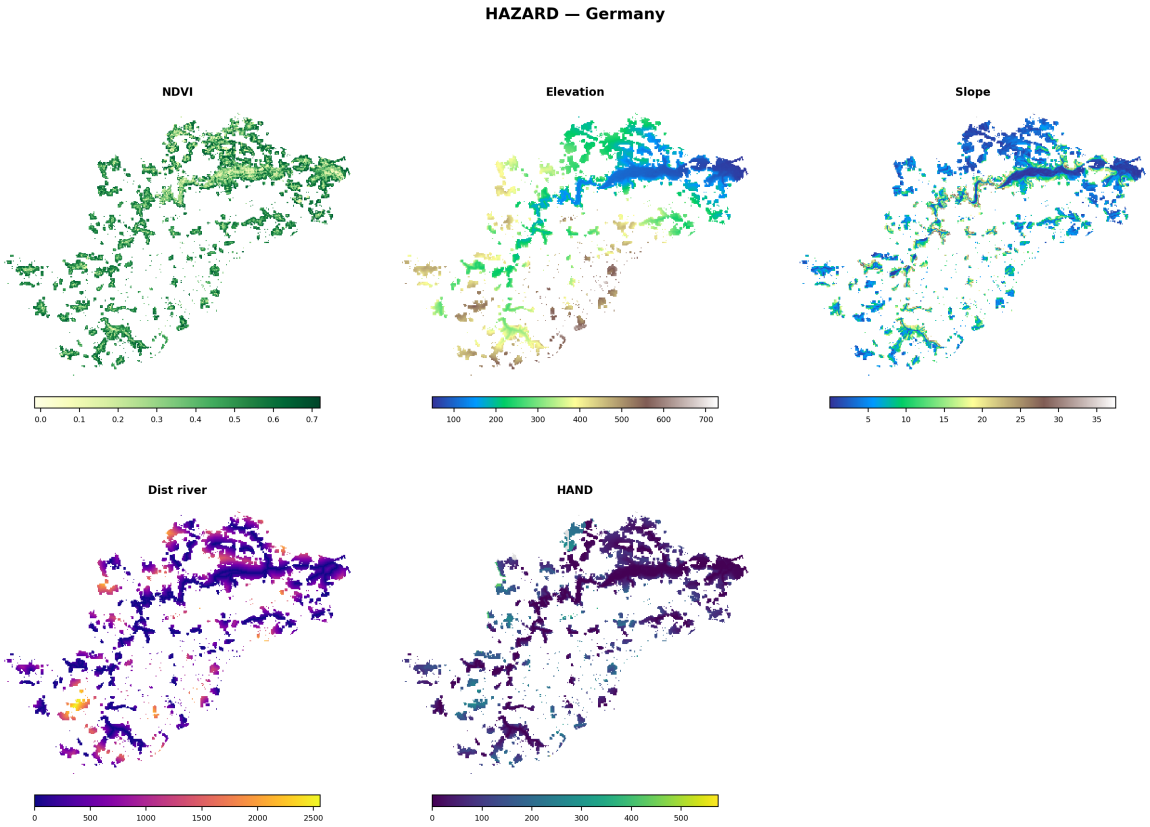


Figure B.1: Choropleths of hazard indicators for Germany.



Figure B.2: Choropleths of physical susceptibility indicators for Germany.

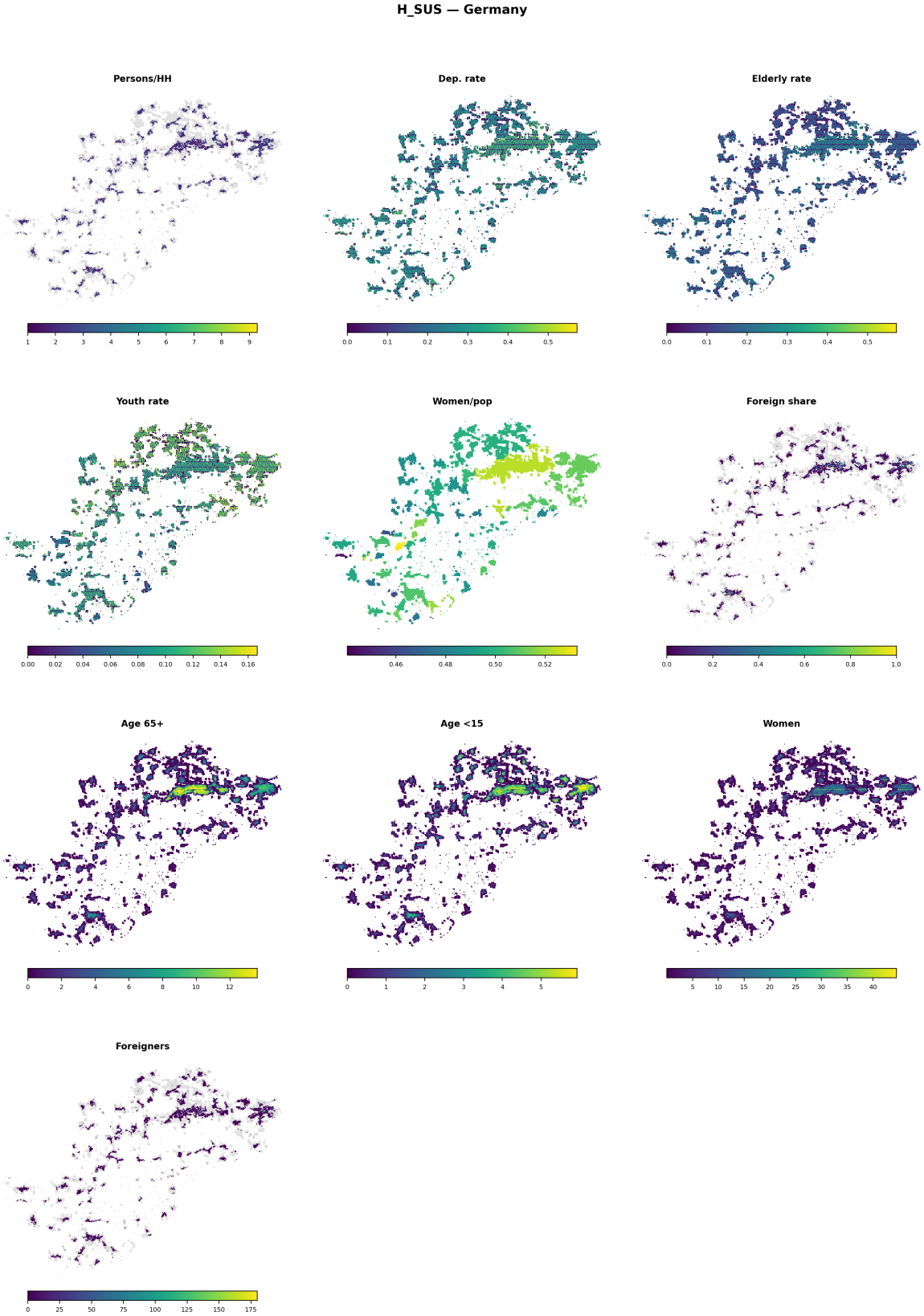


Figure B.3: Choropleths of human susceptibility indicators for Germany.

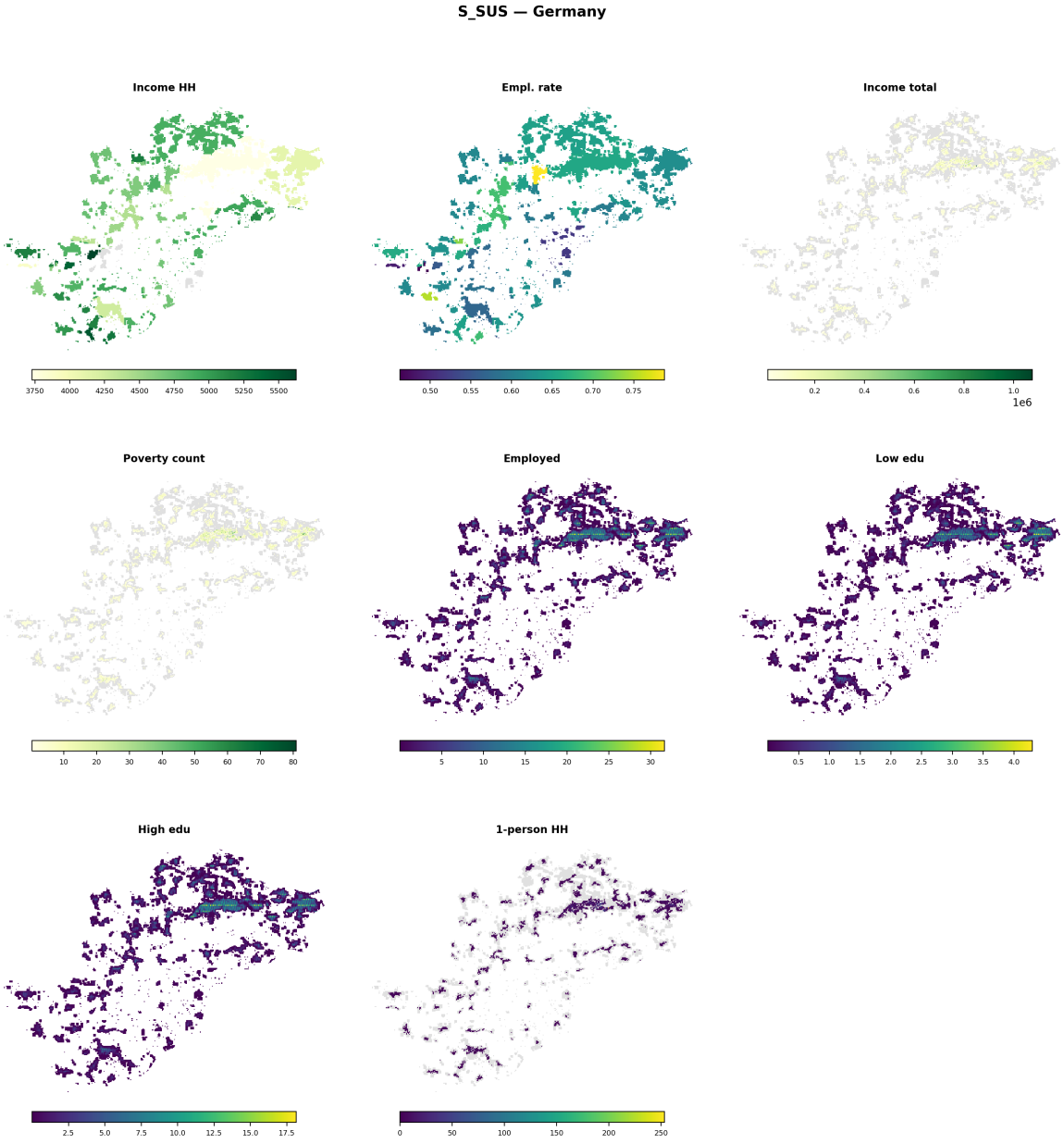


Figure B.4: Choropleths of social susceptibility indicators for Germany.

B.2. Italy

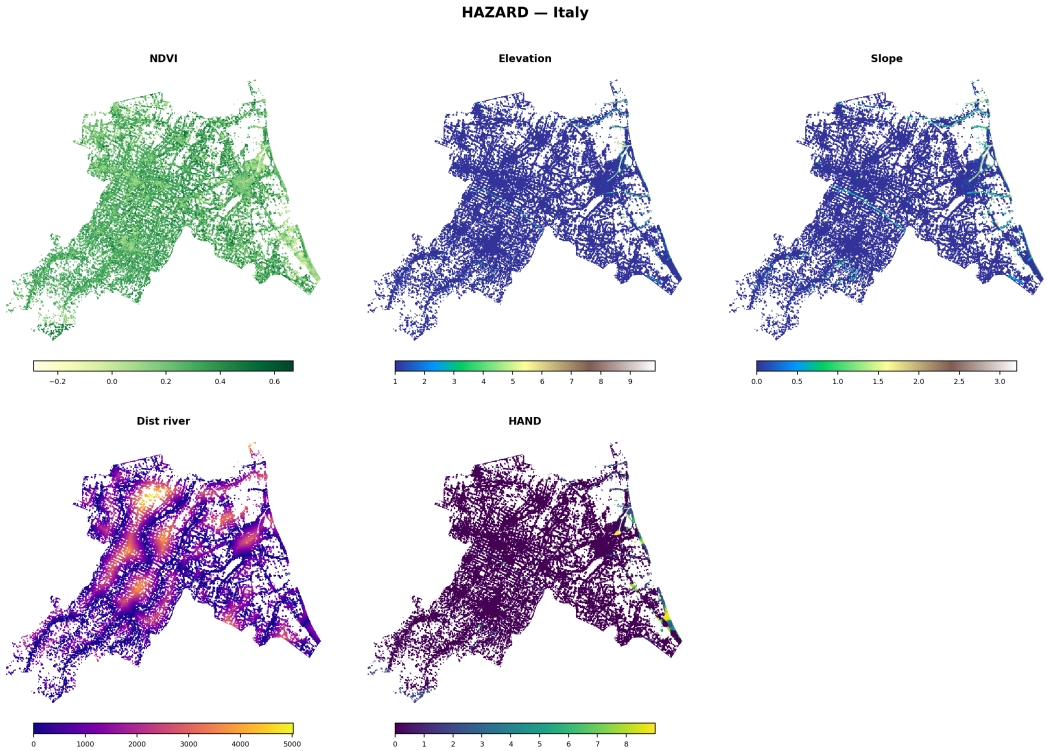


Figure B.5: Choropleths of hazard indicators for Italy.

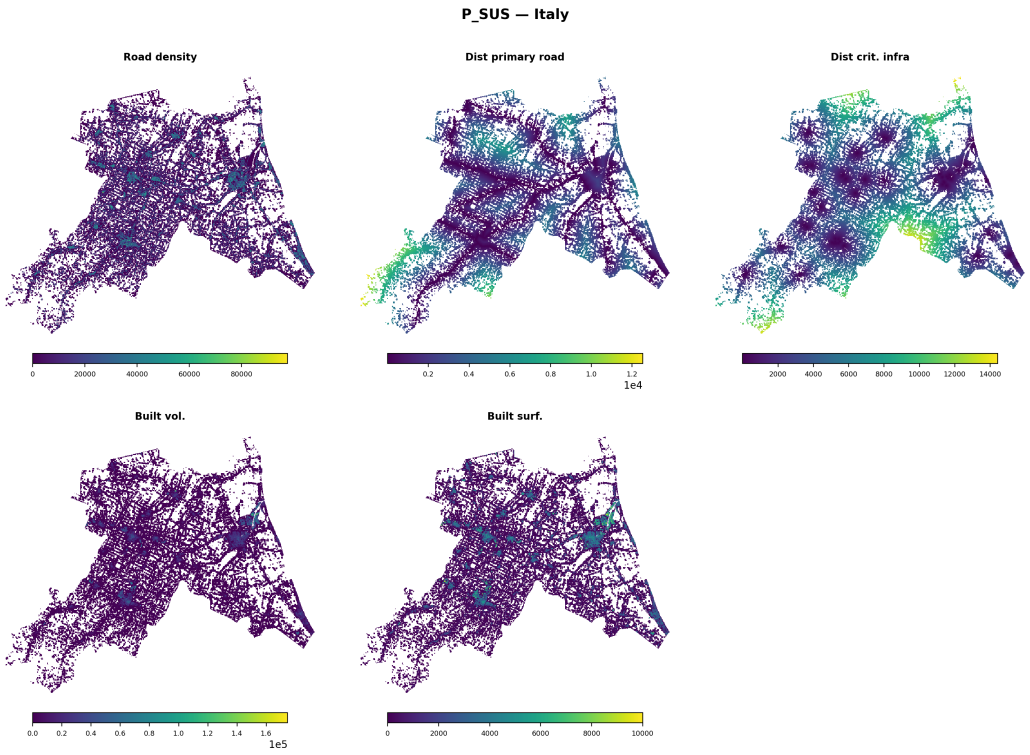


Figure B.6: Choropleths of physical susceptibility indicators for Italy.

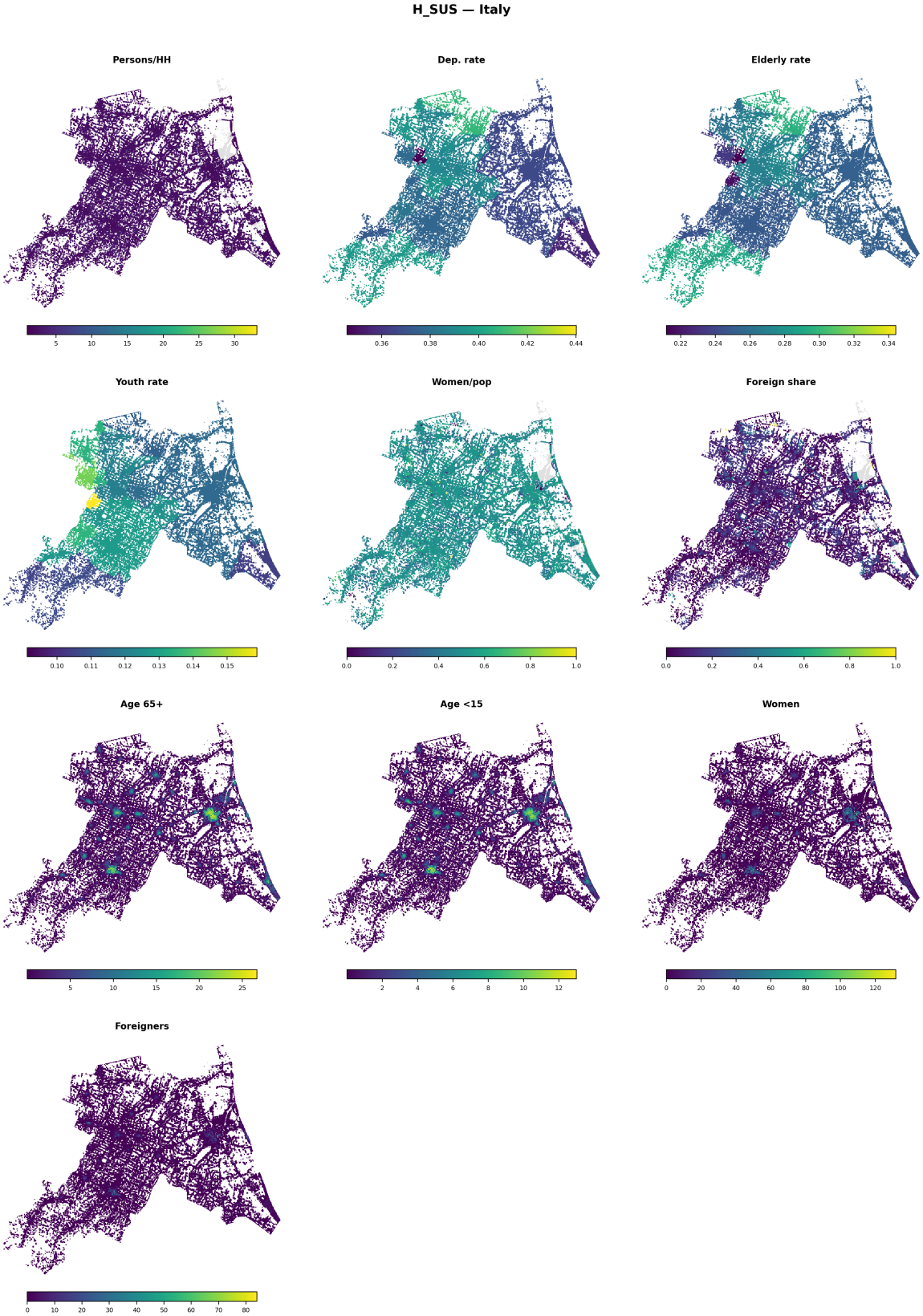


Figure B.7: Choropleths of human susceptibility indicators for Italy.

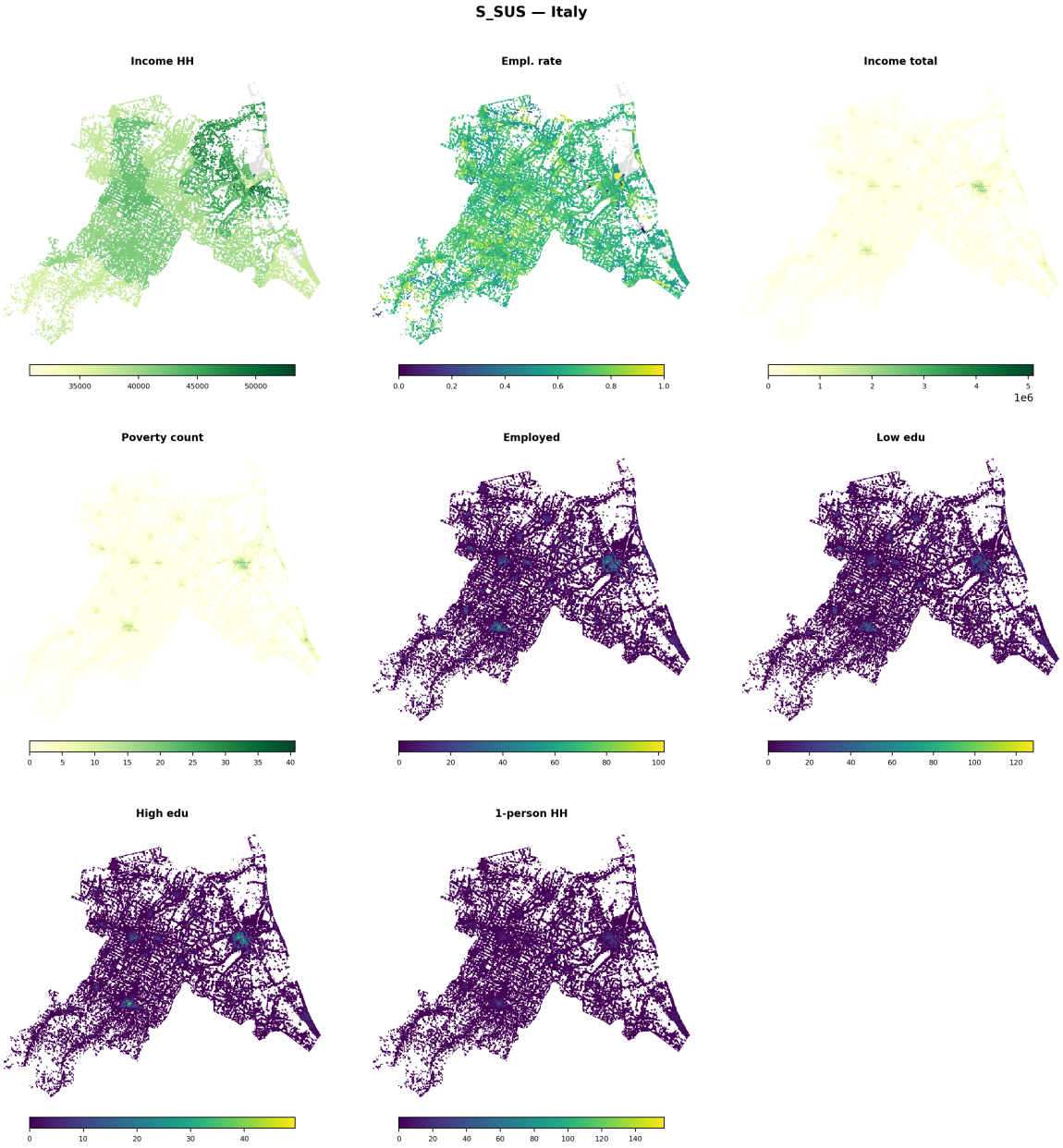


Figure B.8: Choropleths of social susceptibility indicators for Italy.

B.3. Poland

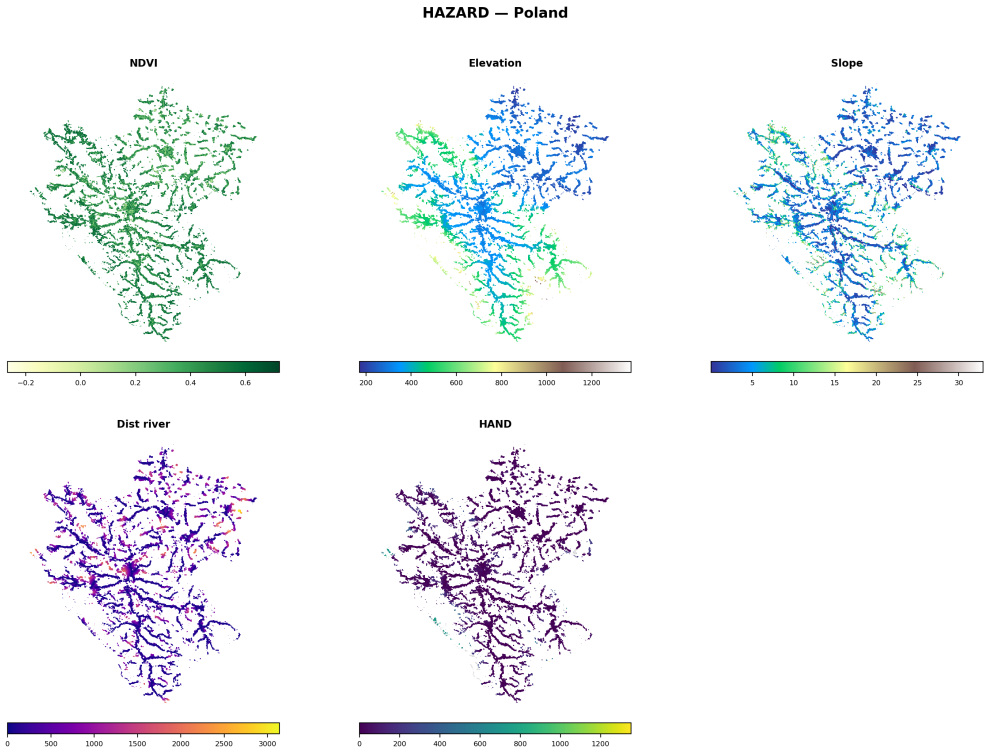


Figure B.9: Choropleths of hazard indicators for Poland.

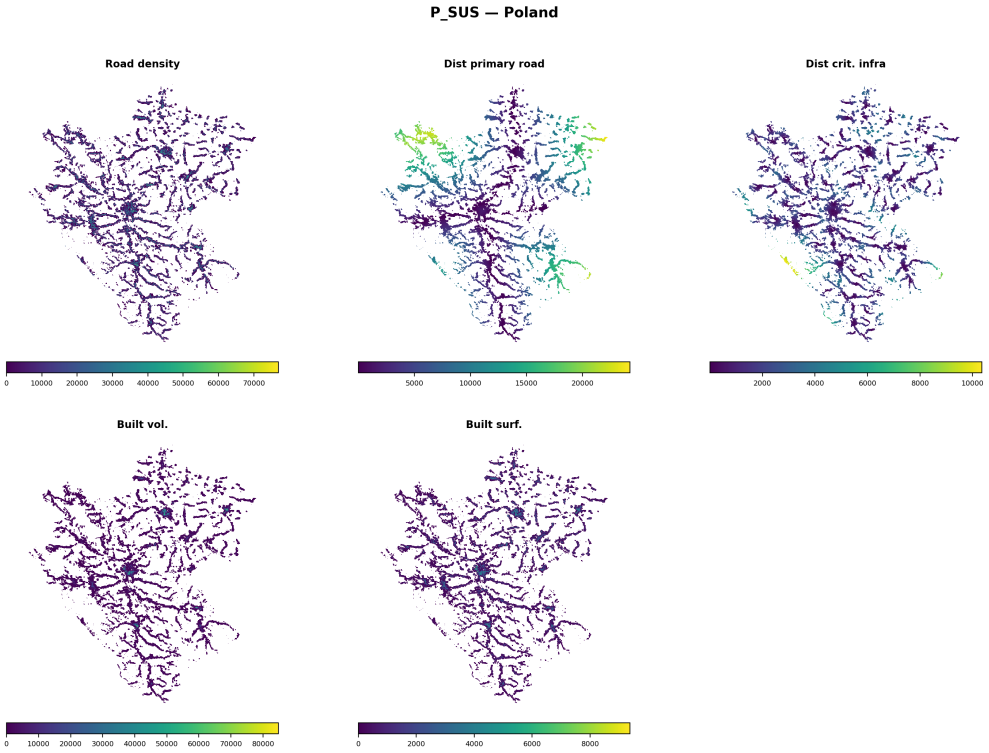


Figure B.10: Choropleths of physical susceptibility indicators for Poland.

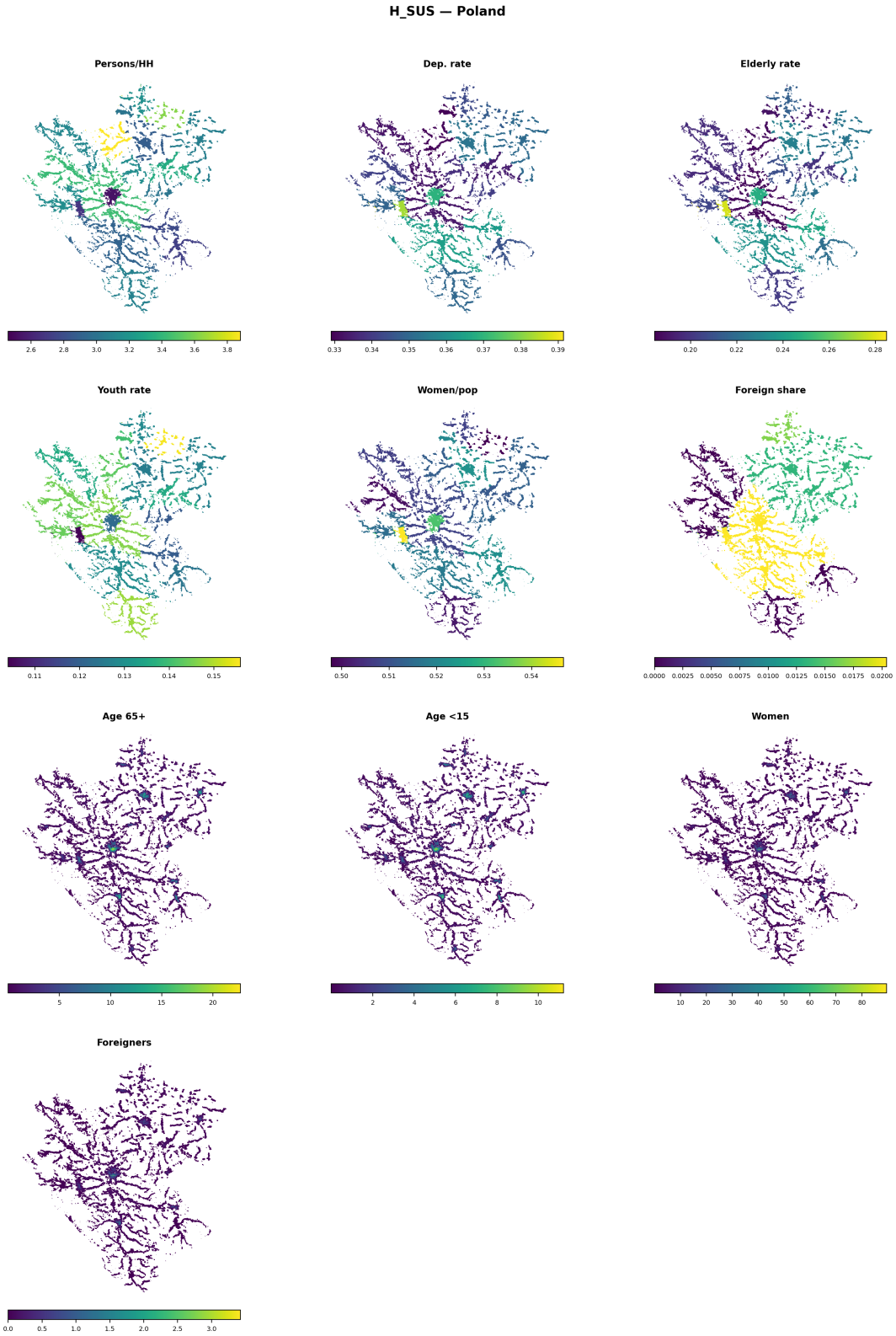


Figure B.11: Choropleths of human susceptibility indicators for Poland.

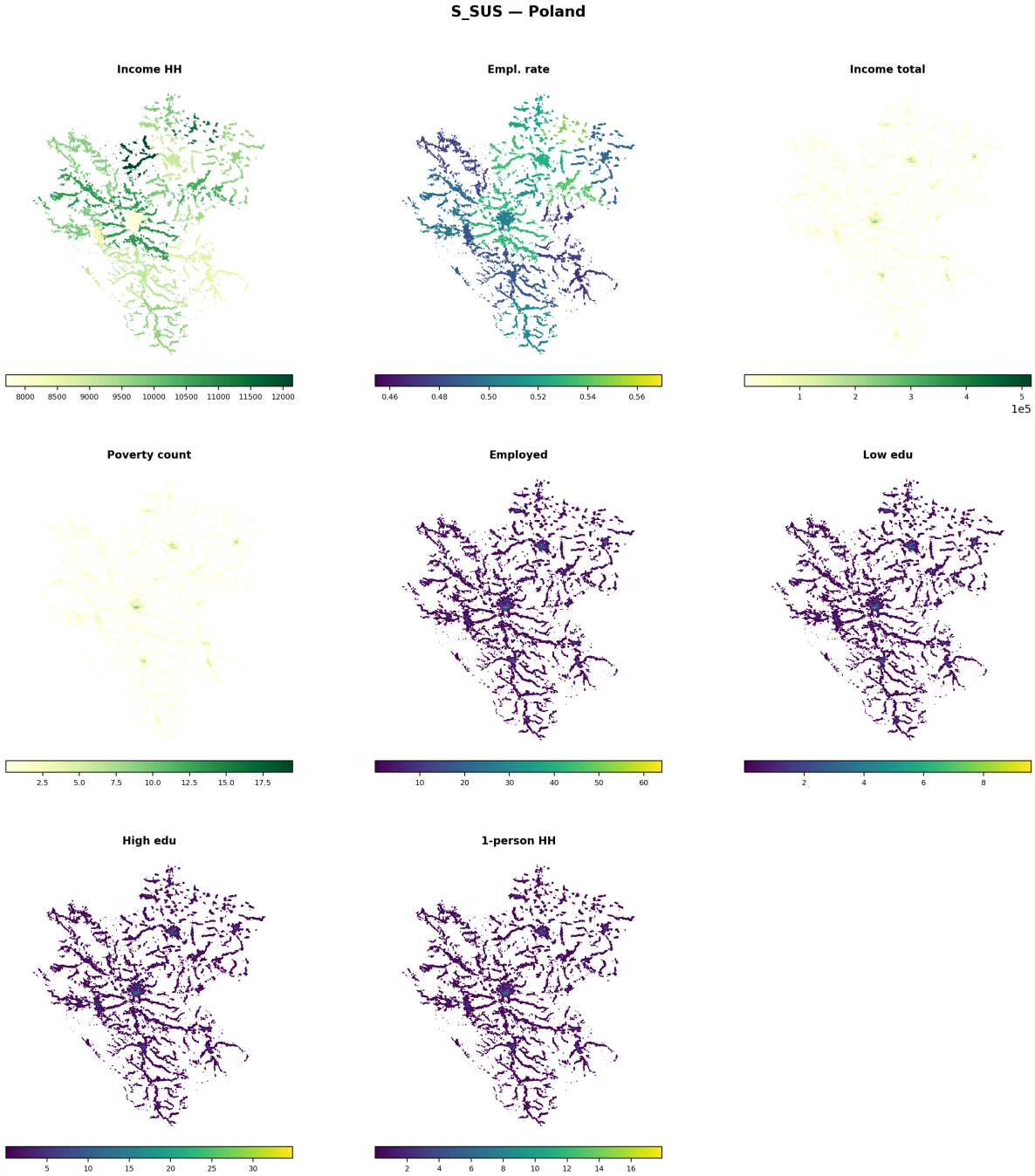


Figure B.12: Choropleths of social susceptibility indicators for Poland.

B.4. Spain

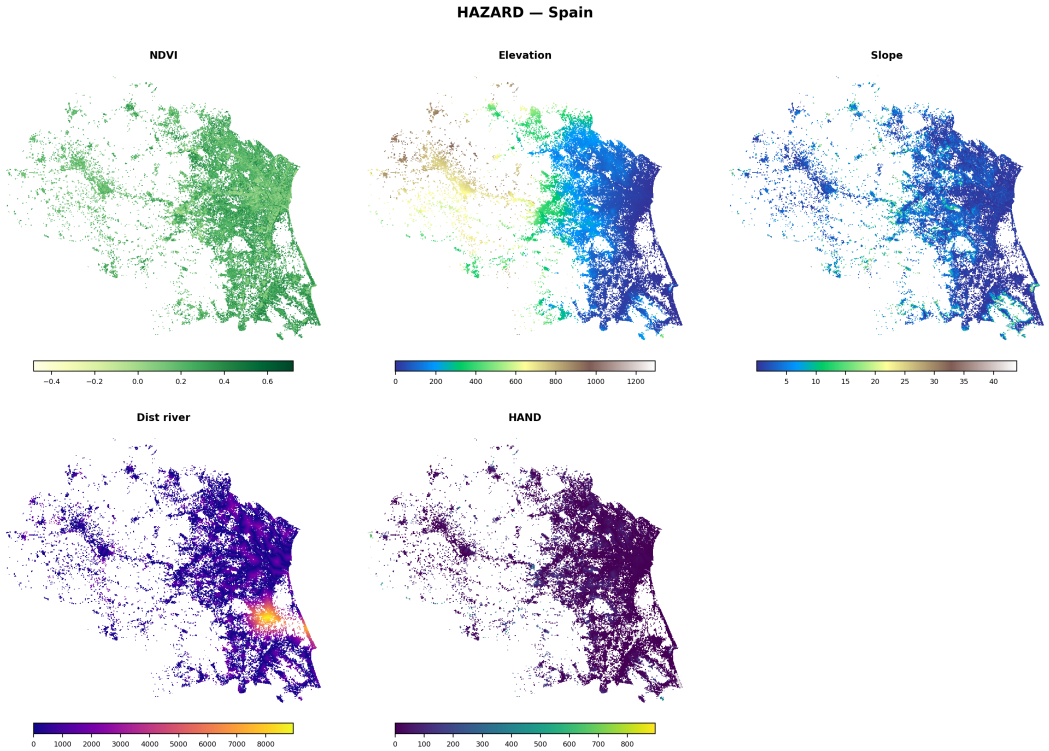


Figure B.13: Choropleths of hazard indicators for Spain.

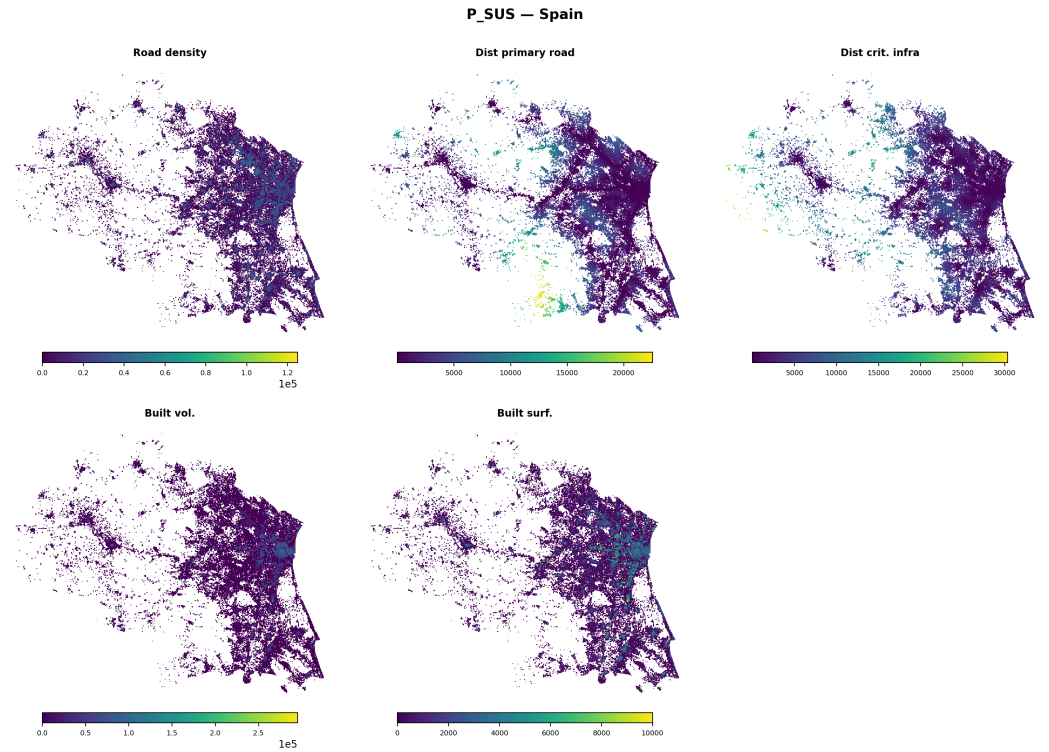


Figure B.14: Choropleths of physical susceptibility indicators for Spain.

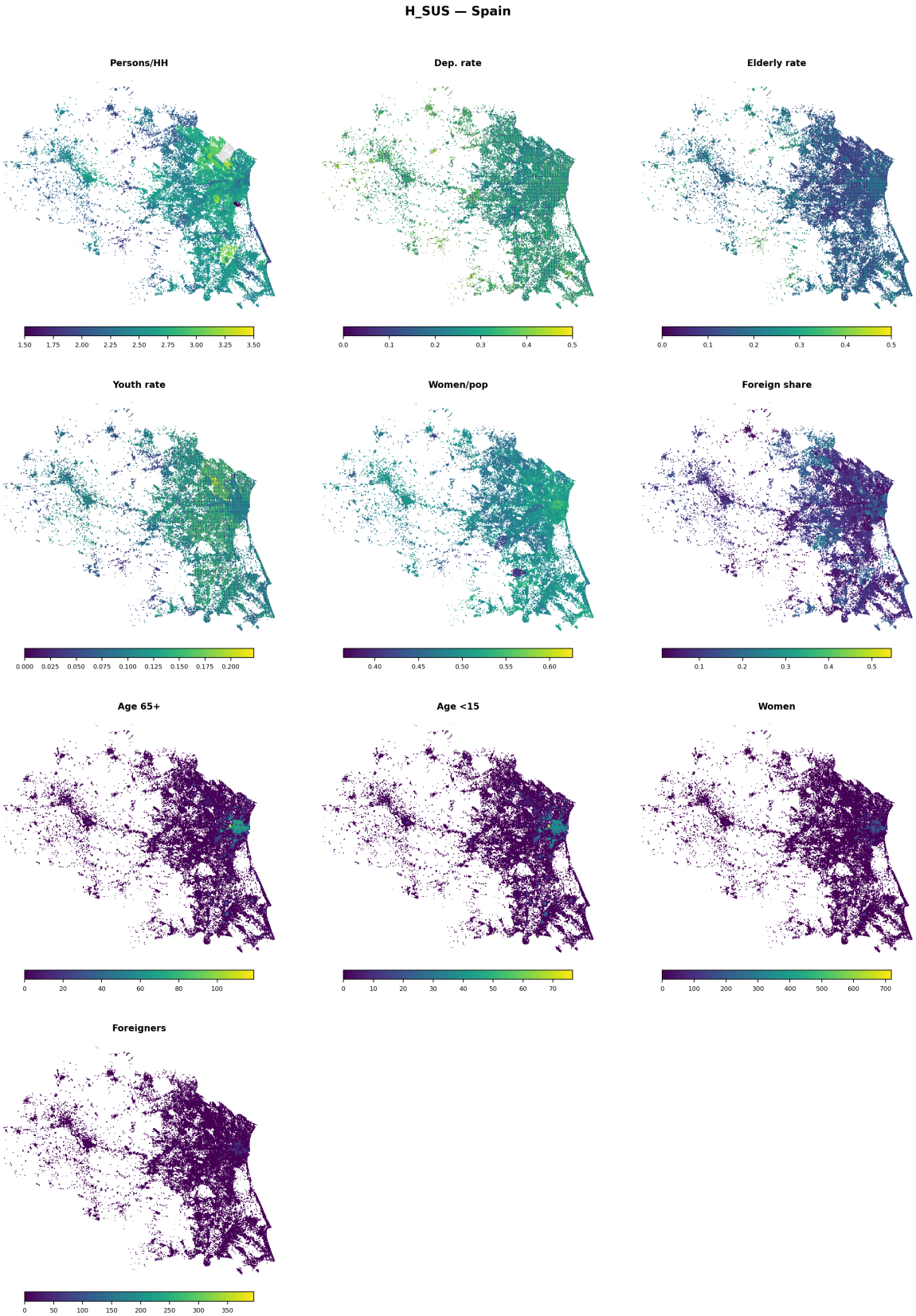


Figure B.15: Choropleths of human susceptibility indicators for Spain.

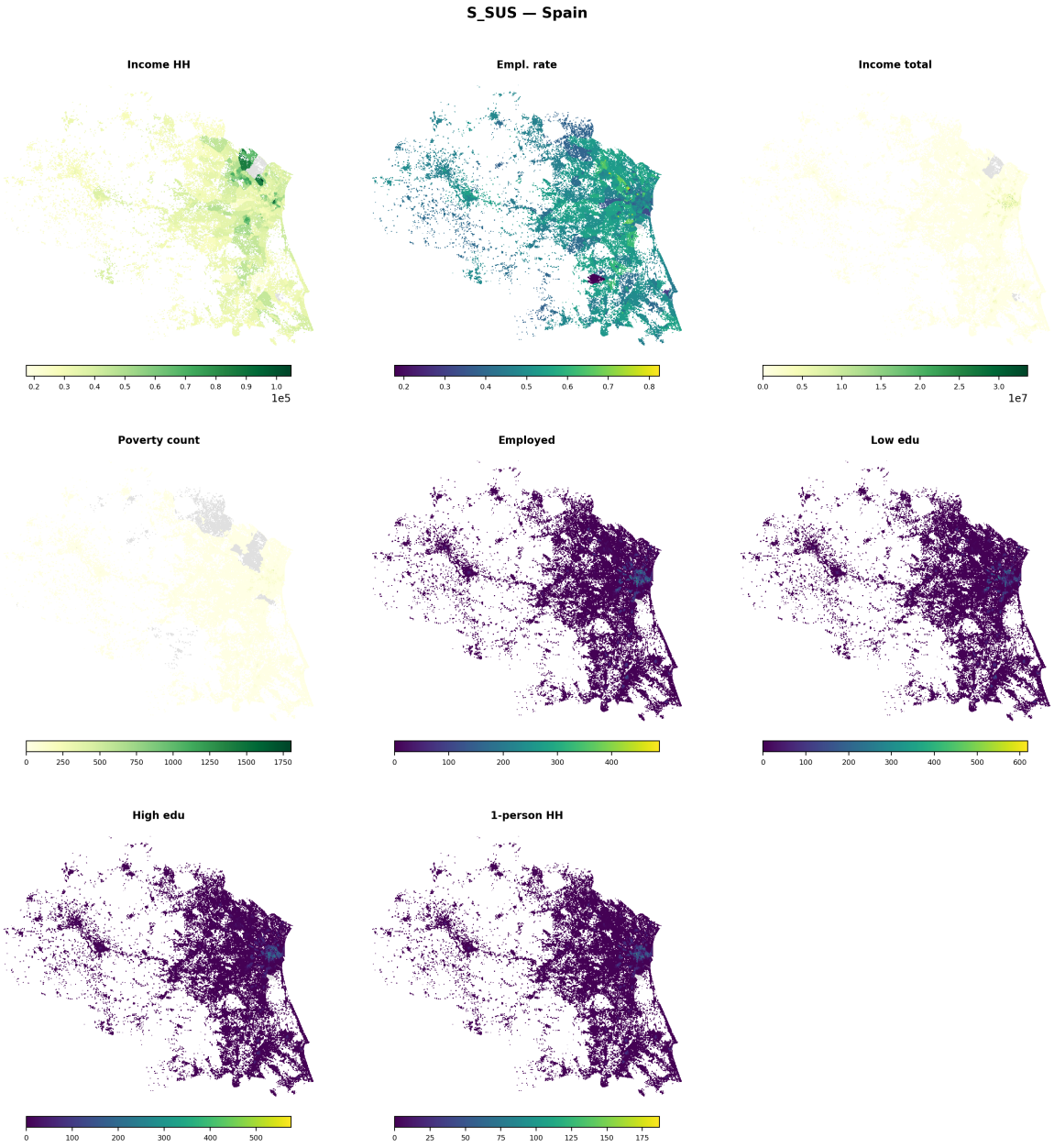


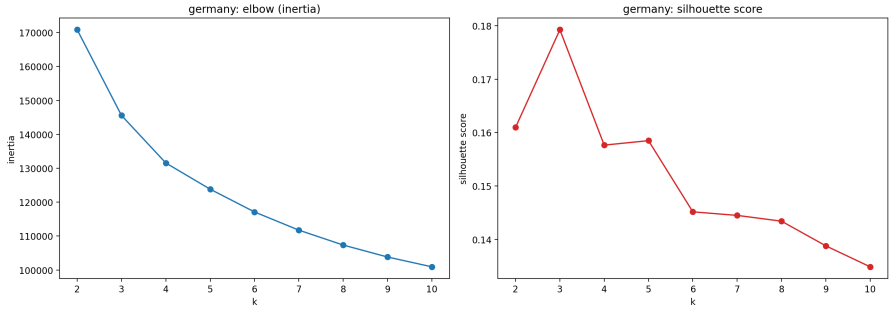
Figure B.16: Choropleths of social susceptibility indicators for Spain.

C

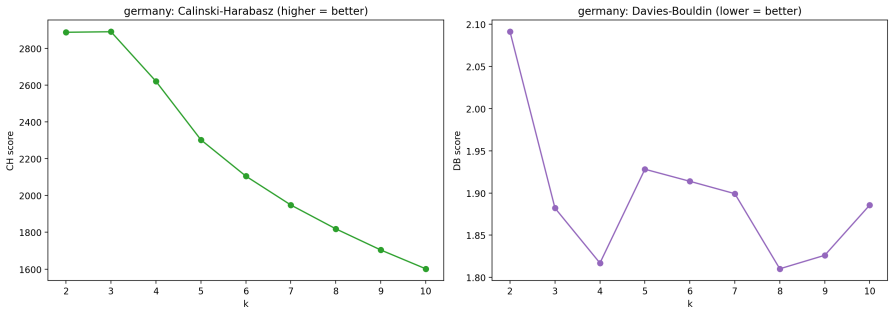
Spatial Clustering K-Value Diagnosis Raw Values

This appendix reports the raw values as results of the k-value diagnostics referenced in Chapter 5. For each region, inertia, silhouette score, the Calinski-Harabasz index, and the Davies-Bouldin index are reported across the full tested range of k, prior to the rescaling described in Chapter 4. The composite-optimal k for each region is shaded.

C.1. Germany



(a) K values for Germany with inertia and silhouette methods



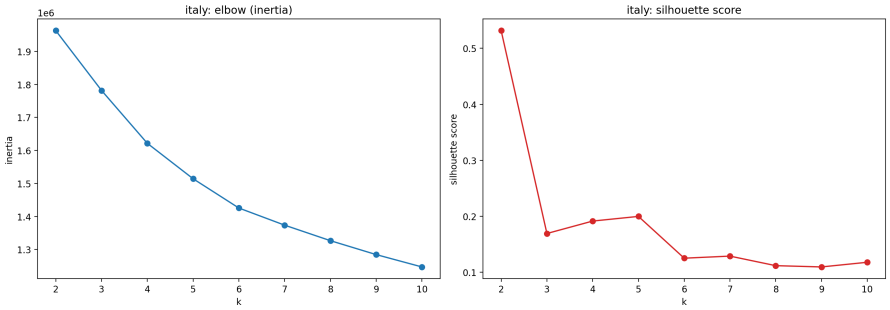
(b) K values for Germany with Calinski-Harabasz and Davies-Bouldin methods

Figure C.1: K value plots according to different methods for Germany.

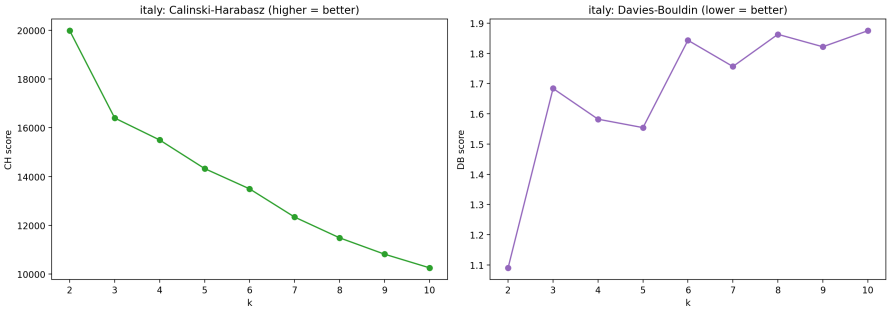
Table C.1: Raw clustering validation indices by number of clusters, Germany

k	Inertia	Silhouette	Calinski-Harabasz	Davies-Bouldin
2	170,831.86	0.161	2,887.18	2.091
3	**145,554.52**	**0.179**	**2,890.09**	**1.882**
4	131,547.38	0.158	2,620.54	1.817
5	123,824.73	0.158	2,302.55	1.928
6	117,116.98	0.145	2,105.13	1.914
7	111,759.95	0.144	1,948.23	1.899
8	107,363.92	0.143	1,818.69	1.810
9	103,837.57	0.139	1,703.72	1.826
10	100,947.60	0.135	1,601.45	1.886

C.2. Italy



(a) K values for Italy with inertia and silhouette methods



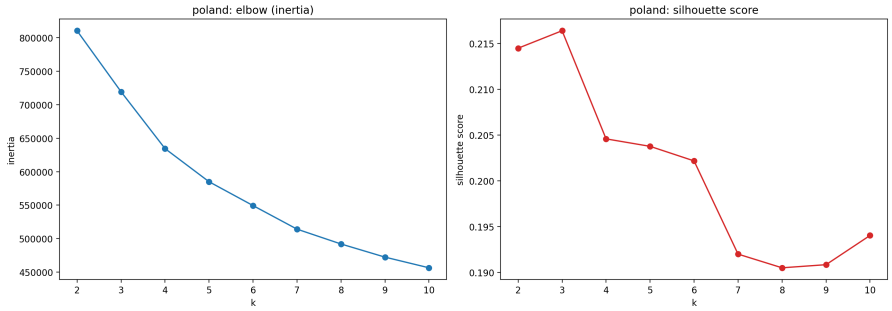
(b) K values for Italy with Calinski-Harabasz and Davies-Bouldin methods

Figure C.2: K value plots according to different methods for Italy.

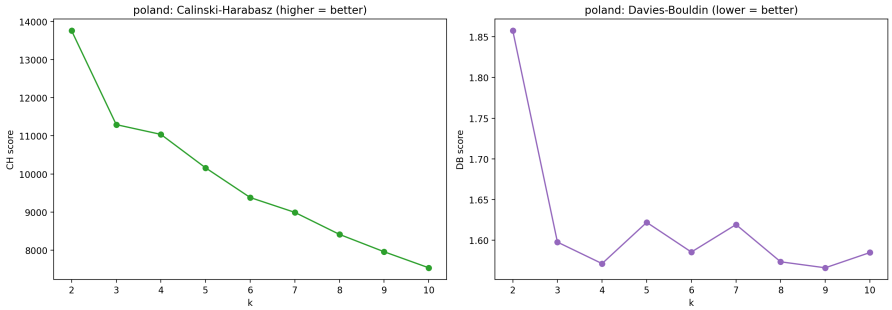
Table C.2: Raw clustering validation indices by number of clusters, Italy

k	Inertia	Silhouette	Calinski-Harabasz	Davies-Bouldin
2	**1,962,806.72**	**0.531**	**19,983.08**	**1.091**
3	1,781,603.82	0.169	16,399.74	1.684
4	1,621,629.45	0.191	15,498.19	1.582
5	1,514,345.66	0.200	14,324.88	1.554
6	1,425,657.07	0.125	13,491.86	1.843
7	1,373,780.38	0.129	12,334.96	1.756
8	1,326,807.94	0.112	11,483.25	1.863
9	1,284,669.12	0.110	10,812.07	1.822
10	1,247,260.89	0.118	10,252.21	1.875

C.3. Poland



(a) K values for Poland with inertia and silhouette methods



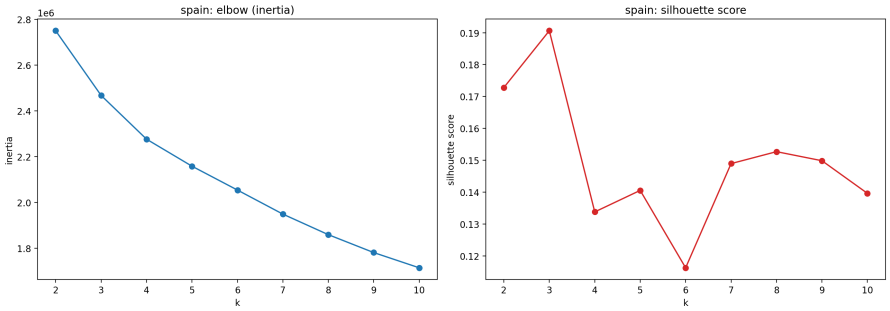
(b) K values for Poland with Calinski-Harabasz and Davies-Bouldin methods

Figure C.3: K value plots according to different methods for Poland.

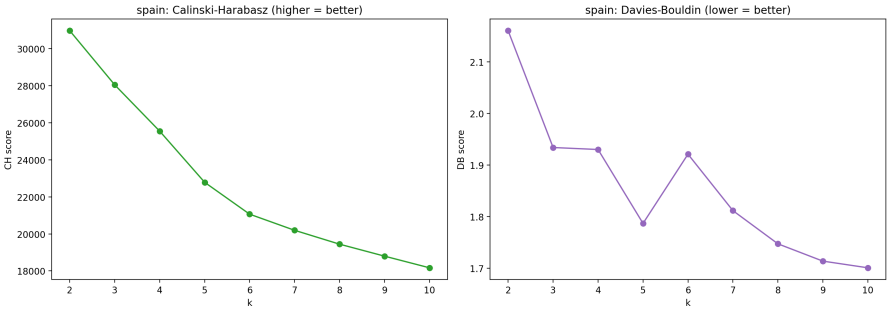
Table C.3: Raw clustering validation indices by number of clusters, Poland

k	Inertia	Silhouette	Calinski-Harabasz	Davies-Bouldin
2	810,339.23	0.214	13,756.03	1.858
3	**719,345.04**	**0.216**	**11,293.72**	**1.598**
4	634,433.63	0.205	11,037.72	1.571
5	585,016.13	0.204	10,161.29	1.622
6	549,422.39	0.202	9,381.86	1.585
7	514,231.80	0.192	8,992.46	1.619
8	492,085.90	0.191	8,414.97	1.573
9	472,462.38	0.191	7,959.81	1.566
10	456,543.45	0.194	7,539.14	1.585

C.4. Spain



(a) K values for Spain with inertia and silhouette methods



(b) K values for Spain with Calinski-Harabasz and Davies-Bouldin methods

Figure C.4: K value plots according to different methods for Spain.

Table C.4: Raw clustering validation indices by number of clusters, Spain

k	Inertia	Silhouette	Calinski-Harabasz	Davies-Bouldin
2	2,750,245.37	0.173	30,969.16	2.160
3	**2,467,611.66**	**0.191**	**28,045.91**	**1.934**
4	2,276,282.72	0.134	25,546.50	1.930
5	2,158,203.17	0.141	22,784.65	1.787
6	2,053,965.02	0.116	21,064.59	1.921
7	1,948,830.51	0.149	20,194.36	1.811
8	1,859,027.88	0.153	19,445.43	1.747
9	1,780,692.11	0.150	18,798.98	1.714
10	1,714,205.00	0.140	18,170.02	1.701

D

Full Spatial Regression Model Results

This appendix reports the full model statistics and coefficient tables for the ordinal spatial lag of X (SLX) models estimated for each of the four countries in the sample. For each country, three model specifications are compared: non-spatial OLS, the non-spatial ordinal logit, and the final ordinal logit with spatial lag (SLX) covariates used in the main text. Model fit is assessed through AIC, BIC, log-likelihood, and McFadden's pseudo-R^2, calculated relative to the null (intercept-only) log-likelihood reported for each country. The improvement in fit from adding spatial lag terms is tested formally with a likelihood ratio test comparing the non-spatial and SLX ordinal logit specifications. Residual spatial autocorrelation is then assessed with Moran's I, computed on the residuals of the OLS baseline and, separately, on the residuals of the final SLX model, to check whether the spatial lag specification adequately accounts for spatial dependence in the data.

For the coefficient tables, each predictor reports the estimated coefficient, standard error, z-statistic, and p-value for both its direct and spatially lagged (WX) effect. int_ and ext_ prefixes denote intensive and extensive variables respectively; full indicator definitions and the composition of each principal component are given in Table 5.1b and its regional equivalents in Chapter 5. The final rows of each coefficient table report the estimated threshold (cutpoint) parameters of the ordinal model.

D.1. Germany

Table D.1: Model comparison statistics for Germany

Model	n	AIC	BIC	Log-lik.	Pseudo R^2
Null (intercept only)	802	—	—	-823.77	—
OLS	802	1588.90	1659.20	-779.45	—
Ordinal logit (no SLX)	802	1492.10	1567.10	-730.05	0.114
Ordinal logit (SLX)	802	1400.40	1541.01	-670.20	0.186

Table D.2: Likelihood ratio test, non-spatial vs. SLX ordinal logit, Germany

LR statistic	119.70
Degrees of freedom	14
p-value	< 0.001
Conclusion	SLX improves fit

Residual spatial autocorrelation is reduced once spatially lagged covariates are added, but remains statistically significant, indicating that the SLX specification does not fully capture the spatial structure present in the data.

Table D.3: Moran's I on model residuals, Germany

	OLS residuals	SLX residuals
Moran's I	0.252	0.200
Expected I	-0.001	-0.001
z_{sim}	14.37	12.39
p_{sim}	0.0025	0.0025
Permutations	399	399

Table D.4: Ordinal SLX model coefficients — Germany (direct and spatially lagged effects)

	Direct				**Spatial Lag (WX)**			
Variable	Coef.	S.E.	z	p	Coef.	S.E.	z	p
Intensive Variables								
int_elderly_dependency_pc	0.254	0.082	3.110	0.002***	0.843	0.248	3.406	<0.001***
int_ndvi	-0.211	0.117	-1.807	0.071*	-0.116	0.273	-0.424	0.672
int_road_density_m_per_km2	0.419	0.108	3.868	<0.001***	-0.265	0.227	-1.169	0.242
int_dist_nearest_primary_road_m	-0.128	0.311	-0.411	0.681	-0.057	0.381	-0.148	0.882
int_dist_nearest_critical_infra_m	-3.468	0.592	-5.861	<0.001***	3.815	0.609	6.264	<0.001***
int_dem_m	0.171	1.129	0.151	0.880	0.289	1.145	0.253	0.801
int_dist_river_m	0.094	0.140	0.673	0.501	-0.105	0.214	-0.489	0.625
int_employment_rate_total	-0.328	0.709	-0.463	0.643	0.299	0.716	0.417	0.677
int_women_per_pop	0.813	1.541	0.528	0.598	-1.402	1.548	-0.906	0.365
int_slope	-0.437	0.162	-2.695	0.007***	1.605	0.300	5.343	<0.001***
int_hand_m	-0.385	0.324	-1.187	0.235	-0.299	0.411	-0.728	0.466
int_income_mean_hh	0.814	1.953	0.417	0.677	-0.611	1.958	-0.312	0.755
Extensive Variables								
ext_built_mass_pc	-0.328	0.167	-1.966	0.049**	-1.448	0.362	-3.995	<0.001***
ext_sociodemographic_mass_pc	0.916	0.189	4.842	<0.001***	2.238	0.401	5.574	<0.001***
Threshold								
$\tau_{0\|1}$	-2.334 (0.128), $z = -18.279, p < 0.001$***							
$\tau_{1\|2}$	0.948 (0.052), $z = 18.383, p < 0.001$***							

Note: $^{*}p < 0.10$, $^{**}p < 0.05$, $^{***}p < 0.01$.

D.2. Italy

Table D.5: Model comparison statistics for Italy

Model	n	AIC	BIC	Log-lik.	Pseudo R^2
Null (intercept only)	10382	—	—	-7784.26	—
OLS	10382	13867.74	14012.70	-6913.87	—
Ordinal logit (no SLX)	10382	13021.16	13173.36	-6489.58	0.166
Ordinal logit (SLX)	10382	12973.19	13263.10	-6446.59	0.172

Table D.6: Likelihood ratio test, non-spatial vs. SLX ordinal logit, Italy

LR statistic	85.97
Degrees of freedom	19
p-value	< 0.001
Conclusion	SLX improves fit

Table D.7: Moran's I on model residuals, Italy

	OLS residuals	SLX residuals
Moran's I	0.248	0.244
Expected I	0.000	0.000
z_{sim}	50.83	54.27
p_{sim}	0.0025	0.0025
Permutations	399	399

Unlike Germany and Poland, residual spatial autocorrelation in Italy does not meaningfully decrease once spatially lagged covariates are included, and its z_{sim} statistic increases slightly. This suggests the SLX specification captures little of the spatial dependence present in Italy's OLS residuals.

Table D.8: Ordinal SLX model coefficients — Italy (direct and spatially lagged effects)

	Direct				Spatial Lag (WX)			
Variable	Coef.	S.E.	z	p	Coef.	S.E.	z	p
Intensive Variables								
int_ndvi	0.207	0.030	6.841	<0.001***	-0.060	0.049	-1.227	0.220
int_hand_m	-0.064	0.059	-1.086	0.278	-0.090	0.070	-1.280	0.201
int_road_density_m_per_km2	0.462	0.028	16.767	<0.001***	-0.007	0.055	-0.133	0.894
int_dist_nearest_primary_road_m	0.074	0.470	0.158	0.874	-0.100	0.471	-0.212	0.832
int_dist_nearest_critical_infra_m	-0.424	0.439	-0.966	0.334	0.290	0.441	0.658	0.511
int_dem_m	0.034	0.042	0.816	0.415	-0.074	0.082	-0.895	0.371
int_dist_river_m	-0.780	0.367	-2.125	0.034**	0.789	0.370	2.135	0.033**
int_slope	0.033	0.047	0.712	0.476	-0.197	0.078	-2.530	0.011**
int_foreign_share	-0.107	0.052	-2.052	0.040**	0.025	0.062	0.408	0.683
int_women_per_pop	-0.098	0.043	-2.297	0.022**	0.054	0.053	1.017	0.309
int_persons_per_household	-0.008	0.047	-0.178	0.858	-0.185	0.058	-3.174	0.002***
int_income_mean_hh	0.008	0.123	0.064	0.949	-0.012	0.127	-0.092	0.927
int_employment_rate_total	0.039	0.046	0.852	0.394	0.003	0.055	0.052	0.958
int_elderly_rate	-0.238	0.174	-1.370	0.171	0.324	0.178	1.821	0.069*
int_youth_rate	-0.074	0.211	-0.352	0.725	0.029	0.214	0.135	0.892
Extensive Variables								
ext_built_mass_pc	0.680	0.039	17.570	<0.001***	0.049	0.066	0.750	0.453
ext_age_income_poverty_pc	0.365	0.064	5.714	<0.001***	-0.166	0.094	-1.777	0.076*
ext_foreign_total	0.004	0.058	0.074	0.941	-0.275	0.087	-3.169	0.002***
ext_edu_high_comp_count	-0.241	0.057	-4.228	<0.001***	0.519	0.095	5.453	<0.001***
Threshold								
$\tau_{0\|1}$	0.634	0.023	27.098	< 0.001***				
$\tau_{1\|2}$	1.358	0.021	64.321	< 0.001***				

Note: $^{*}p < 0.10$, $^{**}p < 0.05$, $^{***}p < 0.01$.

D.3. Poland

Table D.9: Model comparison statistics for Poland

Model	n	AIC	BIC	Log-lik.	Pseudo R^2
Null (intercept only)	1106	—	—	-1115.58	—
OLS	1106	2156.41	2221.52	-1065.20	—
Ordinal logit (no SLX)	1106	1930.03	2000.15	-951.02	0.148
Ordinal logit (SLX)	1106	1897.55	2027.77	-922.77	0.173

Table D.10: Likelihood ratio test, non-spatial vs. SLX ordinal logit, Poland

LR statistic	56.48
Degrees of freedom	12
p-value	< 0.001
Conclusion	SLX improves fit

Table D.11: Moran's I on model residuals, Poland

	OLS residuals	SLX residuals
Moran's I	0.222	0.210
Expected I	-0.001	-0.001
z_{sim}	15.63	14.75
p_{sim}	0.0025	0.0025
Permutations	399	399

As in Germany, residual spatial autocorrelation decreases once spatially lagged covariates are included, though it remains statistically significant.

Table D.12: Ordinal SLX model coefficients — Poland (direct and spatially lagged effects)

	Direct				**Spatial Lag (WX)**			
Variable	Coef.	S.E.	z	p	Coef.	S.E.	z	p
Intensive Variables								
int_ndvi	0.015	0.084	0.183	0.855	0.719	0.168	4.275	<0.001***
int_road_density_m_per_km2	0.415	0.071	5.844	<0.001***	0.066	0.159	0.417	0.677
int_dist_nearest_primary_road_m	-4.272	3.959	-1.079	0.281	4.729	3.959	1.194	0.232
int_dist_nearest_critical_infra_m	-2.406	0.584	-4.122	<0.001***	2.508	0.593	4.230	<0.001***
int_foreign_share	1.272	1.377	0.924	0.356	-0.984	1.389	-0.709	0.479
int_dist_river_m	-0.040	0.152	-0.266	0.790	-0.189	0.208	-0.906	0.365
int_slope	-0.080	0.119	-0.670	0.503	0.326	0.186	1.753	0.080*
int_hand_m	-0.359	0.111	-3.224	0.001***	0.169	0.205	0.827	0.408
int_elderly_rate	-0.080	0.268	-0.298	0.766	0.117	0.292	0.403	0.687
Extensive Variables								
ext_built_mass_pc	0.309	0.095	3.247	0.001***	0.007	0.164	0.040	0.968
ext_sociodemographic_mass_pc	0.225	0.225	0.996	0.319	0.105	0.246	0.426	0.670
ext_foreign_total	0.038	0.185	0.204	0.838	-0.160	0.215	-0.743	0.458
Threshold								
$\tau_{0\|1}$	-0.067	0.074	-0.906	0.365				
$\tau_{1\|2}$	0.771	0.047	16.406	< 0.001***				

Note: $^{*}p < 0.10$, $^{**}p < 0.05$, $^{***}p < 0.01$.

D.4. Spain

Table D.13: Model comparison statistics for Spain

Model	n	AIC	BIC	Log-lik.	Pseudo R^2
Null (intercept only)	10605	—	—	-10547.10	—
OLS	10605	20401.85	20525.42	-10183.92	—
Ordinal logit (no SLX)	10605	18682.24	18813.08	-9323.12	0.116
Ordinal logit (SLX)	10605	18417.97	18665.12	-9174.99	0.130

Table D.14: Likelihood ratio test, non-spatial vs. SLX ordinal logit, Spain

LR statistic	296.27
Degrees of freedom	16
p-value	< 0.001
Conclusion	SLX improves fit

Table D.15: Moran's I on model residuals, Spain

	OLS residuals	SLX residuals
Moran's I	0.341	0.343
Expected I	0.000	0.000
z_{sim}	68.83	72.75
p_{sim}	0.0025	0.0025
Permutations	399	399

Residual spatial autocorrelation in Spain is essentially unchanged after fitting the SLX specification, with Moran's I and z_{sim} both marginally higher than under OLS. As with Italy, this suggests the spatial lag terms capture little of the spatial dependence present in the residuals.

Table D.16: Ordinal SLX model coefficients — Spain (direct and spatially lagged effects)

	Direct				Spatial Lag (WX)			
Variable	Coef.	S.E.	z	p	Coef.	S.E.	z	p
Intensive Variables								
int_elderly_dependency_pc	0.010	0.020	0.466	0.641	0.127	0.049	2.581	0.010***
int_ndvi	-0.006	0.029	-0.220	0.826	-0.183	0.048	-3.798	0.000***
int_road_density_m_per_km2	0.415	0.025	16.444	<0.001***	0.120	0.044	2.717	0.007***
int_dist_nearest_primary_road_m	-0.104	0.429	-0.243	0.808	0.020	0.431	0.047	0.962
int_dist_nearest_critical_infra_m	-0.720	0.649	-1.111	0.267	0.929	0.650	1.430	0.153
int_dem_m	-2.645	1.926	-1.374	0.170	2.616	1.927	1.357	0.175
int_dist_river_m	-1.385	0.186	-7.434	<0.001***	1.190	0.189	6.283	<0.001***
int_slope	0.111	0.042	2.660	0.008***	-0.035	0.056	-0.636	0.525
int_employment_rate_total	0.027	0.062	0.430	0.667	0.052	0.071	0.743	0.458
int_women_per_pop	-0.027	0.079	-0.343	0.732	0.229	0.084	2.718	0.007***
int_foreign_share	-0.042	0.075	-0.564	0.572	0.295	0.081	3.634	0.000***
int_hand_m	-0.255	0.102	-2.490	0.013**	-0.161	0.108	-1.497	0.134
int_persons_per_household	0.073	0.069	1.068	0.285	0.053	0.075	0.707	0.480
int_income_mean_hh	-0.116	0.062	-1.878	0.060*	0.365	0.071	5.128	<0.001***
Extensive Variables								
ext_built_mass_pc	0.175	0.038	4.613	<0.001***	0.427	0.053	8.130	<0.001***
ext_sociodemographic_mass_pc	-0.113	0.039	-2.874	0.004***	0.120	0.052	2.303	0.021**
Threshold								
$\tau_{0\|1}$	-0.120	0.022	-5.488	< 0.001***				
$\tau_{1\|2}$	0.863	0.015	59.315	< 0.001***				

Note: $^{*}p < 0.10$, $^{**}p < 0.05$, $^{***}p < 0.01$.

E

Full Cross-Region Consistency Results

This appendix reports the full results underlying the cross-country and cross-method consistency checks summarized in Chapter 6. It reports the complete classification of every indicator by region, including the consistent but weak, conflicting, scale-dependent, partial, and irrelevant categories summarized only by count in Table 6.3.

Table E.1: Full evidence classification, Germany

Indicator	Cluster z	Cluster signal	Regression signal	Classification
Built-mass PC	1.414	high	− (p < 0.05)	Conflicting
Sociodemographic mass PC	1.414	high	+ (p < 0.05)	Strongly consistent
Elevation	-0.959	low	ns	Partial
Distance to critical infrastructure	-0.993	low	direct − / lag +	Scale-dependent
Distance to primary road	-0.788	no clear pattern	ns	Irrelevant
Distance to river	-0.879	low	ns	Partial
Elderly-dependency PC	1.412	high	+ (p < 0.05)	Strongly consistent
Employment rate	0.726	no clear pattern	ns	Irrelevant
HAND	-0.915	low	ns	Partial
Income per household	-1.083	low	ns	Partial
NDVI	-1.413	low	− (p < 0.10)	Consistent but weak
Road density	1.413	high	+ (p < 0.05)	Strongly consistent
Slope	-1.371	low	direct − / lag +	Scale-dependent
Women per population	0.968	high	ns	Partial
Youth rate	1.353	high	not in model	Partial

Table E.2: Full evidence classification, Italy

Indicator	Cluster z	Cluster signal	Regression signal	Classification
Age-income-poverty PC	1.000	high	direct + / lag −	Scale-dependent
Built-mass PC	1.000	high	+ ($p < 0.05$)	Strongly consistent
High education count	1.000	high	direct − / lag +	Scale-dependent
Foreign population count	1.000	high	− ($p < 0.05$)	Conflicting
Single-person household count	1.000	high	not in model	Partial
Women-labor-education PC	1.000	high	not in model	Partial
Age dependency rate	-1.000	low	not in model	Partial
Elevation	-1.000	low	ns	Partial
Distance to critical infrastructure	-1.000	low	ns	Partial
Distance to primary road	-1.000	low	ns	Partial
Distance to river	1.000	high	direct − / lag +	Scale-dependent
Elderly rate	-1.000	low	+ ($p < 0.10$)	Partial
Employment rate	-1.000	low	ns	Partial
Foreign share	1.000	high	− ($p < 0.05$)	Conflicting
HAND	1.000	high	ns	Partial
Income per household	-1.000	low	ns	Partial
NDVI	-1.000	low	+ ($p < 0.05$)	Conflicting
Persons per household	-1.000	low	− ($p < 0.05$)	Strongly consistent
Road density	1.000	high	+ ($p < 0.05$)	Strongly consistent
Slope	-1.000	low	− ($p < 0.05$)	Strongly consistent
Women per population	1.000	high	− ($p < 0.05$)	Conflicting
Youth rate	-1.000	low	ns	Partial

Table E.3: Full evidence classification, Poland

Indicator	Cluster z	Cluster signal	Regression signal	Classification
Built-mass PC	1.414	high	+ ($p < 0.05$)	Strongly consistent
Foreign population count	1.414	high	ns	Partial
Sociodemographic mass PC	1.414	high	ns	Partial
Age dependency rate	0.785	no clear pattern	not in model	Irrelevant
Elevation	-1.410	low	not in model	Partial
Distance to critical infrastructure	-1.366	low	direct − / lag +	Scale-dependent
Distance to primary road	-1.369	low	ns	Partial
Distance to river	-1.383	low	ns	Partial
Elderly rate	0.766	no clear pattern	ns	Irrelevant
Employment rate	0.115	no clear pattern	not in model	Irrelevant
Foreign share	0.886	high	ns	Partial
HAND	-1.381	low	− ($p < 0.05$)	Strongly consistent
Household income-size PC	-0.875	low	not in model	Partial
NDVI	-1.411	low	+ ($p < 0.05$)	Conflicting
Road density	1.414	high	+ ($p < 0.05$)	Strongly consistent
Slope	-1.407	low	+ ($p < 0.10$)	Partial
Women per population	1.008	high	not in model	Partial
Youth rate	-0.745	no clear pattern	not in model	Irrelevant

Table E.4: Full evidence classification, Spain

Indicator	Cluster z	Cluster signal	Regression signal	Classification
Built-mass PC	1.414	high	+ (p < 0.05)	Strongly consistent
Sociodemographic mass PC	1.414	high	direct − / lag +	Scale-dependent
Elevation	-0.821	low	ns	Partial
Distance to critical infrastructure	-0.993	low	ns	Partial
Distance to primary road	-0.975	low	ns	Partial
Distance to river	0.421	no clear pattern	direct − / lag +	Scale-dependent
Elderly-dependency PC	-0.534	no clear pattern	+ (p < 0.05)	Partial
Employment rate	0.251	no clear pattern	ns	Irrelevant
Foreign share	-0.014	no clear pattern	+ (p < 0.05)	Partial
HAND	-0.869	low	− (p < 0.05)	Strongly consistent
Income per household	0.698	no clear pattern	direct − / lag +	Scale-dependent
NDVI	-1.331	low	− (p < 0.05)	Strongly consistent
Persons per household	0.750	no clear pattern	ns	Irrelevant
Road density	1.406	high	+ (p < 0.05)	Strongly consistent
Slope	-0.889	low	+ (p < 0.05)	Conflicting
Women per population	1.257	high	+ (p < 0.05)	Strongly consistent
Youth rate	0.626	no clear pattern	not in model	Irrelevant

F

Data Validation and Indicator Construction Checks

This appendix documents the validation checks applied during construction of the harmonized 100 m indicator datasets. The analysis combines hazard, built-environment, demographic, socio-economic, and flood-impact data from global, European, and national sources. These sources differ in spatial unit, coordinate reference system, reporting year, value scale, and disclosure-control practice. Validation was therefore applied during source preparation, spatial processing, dasymetric mapping, derived-variable construction, and final dataset assembly.

The checks had two purposes. First, they verified that values retained their intended meaning after conversion to the common analytical grid. Second, they identified source mismatches, implausible values, incomplete coverage, unit inconsistencies, and spatial-allocation problems before the datasets entered PCA, clustering, and regression.

F.1. General Validation Procedures

F.1.1. Spatial Reference and Grid Checks

All datasets were aligned to the common equal-area analysis projection before spatial overlays, distance calculations, and grid-level joins. For each country, vector inputs were checked for the presence of the common grid identifier, `cellid`, before merging. Duplicate grid identifiers were removed where necessary, and merged datasets were checked for duplicate geometry columns.

The combined-data notebooks also verified the coordinate reference systems of input grids before merging. In the Italian and Spanish workflows, the socio-economic, income, impact, and infrastructure grids were reprojected to the common Mollweide projection before merging by `cellid`. In the German workflow, duplicate infrastructure columns created during merging were compared directly. The overlapping primary-road and critical-infrastructure distance columns showed no differing values in cells where both versions were available.

F.1.2. Numerical Screening

Summary statistics were generated repeatedly during construction and after merging. These checks included count, mean, standard deviation, minimum, quartiles, maximum, missing-value coverage, and value ranges. Rate variables were checked for plausible fractional ranges, while count variables were checked for non-negative values and local magnitudes consistent with their denominators.

Selected indicator maps were also produced as visual checks. These maps were used to identify isolated extreme cells, unexpected administrative boundaries, sparse coverage, and patterns inconsistent with the relevant geography. Outlying values were retained when they represented plausible local conditions. Values were corrected or excluded when tracing showed that they resulted from a source, unit, join, or allocation error.

F.1.3. Dasymetric Allocation Checks

Extensive variables were redistributed to the 100 m grid using WorldPop population or source-specific denominators where appropriate. Where original totals and compatible source geometries were available, allocated grid values were aggregated back to the source unit and compared with the original total.

For each extensive variable X_s reported in source unit s, the mass-preservation check was expressed as:

$$\sum_{i \in s} x_i \approx X_s$$

where x_i is the allocated value in grid cell i. Small differences may arise from floating-point precision or spatial intersections. Material differences were investigated before an indicator was retained.

Derived ratios were recalculated after allocation where possible. This applied to variables such as foreign population share, women per population, poverty count, and total income. Recalculation ensured that the numerator and denominator remained internally consistent at grid level.

F.2. Germany

F.2.1. Administrative Identifier and Source-Format Checks

The German workflow combined INKAR data, Local Administrative Unit boundaries, Zensus 2022 grid products, WorldPop, and the 100 m target grid. Administrative identifiers required normalization because INKAR identifiers and boundary-layer identifiers used different leading-zero conventions. The workflow standardized identifiers before joining municipality and Kreis-level statistics to the spatial boundaries.

German decimal and thousands-separator conventions were also handled during source preparation. Numeric values were converted after removing source-specific thousands separators and converting decimal commas to decimal points. Indicator names and area-reference labels were normalized to account for inconsistent encoding of German umlauts and special characters.

F.2.2. German Zensus Data and Disclosure-Control Checks

Selected German Zensus grid products use disclosure-control encoding for small counts. A placeholder value in the relevant exports was checked against associated source documentation and treated as a true zero value for the affected indicators. This correction was applied before summary statistics, missingness screening, and dimensionality reduction.

Several Zensus-derived indicators were available at municipality or association level rather than directly on the target grid. The workflow mapped municipality-level data to Local Administrative Units and expanded association-level records to their constituent municipalities before constructing reporting polygons.

F.2.3. Education Data Allocation

Educational-attainment variables were derived from German administrative education files. Low educational attainment was calculated from ISCED levels 1 and 2. Higher educational attainment was calculated from the available tertiary-level ISCED counts.

The resulting municipality and association-level totals were redistributed to grid cells using WorldPop population weights. Where a reporting unit had zero population weight, an equal-area fallback allocation was available to avoid losing the reported total. Summary statistics were inspected after redistribution, and the output grid retained the expected count-variable structure.

F.2.4. Correction of Count-Variable Allocation

During early processing, several German count variables were attached through direct spatial joins that repeated administrative totals across grid cells. These joins were replaced with population-weighted dasymetric redistribution. The correction reduced implausible grid-cell maxima and restored consistency between grid-level values and administrative totals.

Source-variable definitions were also checked against the INKAR indicator catalog. This identified a small number of mismatches between unified variable names and the underlying source concept. Such variables were remapped to the appropriate source series before inclusion in the final dataset.

F.3. Italy

F.3.1. Coordinate Reference and Overlay Checks

The Italian workflow integrated ISTAT census sections, CAP-level income data, WorldPop population data, and the 100 m target grid. Before overlays were carried out, census-section and income polygons were reprojected to a common metric coordinate reference system. The workflow checked that overlay operations produced non-empty intersections and retained stable identifiers for both census tracts and CAP polygons.

A coverage metric was calculated for each census tract:

$$\text{CAP coverage fraction} = \frac{\text{area of CAP intersections within the tract}}{\text{total tract area}}$$

Values slightly above one, caused by small overlapping CAP polygons, were capped at one. Census tracts with no CAP intersection received a coverage value of zero.

F.3.2. Household-Weighted Income Allocation

CAP-level income totals were initially explored using population-based allocation. This produced implausible income-per-household values in sparsely populated census sections because the income numerator was distributed using WorldPop population while the denominator came from ISTAT household counts.

The final procedure allocated CAP-level income totals to census tracts using ISTAT household counts as the primary weight. Where a CAP polygon had no recorded household weight across its intersecting tracts, area weighting was used as a fallback. The resulting tract-level income total was divided by the ISTAT household count to derive mean household income.

The final income indicator was retained only where the tract had at least 75% CAP coverage. Notebook output confirmed that census tracts below this threshold had no non-null values for the final income-per-household variable. The retained indicator had a range from approximately EUR 30,567 to EUR 53,341 per household.

F.3.3. Income and Poverty Allocation Checks

The CAP-level allocation was checked by comparing source totals with allocated grid totals. The final notebook output showed near-zero relative differences for the allocated extensive variables:

- total income;
- poverty count; and
- number of tax units.

The allocation check therefore confirmed that the grid-level redistribution preserved source totals within numerical precision.

The poverty-rate denominator was also checked against the population represented in the source income brackets. The denominator was adjusted so that the poverty count and poverty rate referred to the same source population.

F.4. Poland

F.4.1. API Retrieval and Metadata Checks

Polish indicators were retrieved from the GUS Local Data Bank API using a metadata table that specified the variable identifier, year, source level, and standardized indicator name. The retrieval workflow recorded the endpoint used, number of rows downloaded, and request status for each indicator. Failed requests were logged instead of silently omitted.

The downloaded data were converted to numeric values, checked for duplicate indicator-unit-year combinations, and reshaped into separate tables by administrative level. This allowed municipal, powiat, regional, and locality-level data to be processed according to their source geography.

F.4.2. Hierarchy and Derived-Indicator Checks

Polish indicators were reported at different administrative levels. Intensive variables reported at regional or powiat level were attached to municipalities through the administrative hierarchy. Extensive variables reported at locality level were aggregated to municipalities. The workflow used unit identifiers and hierarchy prefixes to map higher-level values to their constituent municipalities.

Several final indicators were derived through explicit row-wise operations. These included total income, poverty count, foreign share, low educational attainment count, and women per population. Ratios were computed with zero denominators converted to missing values before division.

The regional household-income proxy was documented as a derived measure. It combined NUTS-2 mean household income with municipality-level persons-per-household values. It is therefore interpreted as a spatially refined proxy and not as a direct municipality-level household-income observation.

F.4.3. Foreign Population Allocation

Foreign population count was available at a higher administrative level than several other indicators. Copying this total directly to each municipality would have overstated local values. The total was redistributed according to population weights.

The allocation procedure preserved the higher-level total while producing a geographically differentiated municipality distribution. Final grid-level count indicators were then redistributed from municipalities using the same extensive-variable logic.

F.5. Spain

F.5.1. Raster and Census-Tract Checks

The Spanish workflow combined census-tract data, WorldPop rasters, infrastructure data, impact layers, and the 100 m target grid. Negative WorldPop raster artifacts were set to zero during preprocessing, while no-data pixels were converted to missing values.

Grid cells were assigned to census tracts through a largest-overlap rule when they intersected more than one tract. This prevented duplicate tract assignment before count-variable allocation. Census rates were copied to assigned grid cells, while count variables were redistributed through population weights.

F.5.2. Grid Merge and Duplicate-Column Checks

The Spanish combined-grid workflow checked that socio-economic, impact, and OpenStreetMap grids shared the same coordinate reference system and `cellid` structure. Where duplicate infrastructure columns arose during merging, the duplicated versions were compared and redundant columns were removed after confirming consistency.

Descriptive statistics were generated after raster sampling and after final merges. These checks covered elevation, slope, NDVI, distance to river, HAND, built surface, built volume, age variables, and dependency measures.

F.5.3. Province-Level Employment Allocation

A province-level employed-women total was redistributed across Valencia grid cells using the relevant employment denominator as the weighting surface. Cells outside Valencia received zero for this province-specific variable. The procedure was designed to preserve the province total while assigning larger values to cells with a greater share of the relevant local denominator.

F.6. Hazard, Infrastructure, and Impact Checks

F.6.1. Hazard Indicators

Elevation, slope, NDVI, distance to river, HAND, built surface, and built volume were sampled or aggregated to the target grid. Summary statistics were inspected after sampling. Hazard grids were also compared visually with known terrain and hydrographic patterns.

HAND and distance-to-river outputs were checked against EU-Hydro drainage lines. Flat terrain caused incomplete HAND coverage in Italy. A nearest-neighbor procedure was used to fill selected missing HAND val-

ues. This choice is a limitation because a raster-based recalculation using a corrected elevation model would provide a stronger representation of local drainage conditions.

F.6.2. Infrastructure Indicators

Road density, distance to primary roads, and distance to critical infrastructure were derived from OpenStreetMap features. Selected maps and summary statistics were inspected to confirm that road-density values concentrated in built-up areas and that distance values decreased near the corresponding mapped features.

Built surface and built volume were checked for non-negative values and grid alignment. Their strong correlation was expected because both products describe related dimensions of the built environment. They were retained during data construction and later reduced through blockwise PCA.

F.6.3. Flood-Impact Indicators

Copernicus EMS grading layers were checked for thematic category, geometry type, damage grade, and spatial overlap with the observed-event footprint. Damage grades were recoded as 1 for possibly damaged, 2 for damaged, and 3 for destroyed.

The combined damage variable summed the maximum grade recorded for built-up areas, facilities, and transportation within each 100 m cell. The resulting score ranged from 0 to 9. Spatial outputs were inspected against the original Copernicus layers to verify that damaged grid cells corresponded to mapped damage features.

Cells without a Copernicus damage grade were coded as zero damage. This assumes that missing grades indicate no observed damage. Incomplete mapping coverage would violate this assumption and remains a limitation of the impact measure.

F.7. Final Screening Before Analysis

Before PCA, clustering, and regression, each regional dataset was screened using the following procedures:

- restriction to populated grid cells using WorldPop;
- assessment of missing-value and zero-value coverage;
- removal of indicators with more than 50% null coverage in the relevant regional sample;
- descriptive-statistics checks for implausible ranges and extreme values;
- visual inspection of selected indicator maps;
- verification of rate scales and count-variable plausibility;
- Spearman rank-correlation screening for PCA block formation; and
- inspection of final predictor availability before regression estimation.

These checks did not determine the conceptual relevance of an indicator. They ensured that variables entering the spatial analyses had sufficient coverage, variation, and numerical consistency for the methods used in this thesis.